High-content analysis for ethanol-induced mitochondrial and neuronal toxicity in human iPSC-derived neurons

Inaugural-Dissertation
to obtain the academic degree
Doctor rerum naturalium (Dr. rer. nat.)

submitted to the Department of Biology, Chemistry, Pharmacy
of Freie Universität Berlin

by

ANNIKA ZINK

February 2021

This work was conducted from March 2016 until February 2021 under the direction of Prof. Dr. med. Josef Priller at the Charité – Universitaetsmedizin Berlin and Prof. Dr. Alessandro Prigione at the Max Delbrueck Center for Molecular Medicine in the Helmholtz-Association.

1. Reviewer: Prof. Dr. med. Josef Priller

2. Reviewer: Prof. Dr. Stephan Sigrist

Date of defense: 16.09.2021

Acknowledgement

I would like to thank Josef Priller for the opportunity and the trust to work on the project, for the guidance, critical appraisals, and the lively discussions. Special thanks to Alessandro Prigione who supported me in many ways. I would like to thank him for the guidance, for supporting the project, for giving me the freedom to work independently on my project but also for being available for help. I also want to thank him for involving me in other projects. I would like to thank Prof. Dr. Stephan Sigrist from Freie Universität Berlin who kindly agreed to review my thesis.

Further, I want to thank Erich Wanker for having me as a guest at MDC and allowing me to work in his lab as well as for his feedback during lab meetings.

I want to thank the "Abschlussstipendium" from Charité- Universitaetsklinikum Berlin for their support in finishing my thesis.

I would like to thank the members of AG Prigione for the extremely good teamwork and the help in the lab. Special gratitude to Carmen, Barbara and Gizem not only for scientific input and being amazing colleagues but also for becoming my friends and companions during my time in the lab and beyond.

I also thank the AG Wanker for their warm welcome, for the critical thinking during lab meetings and for helping me to improve my presentation skills. Especially, I would like to thank Martina and Nancy for their advice, help, and for answering all my general questions. Special thanks to my diligent and lovely office neighbour's Lydia and Anne for their help and support, and to the AG Wanker members for joyful discussions, coffee breaks and PALE ALÈ sessions.

I want to thank my close circle of friends for their uplifting and motivating words. Especially, I would like to thank Anne, Aline, and Inga who are always there for me. I am very grateful to have you. Finally, I would like to thank my lovely family for supporting me in every possible way and being an invaluable constant in my life.

Table of Contents

Summary ..... **I**
Zusammenfassung ..... **III**
List of Figures ..... **V**
List of Tables ..... **VII**
Units ..... **IX**
List of Abbreviations ..... **X**
1. Introduction **1**
1.1 Behavioral effects of ethanol 3
1.2 Metabolism of ethanol 5
1.3 Effects of ethanol consumption on different organs 8
1.3.1 Effects of ethanol on stomach, liver, and heart 9
1.3.2 Effects of ethanol on the nervous system 10
1.4 Background on mitochondria 14
1.4.1 Mitochondrial bioenergetics and brain function 16
1.4.2 Effects of ethanol on mitochondrial bioenergetics 17
1.5 Alcohol dependence and alcohol use disorder (AUD) 21
1.5.1 Alcohol use disorder (AUD) 21
1.5.2 Genetic predisposition to alcohol abuse 23
1.6 State of the art treatment of AUD 24
1.7 Disease models of AUD 30
1.8 Induced pluripotent stem cells (iPSCs) and personalized medicine 31
1.8.1 High-content analysis (HCA) and iPSC-driven drug discovery 34
1.9 Current work on iPSC technology to model AUD 36
1.10 Genome editing of iPSC to model AUD 38
2. Aim of the study **41**
3. Material **43**
3.1 Experimental models 43
3.1.1 Cells 43
3.1.2 iPSC-derived models 44
3.2 Laboratory equipment 46
3.3 Chemicals and Consumables 48
3.3.1 General consumables 48

3.3.2 Cellular consumables 49
3.3.3 Molecular and chemical consumables 51
3.3.4 Kits 52
3.3.5 Media 53
3.3.6 Oligonucleotides and sequences 58
3.3.7 Antibodies 60
3.3.8 Plasmids 62
3.4 Software 62
4. Methods[1] 63
4.1 Cell biology 63
4.1.1 Cell culture 63
4.1.2 iPSC generation 67
4.1.3 Generation and cultivation of NPCs 68
4.1.4 Generation and cultivation of neurons 69
4.1.5 Microelectrode Array recordings 70
4.2 Molecular biology 72
4.2.1 Real-Time Quantitative Reverse Transcription PCR (qRT-PCR) 72
4.2.2 Mycoplasma test 73
4.2.3 Immunostaining 75
4.2.4 CRISPR/Cas9 Genome Editing 77
4.2.5 Sanger Sequencing 79
4.3 Mitochondrial Neuronal Health (MNH) assay 84
4.3.1 Protocol parameters for HCA-based MNH assay 85
4.3.2 Ethanol exposure and treatment of neurons 88
4.3.3 Compound screening – MNH assay 90
5. Results[2] 91
5.1 Generation of human neurons from hESCs and iPSCs for the evaluation of ethanol-induced neuronal toxicity 91
5.2 Establishment of the Mitochondrial Neuronal Health (MNH) assay 97
5.2.1 Neuronal branching 97
5.2.2 Mitochondrial membrane potential (MMP) 101
5.2.3 The MNH assay 104
5.3 Applying the MNH assay to quantify the effects of ethanol on human neurons 108
5.3.1 MNH assay-based quantification of the effects of chronic ethanol exposure 110

5.3.2 MNH assay-based quantification of the effects of acute ethanol exposure .. 111
5.4 Generation of AUD-iPSCs and differentiation into NPCs and neurons 115
5.4.1 Differentiation of AUD-iPSCs into NPCs and neurons 118
5.4.2 MNH assay-based quantification of ethanol effects on AUD-neurons .. 120
5.5 Proof-of-concept compound screening for modulators of ethanol-induced human neurotoxicity 125
5.5.1 Assessment of hit compound candidates 129
5.6 Genome editing using CRISPR/Cas9 135
5.6.1 CRISPR/Cas9 vector construction and design 135
5.6.2 Screening for the corrected clones 137
6. Discussion 141
6.1 Generation of iPSC-derived NPCs and neurons 142
6.2 Assessment of ethanol toxicity in iPSC-derived neuronal cultures using the MNH assay 145
6.3 MNH assay development 148
6.4 Genome editing for *KLB* knockout in control iPSC line 150
6.5 HT-screening and neurotoxicity assessment 151
6.6 Concluding remarks 153
7. Contributions 155
8. Bibliography 157
9. Supplementary information 179
9.1 List of selected compounds from the FDA-approved drug screening library (z65122) 179
10. Publications 187
11. Selbstständigkeitserklärung 188

Summary

Ethanol is the most frequently abused drug in the world with a worldwide mortality of three million deaths each year (5.3% in 2016). Excessive ethanol consumption can adversely affect several organs, where it can lead to cellular and mitochondrial toxicity. The brain is particularly susceptible to ethanol toxicity. The exact mechanism by which ethanol affects the brain is still unknown. Dopaminergic neurons are believed to play a role, especially in the rewarding and reinforcing (i.e. addictive) effects of alcohol. Thus, model systems enabling to detect early toxicity in human dopaminergic neurons may help to discover potential treatment strategies.

In this study, I used human induced pluripotent stem cells (iPSCs) from control individuals and from patients with alcohol use disorder (AUD) to generate neural progenitor cells (NPCs) and neuronal cultures containing dopaminergic neurons. I developed a high-content analysis (HCA)-based assay, dubbed Mitochondrial Neuronal Health (MNH) assay, to quantitatively assess mitochondrial neuronal health in iPSC-derived neurons following ethanol exposure. Acute and chronic exposure of ethanol on iPSC-derived neurons led to decreased mitochondrial membrane potential (MMP) and decreased neuronal branching complexity in a dose-dependent manner. Ethanol toxicity was similarly observed in control neurons and in neurons derived from individuals with AUD.

Finally, I adapted the MNH assay to perform a proof-of-concept compound screening to identify modulators of ethanol-induced neurotoxicity. I found that the two drugs disulfiram and baclofen, which are used to treat AUD, and lithium caused neurotoxicity.

In contrast, the spasmolytic drug flavoxate had a positive effect on mitochondrial neuronal health.

Zusammenfassung

Ethanol gehört mit einer weltweiten Sterblichkeit von drei Millionen Todesfällen pro Jahr zu den häufigsten missbrauchten Drogen der Welt (5.3% in 2016). Übermäßiger Alkoholkonsum kann sich nachteilig auf verschiedene Organe auswirken und zu zellulärer und mitochondrialer Toxizität führen. Der genaue Mechanismus, durch den Ethanol das Gehirn beeinflusst, ist noch unbekannt. Es wird jedoch angenommen, dass dopaminerge Neuronen eine Rolle spielen, insbesondere in der belohnenden und verstärkenden (d. H. süchtig machenden) Wirkung von Alkohol. Geeignete Modellsysteme, die es ermöglichen frühe Neurotoxizität in humanen Neuronen zu erkennen, könnten daher helfen, mögliche Behandlungsstrategien zu entdecken.

In dieser Studie habe ich neuronale Vorläuferzellen (neural progenitor cells, NPCs) und Neuronen aus induzierten pluripotenten Stammzellen (iPSC) von Kontrollpersonen und Patienten mit Alkoholkrankheit (alcohol use disorder; AUD) generiert. Darüber hinaus entwickelte ich ein auf High Content Analysis (HCA) basierendes System, den sogenannten Mitochondrial Neuronal Health (MNH) Assay. Diesen Assay nutze ich, um die mitochondriale und neuronale Gesundheit in den generierten Neuronen nach der Alkoholexposition quantitativ zu bewerten. Die akute und chronische Exposition von Ethanol führte zu einer dosisabhängigen Verringerung des mitochondrialen Membranpotentials (MMP) und zu einer Verringerung der Komplexität der neuronalen Verzweigungen in den aus iPSC generierten Neuronen. Eine Ethanol-Toxizität wurde in ähnlicher Weise in Kontrollneuronen und in Neuronen, die von Personen mit AUD stammten, beobachtet.

Schließlich habe ich den MNH-Assay verwendet, um ein Proof-of-concept-Medikamentenscreening durchzuführen mit dem Ziel, Modulatoren der Ethanol-induzierten Neurotoxizität zu identifizieren. Ich fand heraus, dass die beiden Medikamente Disulfiram und Baclofen, die zur Behandlung von AUD eigesetzt werden, sowie Lithium Neurotoxizität verursachten. Das spasmolytische Medikament Flavoxate hingegen beeinflusste die mitochondriale neuronale Gesundheit positiv.

List of Figures

Fig. 1: Percentage (in %) of alcohol-attributable deaths, as a percentage of all alcohol attributable deaths, by broad disease category (status of 2016). 2
Fig. 2: Effects of ethanol in humans related to its concentration in mM or blood alcohol concentration (BAC). 4
Fig. 3: Ethanol metabolism. 6
Fig. 4: Effects of acute and chronic alcohol consumption on neurotransmitters in the brain. 13
Fig. 5: Mitochondrial function. 15
Fig. 6: Alterations of mitochondrial health during alcohol consumption. 20
Fig. 7: Applications of induced pluripotent stem cells. 32
Fig. 8: Generation and characterization of NPCs and neurons. 94
Fig. 9: MEA recordings of 7-8-week-old neurons from control iPSCs (XM001). 96
Fig. 10: Neurite detection using the Cellomics® Neuronal Profiling V4. 98
Fig. 11: HCA-based quantification of neuronal branching. 100
Fig. 12: HCA-based quantification of MMP. 103
Fig. 13: HCA-based quantification of MMP after exposure to modulators. 105
Fig. 14: HCA-based quantification of neuronal branching after exposure to modulators. 106
Fig. 15: Schematic workflow of the MNH assay 108
Fig. 16: MNH assay-based quantification of neuronal health after chronic ethanol exposure. 110
Fig. 17: MNH assay-based quantification of neuronal health after acute (1 hour) ethanol exposure. 113
Fig. 18: Characterization of AUD-iPSCs. 117
Fig. 19: Characterization of NPCs differentiated from AUD patient iPSCs. 119
Fig. 20: Characterization of neurons differentiated from AUD-patient iPSCs. 120
Fig. 21: MNH assay-based quantification of MMP in AUD patient-derived neurons exposed to acute ethanol. 121

Fig. 22: MNH assay-based quantification of neuronal branching in AUD-neurons after acute ethanol exposure. 123
Fig. 23: Proof-of-concept compound screening in human neurons exposed to ethanol. 127
Fig. 24: MNH assay-based quantification of disulfiram and baclofen on iPSC-derived neurons. 131
Fig. 25: MNH assay-based quantification of 4-8-week-old neurons exposed to lithium. 133
Fig. 26: MNH assay-based quantification of 4-8-week-old neurons exposed to flavoxate. 134
Fig. 27: KLB expression in ESCs and hPSC-derived neurons. 135
Fig. 28: Genome editing strategy. 136
Fig. 29:Screening of potential clones. 138
Fig. 30: Schematics of potential applications of the MNH assay. 152

List of Tables

Table 1-A: Medication for alcohol use disorder adapted and modified from (Winslow et al., 2016). 28
Table 3-A: Background information on fibroblasts 43
Table 3-B :Background information on hESCs and iPSCs 44
Table 3-C: Background information on iPSC-derived NPC 45
Table 3-D: Background information on iPSC-derived neurons 45
Table 3-E: Media for mouse embryonic fibroblasts (MEFs) 53
Table 3-F: Media for hESCs and iPSCs 53
Table 3-G: Media for NPCs 55
Table 3-H: Composition of freezing media. 56
Table 3-I: Media for neurons 56
Table 3-J: FACS media 57
Table 3-K: Oligonucleotide sequences for qRT-PCR 58
Table 3-L: Oligonucleotides for CRISPR/Cas9 58
Table 3-M: Mycoplasma analysis 59
Table 3-N: Primary antibodies for immunostaining analysis 60
Table 3-O: Secondary antibodies for immunostaining analysis 61
Table 3-P: Intracellular dyes for MNH assay 61
Table 4-A: qPCR-cycle program 73
Table 4-B: Mycoplasma-PCR reagents and volumes 75
Table 4-C: Mycoplasma-PCR cycle program 75
Table 4-D: AmpliTag Gold PCR reaction mix 80
Table 4-E: PCR-cycle program 80
Table 4-F: Master Mix for RT-PCR 82
Table 4-G: Reaction setup for one reaction (25µl volume) 82
Table 4-H: PCR-cycle program 83
Table 4-I: Cellular targets and dyes used for HCA-based MNH assay. 86
Table 4-J: HCA-based cell properties and BioApplication for MNH assay. 86
Table 4-K: HCA-based BioApplication features for MNH assay. 87

Table 9-A: List of selected compounds from the FDA-approved drug screening library (z65122) 179

Units

°C	degrees Celsius
%	Percentage
g	gram(s)/ gravity
mg	miligram(s)
µg	mycrogram(s)
ng	nanograms(s)
h	hour(s)
min	minutes(s)
sec	second(s)
d	days
kDA	kilo Daltons
M	Mol per liter
mM	millimol per liter
µM	micromol per liter
ml	mililiter(s)
µm	microliter(s)
Hz	Hertz
kHz	Kilohertz
mm	milimeter(s)
U	Unit(s)
v/v	volume per volume
kb	kilobase

List of Abbreviations

2D	Two-dimensional
3D	Three-dimensional
5-HT	Serotonin
Acetyl-CoA	Acetyl coenzyme A
AD	Alzheimer's disease
ADH	Alcohol dehydrogenase
ADH1B*2	Alcohol dehydrogenase IB allele
ADP	Adenosine diphosphate
ALDH	Aldehyde dehydrogenase
ALDH2*2	Aldehyde dehydrogenase *2 allele*
Ant.A	Antimycin A
ATP	Adenosine triphosphate
ATPase	Adenosine triphosphatase
AUD	Alcohol use disorder
AUDIT	Alcohol Use Disorder Ident Test
BAC	Blood alcohol concentration
BBB	Blood-brain-barrier
BD	bipolar disorder
BDNF	Brain-derived neurotrophic factor
BMP	Bone morphogenetic proteins
Ca^{2+}	Calcium ions
cDNA	Complementary DNA
Ch	Channel
CHIR	CHIR99021, GSK-3ß inhibitor
CNS	Central nervous system
Complex V	ATP Synthase
conc.	Concentration
CRISPR	Clustered regularly interspaced short palindromic repeats

CYP2E1	Cytochrome P450 2E1
d	Day
DA	Dopamine
DACH1	Dachshund homolog 1
DALYs	Disability-adjusted life years
dbcAMP	N6,2′-O-Dibutyryladenosine 3′,5′-cyclic monophosphate
DM	Dorsomorphin
DMEM	Dulbecco's Modified Eagle Medium
DMSO	Dimethyl sulfoxide
dn53BP1	Tumor protein p53-binding protein 1
DNA	Deoxyribonucleic acid
DNMT3B	DNA Methyltransferase 3 Beta
dNTPs	Deoxyribonucleotide triphosphates
DPPA4	Developmental Pluripotency Associated 4
DSB	Double strand break
DSM-V	Diagnostic and Statistical Manual of Mental Disorders
EBs	Embryoid bodies
eCas9	Enhanced CRISPR associated protein 9
EDTA	Ethylenediaminetetraacetic acid
ELISA	Enzyme-linked immunosorbent assay
ER	Endoplasmic reticulum
ESCs	Embryonic stem cells
ETC	Electron transport chain
F	Female
FACS	Fluorescence-activate cell sorting
FASD	Fetal alcohol spectrum disorders
FBS	Fetal bovine serum
FCCP	Carbonylcyanide p trifluoromethoxy phenylhydrazone
FDA	Food and Drug Administration

FGF 8/21	Fibroblast growth factor 8/21
Fibs.	Fibroblasts
Fig.	Figure
FOXA2	Forkhead box a2
GABA	Gamma-Aminobutyric acid
GABAA	Gamma-aminobutyric acid receptor
GABRA2	Gamma-Aminobutyric Acid Type A Receptor Subunit Alpha2
GAPDH	Glyceraldehyde 3-phosphate dehydrogenase
GDNF	Glial cell-derived neurotrophic factor
GFAP	Glial fibrillary acidic protein
gRNA	Guide RNA
GSK3	Glycogen synthase kinase 3
GWAS	Genome wide association study
H_2O_2	Hydrogen peroxide
HCA	High-content analysis
HCS	High-content screening
HD	Huntington’s disease
HDR	Homology directed repair
hESCs	Human embryonic stem cells
HPLC	High-performance liquid chromatography
HT	High throughput
HT	High-throughout
IMM	Intermembrane matrix
iPSCs	induced pluripotent stem cells
iPSCs	Induced pluripotent stem cells
K^+	Potassium ions
KLB	ß-klotho
KLF4	Kruppel-like factor 4
KO	Knock out

KO-DMEM	Knockout Dulbecco's Modified Eagle Medium
LMX1A	LIM Homeobox Transcription Factor 1 Alpha
LMX1B	LIM Homeobox Transcription Factor 1 Beta
M	Male
MAP2	Microtubule associated protein 2
MEA	Microelectrode array
MEFs	Mouse embryonic fibroblasts
Mg2+	Magnesium ions
MMP	Mitochondrial membrane potential
MNH	Mitochondrial Neuronal Health
mPTP	Mitochondrial permeability transition pore
mRNA	Messenger RNA
mtDNA	Mitochondrial DNA
MYC	MYC proto-oncogene
N	Number
Na	Sodium
NAc	Nucleus accumbens
NAD/NAD^+/NADH	Nicotinamide adenine dinucleotide/-oxidized/-reduced
NANOG	Nanog homeobox
NEAA	Non-essential amino acids
NESTIN	Neuroectodermal stem cell marker
NHEJ	Non-homologous end joining
NMDA	*N*-methyl-d-aspartate
NPCs	Neural progenitor cells
NURR1	Nuclear receptor related 1 protein
OAZ1	Ornithine Decarboxylase Antizyme 1
OCT3/4	Octamer binding transcription factor 4
ON	Overnight

OXPHOS	Oxidative phosphorylation system
P/S	Penicillin/Streptomycin
PAM	Protospacer adjacent motif
PAX6	Paired box protein
PBMCs	Peripheral blood mononuclear cells
PBS	Phosphate-buffered saline
PCR	Polymerase chain reaction
PD	Parkinson’s disease
PEI	Polyethyleminine
PFA	Paraformaldehyde
Pi	Phosphate
PNS	Peripheral nervous system
PS	Phosphatidylserine
PSCs	Pluripotent stem cells
PTP	Permeability transition pore
PU	Purmorphamine
qRT-PCR	Real-time quantitative reverse transcription polymerase chain reaction
RC	Respiratory chain
RI	See ROCK inhibitor
RNA	Ribonucleic acid
ROCK inhibitor	rho-associated protein kinase inhibitor
ROI	Region of interest
ROS	Reactive oxygen species
RT	Room temperature
SB	SB-431542
SCN	suprachiasmatic nucleus
SCZ	Schizophrenia
SD	Standard deviation
SEM	Standard error of the mean
SHH	Sonic hedgehog
sm	Small molecule

SMA	Spinal muscle atrophy
SMN	Survival motor neuron
SNP	Single nucleotide polymorphism
SOX 2/17	SRY-related HMG-box 2/17
SOX1/2	SRY-Box Transcription Factor 1/2
TALEN	TAL effector nuclease
TGFβ	Transforming growth factor beta
TH	Tyrosine hydroxylase
TMRM	Tetramethylrhodamin-methylester
TRA-1-60	Podocalyxin
tRNA	Transfer ribonucleic acid
TUJ1	Neuron-specific Class III β-tubulin
UKB	United Kingdom biobank
UT	Untreated
VIM	Vimentin
Vit. C	Vitamin C
VTA	Ventral tegmental area
WHO	World health organization
WNT	Wingless-INT
WT	Wild type
ZFN	Zinc-finger nucleases

1. Introduction

Ethanol, also known as ethyl alcohol, belongs to the chemical group of alcohols and is obtained by fermentation of sugar. With its molecular formula C_2H_6O, ethanol is the only type of alcohol that can be consumed. Ethanol is the most frequently abused drug (Guo and Ren, 2010), with about two billion people consuming alcoholic beverages worldwide (van den Brink et al., 2018).

The consumption of alcohol and therefore also intoxication, addiction, and dependency can be dated back to the beginnings of recorded human history with beer being one of the first alcoholic beverages to be consumed (Roget, 2009; Nathan et al., 2016). Nowadays, alcohol is widely accepted in our society, and its consumption is supported by its legality, low cost, and wide availability. The consumption of alcohol at social, cultural, and business events and religious ceremonies has become an integral part of today's society. However, high ethanol concentrations consumed over time can lead to serious health problems as well as behavioral changes including a higher risk for accident-related injuries, problems in social life, domestic violence, and loss of work productivity (Rehm et al., 2009; Fernández-Serrano et al., 2010).

In this context, excessive alcohol consumption is a leading risk factor for disease, disability, and death (Griswold et al., 2018). Worldwide, harmful alcohol consumption accounts for 5.1% of disability-adjusted life years (DALYs). Of all global deaths in 2016, 5.3% were attributed to alcohol, which corresponds to over three million deaths worldwide (WHO et al., 2018). The leading contributors to the alcohol-attributable deaths in 2016 were digestive diseases with 21.3%, unintentional injuries with 20.9%, and cardiovascular diseases and diabetes with 19.0% (Fig. 1).

Introduction

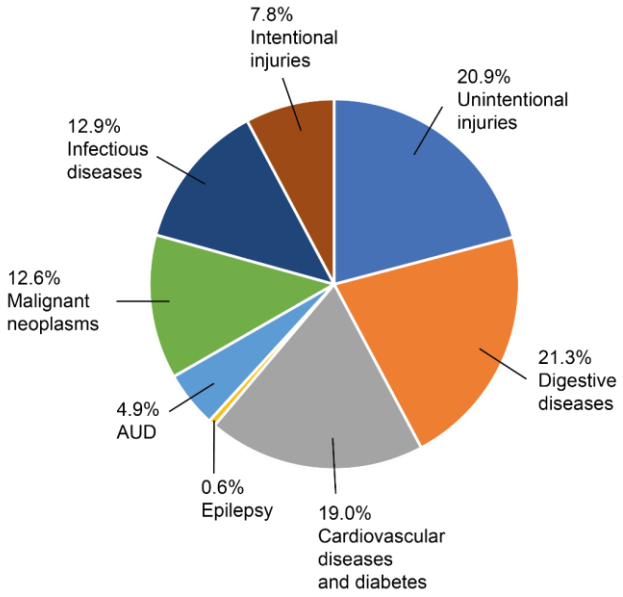

Fig. 1: Percentage (in %) of alcohol-attributable deaths, as a percentage of all alcohol attributable deaths, by broad disease category (status of 2016).
(A) Digestive diseases, unintentional injuries, cardiovascular diseases, and diabetes were the leading contributors to the alcohol-attributable deaths in 2016. Unintentional injuries include road injury, poisonings, falls, fire, heat and hot substances, drowning, and exposure to mechanical forces. Intentional injuries include self-harm and interpersonal violence. AUD: alcohol use disorder. Image adapted from (WHO et al., 2018).

In addition, loss of control over alcohol consumption can lead to more severe diseases which are directly caused by ethanol, meaning that they would not occur in the absence of ethanol, including alcoholic liver diseases and alcohol-induced pancreatitis (Fernandes et al., 2017). Harmful alcohol use accounts for more than 200 diseases and injury conditions in individuals, most notably alcohol dependence, alcohol use disorder (AUD), liver cirrhosis, hypertension, cancers, cardiovascular diseases and injuries with Europe having the highest alcohol-attributable deaths (10.1%) and DALYs (10.8%) in the world (WHO et al., 2018). The degree of alcohol-induced harm is largely determined by the amount consumed, and AUD patients with a very high drinking risk (>60g of ethanol per

day) have a life expectancy that is reduced by 22 years compared with the general population (Rehm et al., 2009).

Reducing ethanol-induced harm should be considered a major public health priority. Nevertheless, identifying new treatment strategies is a major challenge partly due to the multisystemic effects of alcohol and the lack of knowledge which actions underlie the initiation, progression, and maintenance of alcohol addiction as well as a lack of effective human model systems.

1.1 Behavioral effects of ethanol

Ethanol affects the body in a wide range starting from low ethanol concentrations to around 100 mM in alcohol-naïve and occasional consumers of alcohol (Abrahao et al., 2017). However, over time the body can develop a tolerance to the acute effects of ethanol, therefore making it possible for humans with a high tolerance to survive even eight times higher concentrations than alcohol-naïve persons (Abrahao et al., 2017).

The determination of ethanol intoxication is based on the measurement of blood alcohol concentration (BAC), which is defined by the rate of how ethanol is absorbed, distributed, metabolized and excreted (Zakhari, 2006). BACs of 1–20 mM are considered as low concentrations even though they can lead to effects ranging from undetectable effects to a certain degree of sedation and motor incoordination in different individuals. These effects most likely depend on the regularity of alcohol intake as well as physiological properties such as body weight, amount of food in the stomach and overall proportion between liquid and fat.

Introduction

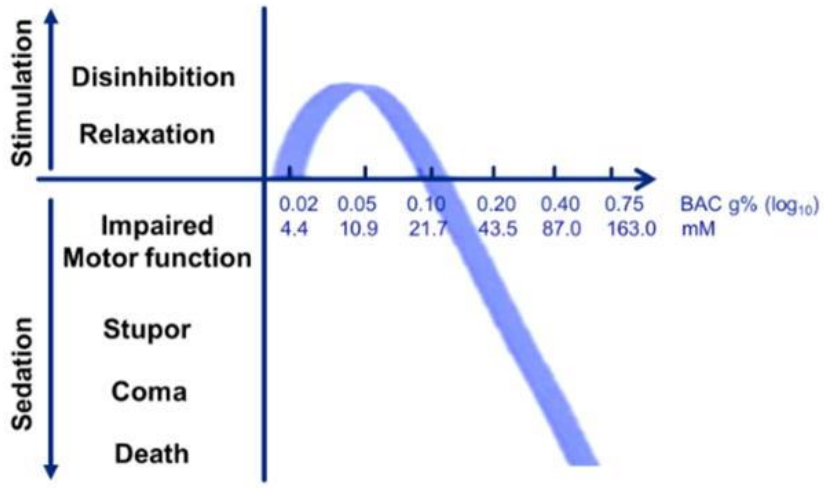

Fig. 2: Effects of ethanol in humans related to its concentration in mM or blood alcohol concentration (BAC).
Below 10 mM ethanol causes disinhibition and relaxation. At higher concentrations ethanol impairs motor function (22-44 mM), and causes stupor (44–65 mM), coma (65–87 mM), and even death (87 mM–and above). Figure from (Cui and Koob, 2017)*.

Blood alcohol concentrations of 10–20 mM typically produce a certain degree of sedation, motor incoordination and cognitive impairment. Starting from 50 mM, ethanol leads to locomotor disruption, cognitive impairment, and sedation. At even higher concentrations, ethanol causes strong sedation with respiratory depression, which can lead to coma and death. Concentrations in the range of 50–100 mM and above are lethal for alcohol-naïve and occasional drinkers but can be tolerated by chronic alcohol consumers (Fig. 2). Tolerance to ethanol is defined as a reduced response to constant amounts of ethanol and/or an increase of the amount of ethanol needed to develop certain effects (Manzo-Avalos and Saavedra-Molina, 2010). In this context, blood alcohol levels of 300 mM have been reported in conscious individuals (Johnson et al., 1982).

*Reprinted from Publication: Cui, Changhai, and George F Koob. Titrating Tipsy Targets: The Neurobiology of Low-Dose Alcohol. *Trends in pharmacological sciences* vol. 38,6 (2017), with permission from Elsevier.

In the case of chronic alcohol consumption, concentrations around 100–200 mM can lead to sedation, anxiolysis and hypnosis, an effect which is often sought by heavy drinkers (Abrahao et al., 2017; Cui and Koob, 2017). Overall, the relation of BACs to intoxication is very complex as tolerance to low and medium doses of ethanol can be obtained.

1.2 Metabolism of ethanol

Ethanol is a small polar molecule with a molar mass of 46 kDa. After oral administration, ethanol is rapidly absorbed by diffusion in the stomach (20%) and absorption through the duodenum and small intestine (80%) (Manzo-Avalos and Saavedra-Molina, 2010; Fernandes et al., 2017). Ethanol is amphipathic, meaning that it has lipophilic and hydrophilic characteristics. Due to its lipophilic characteristic, ethanol can cross biological membranes by passive diffusion. The presence of the hydroxyl group makes ethanol hydrophilic. The attraction between water and ethanol molecules is strong enough to solubilize ethanol, but not strong enough to irrevocably bind to each other (Ferreira and Willoughby, 2008). Consequently, ethanol distributes from blood into all tissues and fluids depending on their relative water content. For example, fat and bone tissue have a relatively low water content, which means that penetration by ethanol is comparatively low (Ferreira and Willoughby, 2008). Moreover, equilibration of ethanol depends on overall mass and blood flow rate (Ramchandani et al., 2001). Hence, the same dose of ethanol per unit body weight can result in completely different blood alcohol concentrations among individuals. Due to their higher body fat percentage, women tend to have lesser volume distribution for ethanol compared to men (Cederbaum, 2012).

In general, most of the ethanol is eliminated through metabolism while a small part (~1–5%) is excreted directly through breath, sweat and urine. Ethanol is mainly metabolized

in the liver via oxidative and non-oxidative pathways through alcohol dehydrogenase (ADH), aldehyde dehydrogenase (ALDH), Cytochrome P450 2E1 (CYP2E1) and catalase enzymes (Manzo-Avalos and Saavedra-Molina, 2010) (Fig. 3).

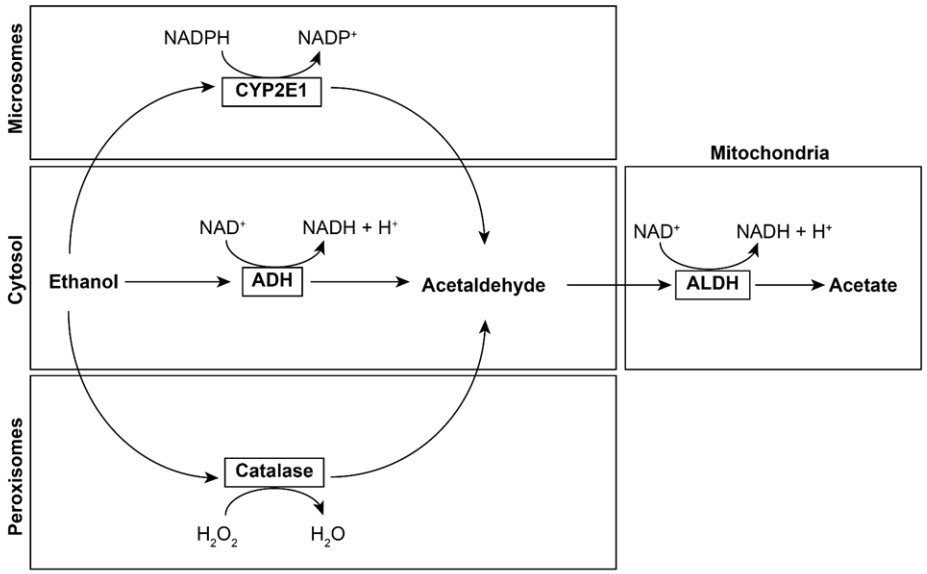

Fig. 3: Ethanol metabolism.
(A**)** Main pathway of ethanol oxidative metabolism. Ethanol is converted into acetaldehyde by ADH, CYP2E1 and Catalase and further oxidized into acetate in the mitochondria by ALDH. Figure adapted from (Manzo-Avalos and Saavedra-Molina, 2010).

In fact, oxidation through ADH accounts for about 90% of ethanol metabolism (Fernandes et al., 2017). Accordingly, ethanol is oxidized to acetaldehyde by class I ADH in the hepatocytes in a reversible manner. The enzyme has a high affinity but therefore also becomes saturated rather fast. Acetaldehyde is highly toxic and is quickly oxidized by the mitochondrial isoform of ALDH into acetate in a non-reversible reaction. Most of the acetate leaves the liver and enters the blood stream, where it is further metabolized to CO_2 in the heart, skeletal muscle, or brain. During ethanol metabolism through ADH and

ALDH, NAD^+ serves as cofactor and is reduced to NADH resulting in an increased ratio of NADH/NAD^+ (Cederbaum, 2012).

NADH/NAD^+ redox couples are essential for maintaining cellular redox homeostasis and for modulating numerous biological events including cellular metabolism. Hence, imbalance of this equilibrium perturbs cellular metabolism (Xiao et al., 2018).

Ethanol is considered a nutrient with a caloric value of 7 kcal/gram (Cederbaum, 2012). In general, the metabolization in the mitochondria of acetyl coenzyme A (acetyl-CoA), the active form of acetate, results in the same nutrients produced through oxidation of carbohydrates, fats, and proteins including ketone bodies, amino acids, fatty acids, and steroids (Agarwal, 2001; Manzo-Avalos and Saavedra-Molina, 2010). Nevertheless, ethanol metabolism does not consist of any minerals, vitamins, carbohydrates, fats, or proteins associated with it, and ethanol-derived calories are produced at the expense of the normal metabolism and displace those essential nutrients (Cederbaum, 2012; Onyekwelu, 2019). Especially under chronic alcohol consumption, this is believed to promote reduced nutrient supply and malnutrition (Lieber, 2000). Moreover, secondary malnutrition can be observed due to alcohol-induced gastrointestinal complications and impaired hepatic metabolism (Lieber, 1995). During chronic alcohol consumption, the generation of acetaldehyde is increased most likely due to metabolic adaptation, resulting in an increased amount of circulating acetaldehyde (Cederbaum, 2012).

In addition to ethanol oxidation through ADH, ethanol is metabolized by CYP2E1, which is predominantly present in the microsomes or vesicles of the endoplasmic reticulum. CYP2E1 activity accounts for only about 10% of ethanol metabolism and is considered a secondary route for ethanol oxidation. However, when ethanol concentrations are

elevated during chronic ethanol consumption, CYP2E1 metabolism is believed to play an important role (Zakhari, 2006).

The third route of ethanol metabolism is through the catalase pathway in the cell peroxisomes. This route accounts for no more than 2% of the hepatic metabolism. Its main activity is the conversion of hydrogen peroxide (H_2O_2) to O_2 and water. However, it is also capable of oxidizing ethanol in the presence of H_2O_2 to produce acetaldehyde (Handler and Thurman, 1988). There is evidence that the brain can metabolize ethanol through the enzyme catalase (Quertemont, 2004). However, the role of ADH and CYP2E1 in the brain is assumed to be minor (Wilson and Matschinsky, 2020).

1.3 Effects of ethanol consumption on different organs

Various mechanisms have been postulated to cause the multiple toxic effects of ethanol observed in several organs. Once ingested, ethanol enters the bloodstream and quickly distributes throughout the whole body, where it can cause damage to various organs including liver, brain, stomach, and heart. Reported mechanisms of ethanol-related organ injury include direct toxicity of ethanol and its primary metabolite acetaldehyde, increase in oxidative stress, impairment in methylation patterns, abnormal posttranslational modifications, dysregulation of lipid metabolism and signaling pathways (Osna and Kharbanda, 2016). Consequently, ethanol affects cell survival and function directly and indirectly through its metabolites. Among the mechanisms causing ethanol-induced tissue damage, ethanol metabolism is considered a predominant factor, particularly through the generation of reactive oxygen species (ROS) and oxidative stress (Zakhari, 2006). The effect of ethanol on various tissues will be discussed in this chapter with a focus on the brain and central nervous system (CNS).

1.3.1 Effects of ethanol on stomach, liver, and heart

It has often been reported that low to moderate alcohol consumption may be associated with better cardiovascular health compared to non-alcohol drinkers or heavy alcohol drinkers. Studies demonstrated that low to moderate alcohol consumption may reduce the risk of heart attacks (Klatsky, 1999; Hines and Rimm, 2001) and minimize the risk of for hypertension (Thadhani et al., 2002), diabetes (Koppes et al., 2005; Baliunas et al., 2009), stress, and depression (Lipton, 1994; Gémes et al., 2019). The presumable beneficial effects of low to moderate alcohol consumption are controversially discussed, partly because there is no universally accepted definition of when alcohol consumption can be determined as moderate drinking.

As noted earlier, contrary to the postulated positive effects of low to moderate alcohol consumption, long-term alcohol abuse, including chronic use, has been found to increase the risk of several diseases (Rehm, 2011). Alcohol abuse increases the risk of heart disease (Ikehara et al., 2008; George and Figueredo, 2010), liver disease (Cederbaum et al., 2009; Osna et al., 2017), and depression (Ramsey et al., 2005). Consequently, binge drinking, a drinking pattern described as consumption of at least five drinks for males and at least four drinks for females on the same occasion (in a period of 2 hours) over the past month (SAMHSA, 2013), as well as chronic alcohol consumption may cause damage to human organs, including brain, liver, heart, lung, skeletal muscle, and bones.. Excessive alcohol consumption can result in cardiovascular diseases as well as enhanced risk of stroke and hypertension, consequently increasing the risk of heart failure (Piano, 2017). Besides causing functional impairment to the liver, gastrointestinal tract, and pancreas, excessive alcohol consumption also directly affects the metabolism of proteins, carbohydrates, and lipids. Moreover, it leads to insufficient immune system responses to

infections, impairs the ability of the host to counteract hemorrhagic shock, and delays wound healing (Manzo-Avalos and Saavedra-Molina, 2010).

1.3.2 Effects of ethanol on the nervous system

The human nervous system consists of the CNS with the brain and spinal cord, and the peripheral nervous system (PNS) which connects the CNS to the rest of the body. The nervous system detects sensory information from the environment as well as from the peripheral tissues, processes the information, and coordinates the responses to the initial stimuli. Therefore, any neurologic dysfunction affects not only the brain itself but can have a major impact on other systems. Damage to the nervous system can for example disturb communication, impair motor function, and cause loss of memory. Massive damage can even result in coma or paralysis. Due to the post-mitotic nature of nerve cells, most injuries to the brain are irreversible. However, the loss of a neuron must not necessarily result in a reduction or loss of function due to neural reserves, the capacity to tolerate lesions, and the ability of adjacent neurons to compensate by re-establishing synaptic contacts and incorporate alternate brain networks (Stern, 2012; Jackson et al., 2019). Though protected by the blood-brain-barrier (BBB), the brain is vulnerable to toxic agents. Simplified, the BBB is a highly specialized structure formed by a tight monolayer of brain endothelial cells, which regulate the movement of ions, molecules, and cells between the blood and the brain. This barrier allows for proper neuronal function and protects the neural tissue from toxins and pathogens (Daneman and Prat, 2015). Neurotoxicity is defined as “any adverse effect on the chemistry, structure or function of the nervous system, during development or at maturity” (Costa, 1998) induced by biological, physical or chemical agents, including natural or artificial toxins.

Ethanol can pass the BBB due to its chemical characteristic of being lipophilic and therefore capable of easily mixing with the fat in the membrane. In this context, ethanol is believed to disturb BBB integrity, which consequently increases the possibility of toxic agents entering the brain. This may represent a critical event in the development and progression of neurological disorders and neurodegeneration (Pratt et al., 1990; Thomsen et al., 1994; Haorah et al., 2008).

Heavy alcohol consumption has long been linked to brain damage and neurobehavioral changes. The risk for brain damage is increased in chronic alcohol abusers due to secondary causes such as poor nutrition, liver disease, and head trauma. Post-mortem studies on the human brain as well as imaging-based analysis and neuropsychological testing suggest that chronic alcohol consumption changes brain structure. The frontal lobes, limbic system, and cerebellum appear particularly vulnerable to AUD-associated brain damage and dysfunction (Oscar-Berman and Marinković, 2007).

Generally, within a year of abstinence, some improvement in brain function and structure can be recorded. However, brain dysfunction may persist even after the individual has become abstinent from alcohol. Additional factors increase the likelihood of developing cognitive, sensory, or motor impairments due to alcohol abuse (Bates et al., 2002; Oscar-Berman, 2003).

The effects of ethanol on the brain are variable and presumably related to a wide range of factors such as gender, genetics, and environment as well as the age at which the individual started drinking, and the duration. The susceptibility to develop alcohol dependence also depends on gender, age, and environment. Individuals with psychiatric disorders including depression, anxiety, post-traumatic stress disorder, psychosis and

drug abuse have a higher risk of developing alcohol dependence (Oscar-Berman and Marinković, 2007).

In the CNS, some of the main effects of ethanol are at least partially due to neuroinflammation, oxidative stress, and excitotoxicity, and can contribute to memory gaps, motor impairment, and inhibition of neurogenesis (Fernandes et al., 2017). Besides indirect tissue damage as described above, ethanol also acts directly on membrane components, ion channels, enzymes, and receptors. In fact, ethanol can alter the synthesis, release, and signaling of several neurotransmitters, including dopamine, *N*-methyl-d-aspartate (NMDA), serotonin (5-HT), and gamma-aminobutyric acid (GABA) (Charlet et al., 2011; Lovinger and Roberto, 2013; Abrahao et al., 2017). Ethanol enhances GABAergic inhibitory activity (Vengeliene et al., 2008) and inhibits NMDA function in a concentration-dependent manner. This ethanol-induced NMDA inhibition may contribute to the neural and cognitive impairments associated with intoxication (Vengeliene et al., 2008). Acute ethanol consumption can increase extracellular 5-HT levels, whereas chronic exposure causes an overall decrease in 5-HT neurotransmission (Sari et al., 2011). Moreover, acute ethanol exposure affects dopaminergic (DA) neurons, resulting in higher firing frequency and increased excitability (Trantham-Davidson and Chandler, 2015), as well as decreased dopamine synthesis and dopamine D2 receptor availability in AUD patients (Morikawa and Morrisett, 2010). In the state of withdrawal from chronic alcohol consumption, DA neurotransmission has been reported to be decreased (Morikawa and Morrisett, 2010). Ethanol's indirect effects on several neurotransmitters may lead to behavioral effects ranging from disinhibition to sedation and hypnosis (Spanagel, 2009). Additionally, the neurotransmitters dopamine and

serotonin are believed to play a role in the initiation of ethanol reinforcement (Charlet et al., 2011). A summary of the effects of ethanol in the CNS is depicted in Fig. 4.

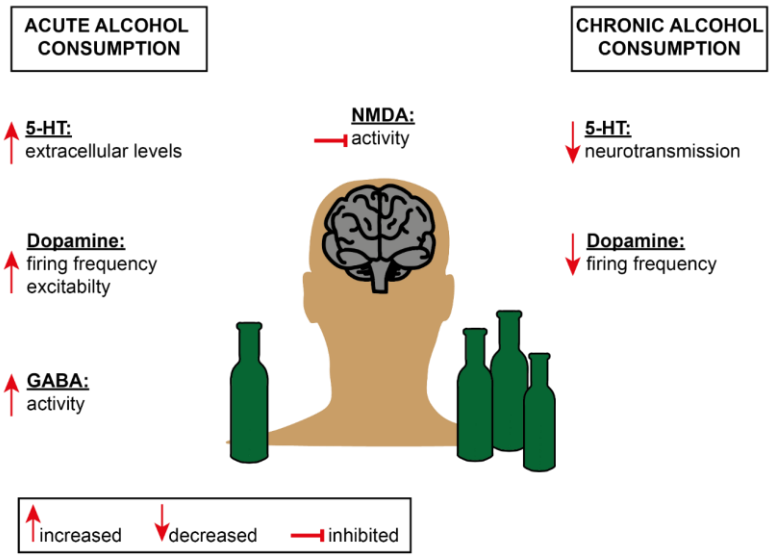

Fig. 4: Effects of acute and chronic alcohol consumption on neurotransmitters in the brain. Schematic overview of the effects of acute and chronic alcohol consumption on neurotransmitters in the brain. Following acute alcohol consumption, increased activity has been observed for 5-HT (serotonin), dopamine and gamma-aminobutyric acid (GABA). Moreover, ethanol inhibits *N*-methyl-d-aspartate (NMDA) receptor function in a dose-dependent manner. Chronic alcohol consumption leads to decreased 5-HT neurotransmission and dopaminergic neuron firing frequency.

Chronic and acute alcohol consumption are known modulators of neuroinflammation (Fernandes et al., 2017). It has been demonstrated that ethanol stimulation in both female and male mice triggered inflammatory mediators, cytokines, gliosis, and neuronal loss in the cerebral cortex (Squeglia et al., 2011; Alfonso-Loeches et al., 2013).

Since 1990, microglia have been suggested to play an important role in ethanol-induced brain damage. Recent studies showed that glial cells are even more sensitive to ethanol-induced degeneration than neurons in the brain (Santos et al., 2013). Increased levels of microglial markers have been observed in post-mortem brains of human alcoholics and

ethanol-treated rodents (Yang and Luo, 2015). A study performed in rats indicates that microglia may be involved in neurodegeneration and cognitive dysfunction during intermitted ethanol exposure (Zhao et al., 2013).

Although ethanol-induced neurotoxicity in the brain can result from various mechanisms, oxidative stress probably plays a key role (Haorah et al., 2008; Harper, 2009). Increased oxidative stress can be observed after chronic ethanol consumption, most likely through ethanol metabolism in mitochondria.

1.4 Background on mitochondria

As mentioned before, mitochondria play an important role in ethanol-metabolism via the enzyme ALDH. The following chapter will focus on the role of mitochondria in cellular function and particularly during ethanol exposure.

Mitochondria are highly specialized organelles found in multiple copies in all nucleated eukaryotic cells in various shapes and numbers depending on the specific tissue type and its energy requirement (Krauss, 2001). Structurally, they contain an outer membrane, inner membrane, intermembrane space, and the matrix. The inner membrane creates a cristae structure by enclosure into the mitochondrial matrix to increase the surface (Dyall et al., 2004). According to the energetic state requirements of the corresponding tissue, the cristae remodel by fusion, fission, mitophagy, and motility. Mitochondria contain their own genome which is maternally inherited. Mitochondrial DNA (mtDNA) is present in multiple copies within the cell and encodes for 13 proteins of the oxidative phosphorylation (OXPHOS) system, as well as for 22 tRNA and 2 ribosomal RNA of the RNA machinery. The remaining mitochondrial proteins are nuclear-encoded and imported into the organelle (Chinnery and Hudson, 2013).

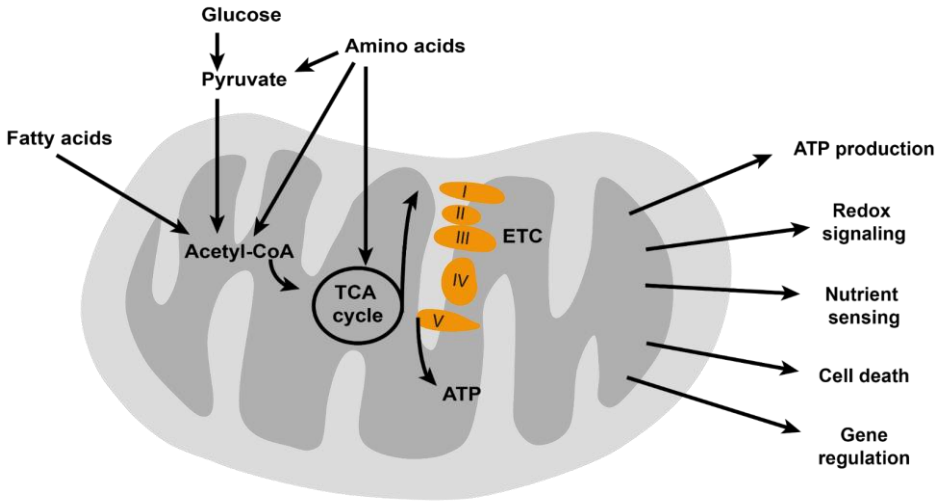

Fig. 5: Mitochondrial function.
During mitochondrial bioenergetics, amino acids, glucose, and fatty acids are converted to acetyl-CoA, which is oxidized to produce ATP. Besides ATP production, mitochondria play essential roles in cell signaling including nutrient sensing, redox signaling, cell death, and gene regulation. ETC: electron transport chain; TCA: tricarboxylic acid. Figure adapted from (Zhang et al., 2018). Original figure licensed under a Creative Commons License.

Mitochondria play a role in the metabolism of fatty acids, amino acids, and steroids, as well as in numerous signaling pathways such as apoptosis, calcium homeostasis, and in the generation of ROS (Fig. 5). The main function of mitochondria is to produce energy in the form of adenosine triphosphate (ATP) through the process of OXPHOS. The core machinery of OXPHOS is the respiratory chain (RC), consisting of the electron transport chain (ETC) complexes I-IV and the ATP-synthase (complex V) located in the inner mitochondrial membrane. The complexes I-IV transport electrons along the ETC thereby releasing protons (hydrogen) out of the mitochondrial matrix into the intermembrane space, leading to a proton gradient across the inner mitochondrial membrane space, also known as mitochondrial membrane potential (MMP). The electrochemical proton gradient is then used by complex V to produce ATP, the main cellular energy resource, by pumping protons into the mitochondrial matrix and driving the reaction between

adenosine diphosphate (ADP) and phosphate (Pi) (Vafai and Mootha, 2012). Besides the generation of ATP, the MMP has also been described to be responsible for mitochondrial calcium (Ca^{2+}) uptake, metabolite and protein transport, production of reactive oxygen species, and the MMP is a key driver in the process of apoptosis (Wong and Cortopassi, 2002).

Mitochondria are highly complex and dynamic organelles that change their shape by opposing and balancing events of fusion and fission (Chan, 2006; Archer, 2013). The dynamic mitochondrial network contributes to the maintenance of cellular homeostasis by enabling the mitochondria to distribute Ca^{2+} and ATP to the destination of need (Bliek et al., 2013). Fusion and fission events rely on a critical balance to sustain proper function. However, fission alone is associated with metabolic stress as well as cellular damage and apoptosis (Reddy, 2014). Fusion instead plays a role in cellular repair mechanisms and cell survival (Ni et al., 2015). Accordingly, imbalance in fusion and fission processes are linked to disturbed mitochondrial dynamics in many neurological diseases (Burté et al., 2015; Mishra, 2016).

1.4.1 Mitochondrial bioenergetics and brain function

The human brain consumes about 25% of the daily intake of glucose (Clarke and Sokoloff, 1999). Given its high energy demand, mitochondria are particularly relevant for the function of the CNS. The brain consumes about 20% of the oxygen inspired at rest (Erecińska and Silver, 2001). Hence, neuronal cells need to be capable of balancing ROS production with antioxidant defense. Any imbalance of this equilibrium is believed to contribute to excessive oxidative stress and neurodegeneration (Lin and Beal, 2006).

Neurons require cytoplasmic calcium for the regulation of neurotransmitters and therefore rely on proper calcium homeostasis (Neher and Sakaba, 2008). In addition to the plasma membrane and the endoplasmic reticulum (ER), mitochondria play a critical role in the cellular homeostasis of calcium. Due to their ability to move independently, mitochondria can travel to areas of high calcium overload and lower the calcium concentration (Wang and Schwarz, 2009; Williams et al., 2013). Chronic alcohol consumption has been shown to alter calcium regulation by increasing its cytoplasmic levels. The increase in cytoplasmic calcium in turn can induce further mitochondrial damage through ROS formation, and can destabilize the ETC (Ji, 2011; Tapia-Rojas et al., 2017). Moreover, calcium overload within the mitochondria can trigger cell death through the opening of the mitochondrial permeability transition pore (mPTP) in the mitochondrial membrane (Giorgi et al., 2012). Increase in mitochondrial permeability is associated with mitochondrial impairment in the brain (Marzo et al., 1998; Pérez and Quintanilla, 2017), and can be induced by mitochondrial calcium overload, oxidative stress, and changes in the pH (Tsujimoto and Shimizu, 2007).

1.4.2 Effects of ethanol on mitochondrial bioenergetics

Various *in vitro* and *in vivo* studies (Manzo-Avalos and Saavedra-Molina, 2010) observed that ethanol increases ROS production (Reddy et al., 2013), alters mitochondrial respiration (Haorah et al., 2013; Reddy et al., 2013), impairs ATP production (Bustamante et al., 2012; Jung, 2015), and ultimately induces cell death by opening of the mPTP (Lamarche et al., 2013).

As mentioned in chapter 1.2, mitochondria play a role not only in ethanol metabolism, but their dysfunction may also be crucial in driving the ethanol-induced impairment of several organs, including liver and heart (Manzo-Avalos and Saavedra-Molina, 2010). Bonet-Ponce and colleagues demonstrated that ethanol causes an increase in mitochondrial fission in human retinal pigment epithelial cells in a dose-dependent manner through mitochondrial translocation and proteolytic cleavage (Bonet-Ponce et al., 2015). Ethanol is known to dramatically increase oxidative stress which has been shown in various *in vitro* and *in vivo* studies (Ramachandran et al., 2003; Lee et al., 2005; Ozkol et al., 2017). During the metabolism of ethanol by ADH, ALDH and CYP2E1 (details are described in chapter 1.2), acetaldehyde is formed, which is known to contribute to neuronal damage in the brain possibly by its ability to increase ROS formation (Yan et al., 2015; Auta et al., 2017). This was confirmed by experiments in rats showing that chronic ethanol exposure promotes the production of ROS and reactive nitrogen species (Reddy et al., 2013; Casañas-Sánchez et al., 2016). Ramachandran and colleagues treated cultured fetal cortical neurons with the antioxidant glutathione that prevented ROS production and ultimately inhibited ethanol-induced apoptosis. They concluded that an imbalance between the oxidant response and antioxidant pathways may contribute to ethanol-induced oxidative damage (Ramachandran et al., 2003).

Extensive opening of the mPTP may lead to mitochondrial swelling as a result of the influx of ions and water, thereby inducing cytochrome c release, followed by caspase activation and DNA fragmentation, which are two known events causing programmed cell death or apoptosis (Kim et al., 2003, 2005). Lamarche and colleagues demonstrated that neuronal cultures presented permanent mPTP opening and neuronal cell death after exposure to ethanol (Lamarche et al., 2013). Additionally, further studies demonstrated

that changes in expression of mitochondrial complexes I and IV were leading to bioenergetic deficits as indicated by low ATP concentrations (Das and Vasudevan, 2007; Haorah et al., 2013; Reddy et al., 2013; Yan et al., 2015; Casañas-Sánchez et al., 2016). Decreased activity in the mitochondrial complexes I, III, IV and Na^+/K^+-ATP-ase in alcohol-administered rats has been reported, suggesting that ethanol alters the mitochondrial membrane properties and leads to mitochondrial dysfunction via mitochondrial ROS and reactive nitrogen species (Reddy et al., 2013).

Additionally, various studies observed a loss of MMP in different patterns of alcohol consumption, including heavy episodic drinking, binge-drinking, AUD, alcohol withdrawal, and hangover (Das and Vasudevan, 2007; Reddy et al., 2013; Bonet-Ponce et al., 2015; Jung, 2015; Karadayian et al., 2015).

A study using human retinal cells demonstrated that low ethanol concentrations (80 mM) for 24 hours led to an increase in MMP, whereas at high doses (400 mM) MMP collapsed (Bonet-Ponce et al., 2015). Additionally, a study investigated the influence of ethanol on intracellular events in cultured postnatal day 8 neonatal rat cerebellar granule cells (Heaton et al., 2011). They observed MMP dysfunction following ethanol exposure, which was blunted by co-treatment with the antioxidant vitamin E or the neurotrophin brain-derived neurotrophic factor (BDNF). Moreover, MMP and permeability were decreased in the state of ethanol hangover in cerebellar mitochondria of mice (Karadayian et al., 2015).

Altogether, chronic alcohol intake has detrimental effects on the mitochondria including changes in structure and function, increased ROS production, altered expression of the ETC complexes I and V, and altered ATP synthesis. Moreover, MMP can be seen as an essential parameter for viable cells and its normal function is influenced by the efficiency

of mitochondrial bioenergetics (Chen, 1988). Sustained changes in the MMP may serve as an early marker for reduced cell function and an indirect target for treatment strategies to circumvent neuronal cell loss and brain damage. Alterations of mitochondrial health during acute and chronic alcohol consumption is depicted in Fig. 6.

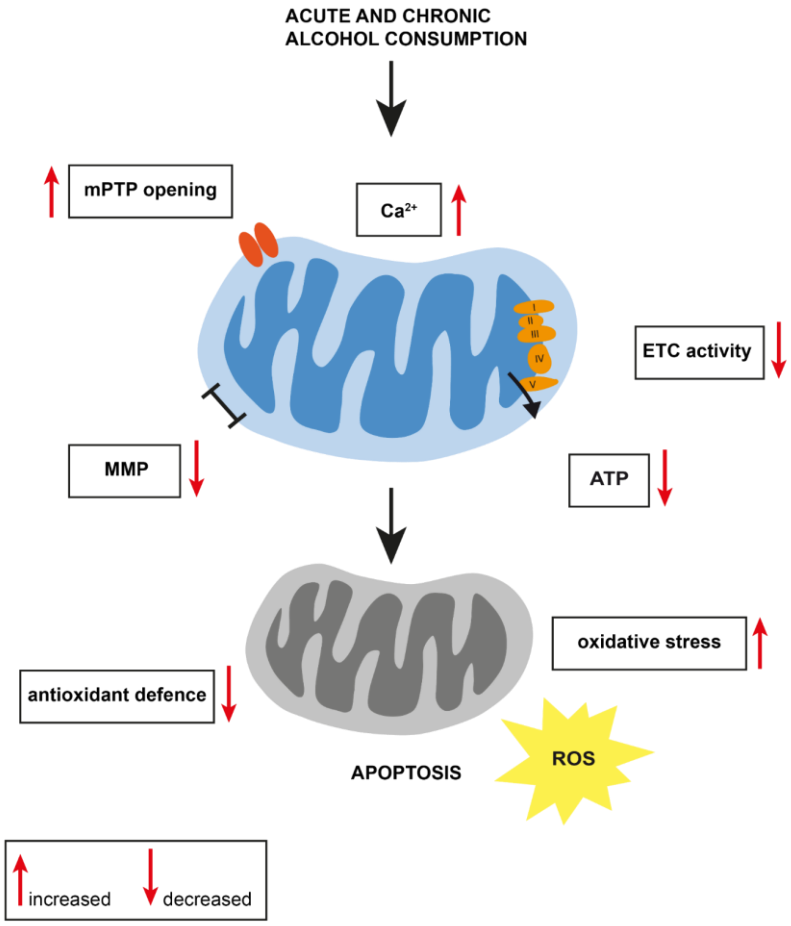

Fig. 6: Alterations of mitochondrial health during alcohol consumption.
A representative scheme summarizing the alterations of ethanol on mitochondrial health causing increased ROS production and reduced antioxidant defense. Alcohol consumption is associated with decreased ATP production and opening of the mPTP. Moreover, decreased activity of the electron transporter chain, loss of the MMP, and high extracellular Ca^{+2} concentrations are observed. Chronic ethanol exposure causes prolonged opening of the mPTP that eventually triggers apoptosis. Figure adapted from (Tapia-Rojas et al., 2017). The original figure is licensed under a Creative Commons License.

1.5 Alcohol dependence and alcohol use disorder (AUD)

It is known that the pathogenesis of alcohol addiction results from a complex interplay of genetic, psychological, and environmental factors, where CNS neurotransmitters may play an important role (Goldman et al., 2005; Hiroi and Agatsuma, 2005; Volkow and Li, 2005). In this chapter, the question why some individuals develop AUD and others do not will be addressed, including recent genome-wide association studies (GWAS) and studies focusing on the role of neurotransmitters in alcohol dependence. Several studies aimed to identify the specific genes that can influence a person's likelihood of developing AUD (Lieberman et al., 2015, 2018; Verhulst et al., 2015; De Filippis et al., 2016). Nevertheless, the risk factors for the development of AUD are quite complex, and it is highly likely that an individual with AUD carries several single nucleotide polymorphisms (SNPs) in several genes, or even in non-coding regions. Even though each individual variant may only exert a small effect on AUD risk, the additive sum of these variants together may yield a significant impact (Mayfield et al., 2008) .

1.5.1 Alcohol use disorder (AUD)

AUD is described as a chronic relapsing brain disorder diagnosed based on the Diagnostic and Statistical Manual of Mental Disorders (DSM-V) (American Psychiatric Association, 2013) and the ICD-10 Classification of Mental and Behavioral Disorders (WHO, 1992). AUD comprises alcohol abuse and alcohol dependence causing behavioral, cognitive, and physiological phenomena that develop after repeated alcohol use. Those phenomena include a strong desire to consume alcohol (craving) despite the

existence of harmful consequences. Individuals have difficulties controlling alcohol intake and prioritize alcohol over other activities (American Psychiatric Association, 2013; Kim et al., 2018). Moreover, withdrawal symptoms occur when a person suddenly stops or drastically reduces drinking after prolonged and heavy alcohol consumption. Symptoms vary in their severity and can range from headache, nausea, sweating, and vomiting to more serious health problems including hallucination, seizures, and a state of delirium tremens. This so-called alcohol withdrawal syndrome is caused by a readjustment of several neurotransmitter circuits, particularly those involving GABA and NMDA receptors, and leads to a hyperexcitability of the central nervous system (Sychla et al., 2017).

AUD is among the most prevalent mental disorders in industrialized countries. Throughout the world AUD belongs to the top five risk factors for disease, disability, and death (Kessler et al., 2005). AUD and chronic exposure to ethanol have a major impact on general society, including failed relationships, higher rate of unemployment, as well as increased risk for psychiatric symptoms and health problems. Chronic alcohol consumption is a major health care burden with an economic burden for AUD treatment of $250 billion nationally, and deploys notable resources for psychiatric care, organ transplants and overall long-term medical treatment (Sacks et al., 2015). The risk of developing AUD is higher in individuals with parents suffering from AUD, with a heritability of approximately 40–60% (Verhulst et al., 2015; Scarnati et al., 2019). Moreover, children adopted into households with alcohol abuse have the same increased risk of developing AUD as do children of chronic alcohol consumers (Scarnati et al., 2019). This suggests that genetic and environmental factors together influence the occurrence and severity of alcohol dependence.

1.5.2 Genetic predisposition to alcohol abuse

The most prominent SNPs associated with alcohol abuse can be linked to liver enzymes such as ADH and ALDH where the variant gene alleles *ADH1B*2* and *ALDH2*2* have been consistently documented to reduce the risk of developing alcohol dependence across ethnic groups (Tawa et al., 2016).

A genome-wide association study (GWAS) using a UK Biobank (UKB; N=121,604) of self-reported alcohol consumption of 112,117 individuals identified significant genome-wide associations at 14 loci. Among those loci, SNPs in the ethanol metabolizing genes *ADH*, and two loci in ß-klotho (*KLB)* were found (Clarke et al., 2017). Interestingly, a SNP in *KLB* has already been associated with alcohol consumption in humans and the gene product, β-klotho, was found to regulate alcohol preference in mice (Schumann et al., 2016).

A more recent GWAS study using the same UK Biobank and 23andMe (N=20,328) obtained quantitative measures using the Alcohol Use Disorder Identification Test (AUDIT). They identified 10 associated risk loci and were able to replicate previously identified genes including *KLB* (Sanchez-Roige et al., 2019).

Moreover, a variation in the $GABA_A$ subunit gene *GABRA2* has been associated with alcohol dependence in a reproducible manner and has been further studied by Lieberman and colleagues in human neural cells derived from induced pluripotent stem cells from social drinkers and heavy drinkers (Lieberman et al., 2015).

Besides GABA, a wide range of neurotransmitter were identified of being related to alcohol dependence including dopamine, serotonin, and glutamate (Banerjee, 2014). Preclinical and clinical data suggest that ethanol activates the mesolimbic dopamine system (Jayaram-Lindström et al., 2016), which is known as the reward system

modulating physiological functions related to survival including the intake of food and water, and sexual behavior. It is believed that ethanol induces its rewarding properties through its ability to excite dopaminergic neurons in the ventral tegmental area (VTA), resulting in an increased dopamine release in the nucleus accumbens (NAc). Moreover, this increase is involved in the affirmative and reinforcing effects of ethanol and other drugs of abuse (Wise and Rompre, 1989; Tapert et al., 2004; Heinz et al., 2009). So far, the exact mechanisms through which ethanol modulates the mesolimbic dopamine system are still not completely understood (Gonzales et al., 2004), and it is not entirely known if ethanol affects dopaminergic neurons directly, or acts indirectly through its effect on GABAergic or other interneurons, which in turn influence the activity of dopaminergic neurons (Charlet et al., 2011). Neuronal communication is affected by ethanol, since it alters the synthesis, release and signaling of neurotransmitters, including GABA, glutamate and dopamine (Fernandez et al., 2017). Alterations in dopamine signaling, induced by chronic alcohol consumption have been shown to produce alterations in the prefrontal cortex in human alcoholics. Interestingly, alcohol dependence is characterized by a disruption in the reward-related brain areas including fewer dopamine D2 receptors in the ventral striatum (Diana, 2011; Koob, 2013; Jayaram-Lindström et al., 2016). Those changes have a major impact on the quality of life and may increase the probability of relapse (Trantham-Davidson and Chandler, 2015).

1.6 State of the art treatment of AUD

Despite alcohol addiction and AUD having a high overall prevalence, in 2007 only about 25% of people with alcoholism received effective, evidence-based treatments in the United States (US) (Hasin et al., 2007). A study from 2015 reported that 8.3% out of 15.8

million adults with heavy alcohol consumption received appropriate treatment (Kranzler and Soyka, 2018). Health professionals may also fail to inquire about alcohol consumption. Only one of six US adults, including binge drinkers, reported ever being asked about their alcohol consumption by a health professional in 2011 (McKnight-Eily et al., 2014; Kranzler and Soyka, 2018).

Even though the prevalence of AUD is high and systematic strategies for their identification have become more prominent, only a small fraction (about 3%) of patients diagnosed with alcoholism receive any prescription medication (Mark et al., 2009; Harris et al., 2010; Heilig et al., 2019). Common sources of help for people with AUD are based on behavioral treatments, medications, and mutual-support groups with modest effect sizes.

Currently, there are 3 drugs approved by the Food and Drug Administration (FDA) for the treatment of AUD: disulfiram, acamprosate, and naltrexone (Fairbanks et al., 2020).

Disulfiram is used to treat chronic alcoholism. It produces acute sensitivity to ethanol by inhibiting the enzyme ALDH and preventing the breakdown of acetaldehyde. The accumulation of acetaldehyde in turn produces unpleasant physiological reactions, including flushing, nausea, headache, palpation, vomiting, and hypotension (Kim et al., 2018). Hence, disulfiram is used as a psychological deterrent, which induces unpleasant physiological reactions if taken together with alcohol. The efficacy of disulfiram is low due to poor medication compliance. Possible side effects of disulfiram include drowsiness and hepatotoxicity, and it should not be given to someone in a state of alcohol intoxication.

Acamprosate is used to medicate alcohol dependence, since it demonstrated to maintain abstinence, presumably by reducing craving. The exact molecular function of

acamprosate is not well known. It is thought that acamprosate acts as NMDA antagonist and modulator of GABA that stabilizes the chemical balance in the brain that would be disrupted by alcohol withdrawal (Mason et al., 2002; Seneviratne and Johnson, 2015; Kim et al., 2018).

Naltrexone acts as opiate antagonist, which blocks the action of the endogenous opioid peptide dynorphin. Potentially, it reduces the endorphin-mediated rewarding effects of alcohol and results in reducing the consumption of alcohol (Mason et al., 2002; Kim et al., 2018; Fairbanks et al., 2020). Naltrexone induces acute opioid withdrawal in patients with opiate use. Hence, it should not be taken together with opioids. Naltrexone appears to be the first-line therapy for many patients who seek to reduce drinking, since it can be taken while a patient continues to consume alcohol (Fairbanks et al., 2020).

Besides the mentioned FDA-approved drugs, there are 3 additional drugs that could be used for treatment of AUD: baclofen, chlomethiazole and diazepam.

Baclofen, a GABA-B antagonist, is approved for spasticity treatment and is used in alcohol dependence as an off-label drug (de Beaurepaire et al., 2019). GABA-B receptors interact with many biological systems, which are potentially involved in AUD including neurotransmitter systems (dopamine, serotonin, norepinephrine, and glutamate). In clinical studies, baclofen appeared to suppress alcohol consumption, craving for alcohol, and alcohol withdrawal symptoms (Agabio and Colombo, 2014). Nevertheless, the possible mode of action of baclofen for AUD is still not fully clarified (de Beaurepaire, 2018).

Chlomethiazole, structurally related to thiamine, is used to treat and prevent symptoms of alcohol withdrawal. As mentioned before, abrupt reduction or cessation of alcohol consumption causes a reduced GABAergic activity and increased glutamatergic activity,

and results in a hyperexcitable state (Attilia et al., 2018). By enhancing the action of the neurotransmitter GABA at its receptor, chlomethiazole acts like a sedative, hypnotic, anticonvulsant, and muscle relaxant, thereby leading to reduction of the withdrawal symptoms. (Sychla et al., 2017).

Diazepam belongs to the group of benzodiazepines and is used in alcohol withdrawal. By stimulating the inhibitory GABA-signaling pathways, it suppresses the symptoms and complications of withdrawal, including autonomic hyperactivity, agitation, combativeness, hallucinations, seizures, delirium, and death (Weintraub, 2017).

Finally, in addition to the above mentioned drugs available for the treatment of alcohol dependence and withdrawal symptoms, lithium carbonate (further referred to as lithium) has been considered for the treatment of AUD (Fawcett et al., 1987; Clark and Fawcett, 1989). Lithium is known for its use in the treatment of bipolar disorders (BD). Although the mechanisms underlying the positive effects of lithium in AUD patients is still not entirely understood, lithium has been described to have various effects on neurotrophic factors, neurotransmitters, oxidative metabolism, apoptosis, second messenger systems, and biological systems (Won and Kim, 2017). Lithium has been reported to modulate neurotransmitters including glutamate, dopamine, GABA, acetylcholine, and glycine. For these reasons, lithium is being considered in the treatment of alcohol dependence as well as in the treatment of side effects including depression. Nevertheless, lithium has also been reported to cause neurotoxicity, even at concentrations normally used in the therapy of BD (Lang and Davis, 2002; Mignarri et al., 2013; Shah et al., 2015).

Overall, treatment options for alcohol abuse and dependence including AUD are limited and not without risks. Moreover, most drugs of abuse may have inherent neurotoxic effects (Mohammad Ahmadi Soleimani et al., 2016). Therefore, there is a need to identify

new treatment strategies to counteract the negative consequences of acute and chronic alcohol consumption. However, this is not an easy task, as also seen by the lack of new medication approved since 2004 (Heilig et al., 2019). A summary of possible adverse effects of each FDA-approved drug including non-FDA approved drugs for AUD is depicted in Table 1-A.

Table 1-A: Medication for alcohol use disorder adapted and modified from (Winslow et al., 2016).

Medication	Application	FDA approved for AUD	Adverse effects
Acamprosate	Alcohol dependence	Yes	Diarrhea, insomnia, anxiety, depression, asthenia, anorexia, pain, flatulence, nausea, dizziness, pruritus, dry mouth, paresthesia, sweating
Disulfiram	Alcohol dependence	Yes	Flushing, palpitations, nausea, vomiting, headache, optic neuritis, peripheral neuritis, polyneuritis, peripheral neuropathy, hepatitis, drowsiness, fatigability, impotence, headache, acneiform eruptions, allergic dermatitis, metallic or garlic-like aftertaste
Naltrexone	Reduce alcohol consumption	Yes	Nausea, vomiting, headache, dizziness, nervousness, fatigue, low energy, insomnia, anxiety, difficulty sleeping, abdominal pain or cramps, joint or muscle pain

Baclofen	Reduce alcohol consumption	No	Sedation, dizziness, weakness, nausea, headache, skin rash, itching, shortness of breath, problems in micturition, bowel changes, irregular heartbeat, and chest pain (Franklin et al., 2009)
Chlomethiazole	Alcohol withdrawal symptoms	No	Sedation, nasal irritation and sneezing, headache, excitement, confusion, dependence, gastrointestinal disturbances, rash, bullous eruption drowsiness and anaphylaxis (Wilby and Hutchinson, 2004)
Diazepam	Alcohol withdrawal symptoms	No	CNS and respiratory depression. Severe adverse effects include seizures and cardiovascular collapse, dependency, and abuse. Common adverse effects include sedation, fatigue, depression, ataxia, headache, nausea, incontinence, rash and may more. A detailed list of adverse effects is reported in (Dhaliwal et al., 2020)

1.7 Disease models of AUD

One of the reasons underlying the lack of effective treatment strategies is our incomplete knowledge of the molecular mechanisms of alcohol toxicity and alcohol dependence in human brain cells. Animal models are instrumental to retrieve important information regarding disease pathogenesis and treatment. However, they not fully recapitulate the human disease state, particularly in the context of human conditions such as addiction, including AUD (Goldman, 2016).

Given the impracticability of studying live brain cells, investigations are mostly based on post-mortem tissue. However, post-mortem tissue correlates with an end-stage of the disease and cannot be used to investigate the molecular aspects of early changes and compensatory pathways of live human neuronal cells. Other ethanol studies focus on brain imaging, which can provide macroscopic and functional data of live brain. However, this approach does not allow to gain information at the cellular and molecular level. Taken together, given the difficulty of modeling neuropathologies, there is high attrition rate in brain disease drug development, with only approximately 8% of successful clinical trials (Miller, 2010; Sherman and Bang, 2018). There is a high need for the development of human cell-based model systems capable of assessing the complexity of human neurotoxicity. Such systems would be extremely useful in the context of AUD, and they might lead to the identification of substances capable of counteracting ethanol toxicity in human neuronal cells.

To circumvent the limitations of the current model systems of neurological defects, stem cell technology can be harnessed to generate human neuronal cells in a dish. This approach allows to investigate the molecular aspect of biology and disease in a relevant cellular context.

1.8 Induced pluripotent stem cells (iPSCs) and personalized medicine

Stem cells are potent, unspecialized cells that are capable of self-renewal. They can be found in different human tissues and give rise to different specialized cell types. Unlike somatic or adult stem cells, which retain the ability to differentiate only into specialized cell types of the tissue or organ in which they reside, pluripotent stem cells (PSCs), such as embryonic stem cells (ESCs), can give rise to progenies of all three germ layers (endoderm, ectoderm, and mesoderm), including heart muscle cells, blood cells, and nerve cells. Human ESCs (hESCs) were first derived out of the inner cell mass of human blastocysts and cultured in vitro in 1998 by Thomson and colleagues (Thomson et al., 1998). Despite of their potential role in drug discovery, transplantation medicine, and human developmental biology, their use is associated with ethical controversies, which hinder their clinical application. The limitations can be overcome by inducing the pluripotent state in somatic cells (such as fibroblasts or peripheral blood mononuclear cells (PBMCs)). This can be achieved by reprogramming somatic cells into ESC-like cells, e.g. by forcing the ectopic expression of ESC-associated factors, such as OCT3/4, SOX2, KLF4, and c-MYC (Takahashi and Yamanaka, 2006). The generated induced pluripotent stem cells (iPSCs) resemble ESCs in morphology, proliferative capacity, and developmental potential. Human iPSCs circumvents the ethical controversies related to hESCs and may serve as a tool for regenerative medicine applications by reducing the risk of allogenic reactions upon autologous transplantation (Jiang et al., 2014). Despite acquiring new pluripotency properties, iPSCs retain the genetic background of the original somatic cells from which they were derived, including any disease-associated genetic traits (Guenther et al., 2010; Zhao et al., 2017). This feature enables the generation of patient-specific cell lines that recapitulate the genetic background of the donor. Hence,

the iPSC technology allows the establishment of innovative cellular disease models that can be used for studying the cellular and molecular pathophysiology of complex human diseases, as well as for the conduction of personalized drug development strategies (Fig. 7). Enormous progress in the development of *in vitro* differentiation protocols has enabled the robust generation of specific affected cell types and decreased the issue of cell-to-cell variability.

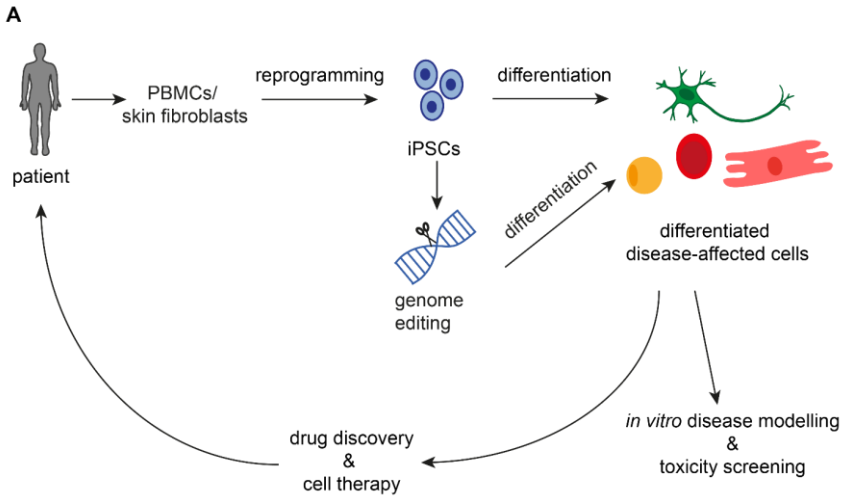

Fig. 7: Applications of induced pluripotent stem cells.
PBMCs or skin fibroblasts can be reprogrammed into patient iPSCs, which can be differentiated into disease-affected cells. Those cells may serve as *in vitro* disease models for mechanistic studies, toxicity screenings and drug screenings. Genetically engineered cells can be used for cell therapy and enable the investigation of individual or combinatorial genes and their contribution to a disease. iPSCs: induced pluripotent stem cells; PBMCs: peripheral blood mononuclear cell.

Several patient-specific iPSCs have been used to model a growing list of neurological diseases such as Alzheimer's disease (AD), Huntington`s disease (HD) and Parkinson's disease (PD) (Bahmad et al., 2017), and psychiatric disorders including schizophrenia (SCZ) (Brennand et al., 2011; Chiang et al., 2011) and bipolar disorder (BD) (Mertens et al., 2015). For example, iPSCs derived from PD patients were used to gain mechanistic insights into the gene-environmental interaction involved in the disease pathogenesis and

to identify new pathways as therapeutic targets (Ryan et al., 2013). Human iPSC-derived cortical neurons were used to establish a cellular AD model to analyze Aβ-induced synaptic disease mechanisms and develop new therapeutic approaches (Nieweg et al., 2015).

Among psychiatric disorders, SCZ was the first disorder whose disease pathology was modelled using patient-derived iPSCs. In those studies, patient-derived iPSCs were differentiated into neurons to study their connectivity, synapse number, spine density, and expression of glutamatergic receptors (Brennand et al., 2011; Chiang et al., 2011).

Mertens and colleagues developed an iPSC model derived for human BD, a neuropsychiatric disorder that is characterized by intermittent episodes of mania and depression. With this model they investigated the cellular phenotypes of hippocampal dentate gyrus-like neurons derived from those patient iPSCs. They observed mitochondrial abnormalities in young neurons and hyperactive action-potential firing. Using lithium, the patient-specific hyperexcitability was selectively reversed. This effect was specifically observed in neurons derived from those patients who responded to clinical treatment with lithium (Mertens et al., 2015). Hence, iPSCs can be used to study disease relevant phenotypes *in vitro* that are directly translatable to the clinic.

Another strategy to improve iPSC-based disease modelling is the use of gene editing technology. Besides TAL effector nuclease (TALEN) and zinc-finger nucleases (ZFN), one of the leading-edge genome editing tools is the clustered regularly interspaced short palindromic repeats (CRISPR)/Cas9 system (Jinek et al., 2012; Gupta and Musunuru, 2014). Genome editing enables the investigation of individual or combinatorial genes and their contribution to a disease or for studying the effect of one or more genetic variants including single nucleotide polymorphisms (Fig. 7) (Prytkova et al., 2018).

1.8.1 High-content analysis (HCA) and iPSC-driven drug discovery

For modern drug discovery, one major challenge is the establishment of suitable *in vitro* systems in which the efficacy and toxicity of compounds can be validated. A vastly used high-throughput (HT) system for drug discovery is the imaging-based high content analysis (HCA). HCA was introduced in 1997 by Cellomics, Inc. (Pittsburgh) as a new advance in cell analysis (Giuliano et al., 1997). HCA is a cell based high-throughput technique that enables automatic measurement and analysis of fluorescence images of a vast number of cells or samples. HCA provides quantitative and qualitative information from complex biological systems beyond typical assay formats. One major advantage is that HCA makes it possible to monitor multiple independent measurements and diverse responses on a single cell-level. In recent years, various HCA methods have been established (Saunders et al., 2014; Iannetti et al., 2015; Gelles and Chipuk, 2016; Daniele et al., 2017; Kepiro et al., 2018; Arias-Fuenzalida et al., 2019; Varkuti et al., 2020). Using a mitochondrial-targeted high-throughput small molecule screen comprised of 24,000 compounds, Varkuti and colleagues identified potential structural and functional classes of mitochondrial modulators. They identified potential compounds that promote mitochondrial health, enhance oxygen consumption rate, and protect neurons against toxic insults (Varkuti et al., 2020).

Despite of these successes in high-throughput drug discovery, most of the identified drug candidates fail in late-stage drug development. A reason why many drug candidates fail in clinical settings is the poor performance and predictability of preclinical model systems. Rodents are predictive of human toxicity in only half of the cases (Olson et al., 2000; Uhl and Warner, 2015). Unfortunately, drug candidates often fail due to species-

specific differences in disease pathology (Heilker et al., 2014), leading to high drug attrition rates (Grskovic et al., 2011).

Furthermore, the early steps of drug validation are mainly performed in disease-unrelated cell lines, while disease-relevant primary cell systems or animal models are only used at later stages in preclinical development.

Human iPSC-derived cells may thus hold great promises in circumventing the above-mentioned issues by serving as human disease-relevant cell types on which drug candidates can be tested already in early stages of drug development reducing the risk for toxic side effects. The combination of HCA with human iPSC technology has in fact the potential to enable the identification of drug candidates for neurological diseases that may be better predictive of clinical efficacy in humans.

Daniele and colleagues developed stable autophagy and mitophagy reporter-iPSCs and established a HT phenotyping platform utilizing automated HCA. With this tool, they enabled the evaluation of autophagy and mitophagy homeostasis in basal conditions and in response to stress conditions (Daniele et al., 2017). Ebert and colleagues where the first to show that human iPSCs can be used to model the specific pathology seen in the genetically inherited disease spinal muscular atrophy (SMA), a group of neuromuscular disorders that result in the loss of motor neurons and progressive muscle atrophy (Ebert et al., 2009). The biopharmaceutical company iPierian established an integrated iPSC-based drug discovery strategy targeting SMA. They derived iPSCs from several patients with type 1 SMA. In accordance with previous findings (Burghes and Beattie, 2009), patient-derived cells showed reduced survival motor neuron (SMN) levels. Those patient derived-iPSCs were differentiated into motor neurons and used for screening against a library of 200,000 compounds geared towards the identification of small molecules with

the capacity to increase SMN levels to those found in non-diseased motor neurons (Grskovic et al., 2011).

Additionally, I contributed to the establishment of a phenotypic high-content drug screening targeting the MMP in patient-derived neuronal progenitor cells (NPCs) carrying a *MT-ATP6* mutation causing neurological diseases such as Leigh syndrome (Lorenz et al., 2017).

All these studies underpin the possibilities and potentials of iPSC-technology. Combined with the fast-growing knowledge of efficient differentiation protocols, HCA, and gene editing, iPSCs may become a crucial tool for the development of drug discovery platforms in disease-relevant and cell type-specific environments. This new strategy will allow circumventing the drawbacks of conventional target-centered drug discovery systems and may potentially lead to the identification of novel drug candidates, opening the way to personalized drug discovery approaches.

1.9 Current work on iPSC technology to model AUD

Despite of the advances in human iPSC technology, improved treatment strategies for AUD have not yet emerged. Understanding the molecular, cellular, and synaptic plasticity mechanisms of AUD in the human CNS is instrumental for the development of effective therapeutics for AUD, considering that current treatments for alcoholism and AUD only exhibit a limiting rate of success.

To date, the use of iPSCs to study AUD is in its nascent stage. Lieberman et al. investigated the acute and chronic effects of ethanol exposure on human iPSC-derived neural cells from alcoholic and non-alcoholic donors. They focused their study on NMDA receptor function and receptor subunit messenger-RNA (mRNA) expression levels. They

exposed the iPSC-derived neurons to 50 mM ethanol and observed attenuated NMDA receptor mediated currents. These results were in line with data obtained from animal models (Lieberman et al., 2012). At the same time, electrophysiological recordings of the $GABA_A$ response in human iPSC-derived neuronal cells following acute ethanol exposure (50 mM) revealed data that was contradictory to the findings obtained from animal models (Lieberman et al., 2018). Similarly, mRNA expression analysis of $GABA_A$ receptor unit expression levels observed in iPSC-derived neuronal cells following chronic ethanol exposure differed from the results obtained *in vitro* and in *in vivo* animal models (Kumar et al., 2009; Lieberman et al., 2018). De Filippis et al. investigated patient-derived iPSCs which were further differentiated into neural cell types including NPCs and neurons. With this model system they studied the effect of ethanol on pluripotency (iPSCs), neurogenesis (NPCs) and differentiation (post-mitotic neurons) (De Filippis et al., 2016). In a recently published study, iPSC-derived three-dimensional cerebral organoids were used to model alcohol-induced neurotoxicity (Arzua et al., 2020). This study may help to better understand the neurotoxic effects of binge drinking during pregnancy.

So far, the data underlines the necessity of human neuron-based studies considering the observed contradictions in data obtained from animal and human models. Accordingly, advantages of iPSC-technology include the possibility to study patient-specific cells as well as different cell types and their response to ethanol. Moreover, iPSC-technology enables the generation of genetically engineered cells which becomes especially interesting when studying the underlying genetic variations associated with alcohol dependence.

Overall, the data underpins the importance of human neuronal models in understanding the cellular response and effects following alcohol consumption in humans. For these reasons, it is of great importance to focus on developing innovative patient-specific iPSC-driven approaches to enable the discovery of effective treatment strategies for ethanol neurotoxicity and AUD.

1.10 Genome editing of iPSC to model AUD

Several studies aimed to identify the specific genes that can influence a person's likelihood of developing AUD (Lieberman et al., 2015; Verhulst et al., 2015; De Filippis et al., 2016). Recent genome wide association studies identified a polymorphism in the gene ß-klotho (*KLB),* which is associated with alcohol consumption (Schumann et al., 2016). *KLB* encodes for the transmembrane protein KLB that functions as co-receptor for the hormone fibroblast growth factor 21 (FGF21), which is secreted by the liver and regulates critical metabolic pathways including sweet and alcohol preference (Talukdar et al., 2016). KLB is highly expressed in adipose tissue, pancreas and liver. In mice, *Klb* is selectively expressed in the hypothalamus in the suprachiasmatic nucleus (SCN) (Bookout et al., 2013), and to a lower extent in the VTA and NAc (Talukdar et al., 2016). Nevertheless, the level in the human brain is reported to be low. Although there is an indication of KLB expression in human brain (The Human Protein Atlas), restricted expression to specific areas has not been demonstrated so far (Staiger et al., 2017).

KLB-knockout (KLB-KO) experiments in mice demonstrated that KLB expression in the brain significantly influences the FGF21 effect on alcohol drinking (Schumann et al., 2016). It is known that alcohol can rapidly cross the blood-brain barrier and that it increases the release of dopamine in the ventral striatum in humans (Boileau et al., 2003).

However, the molecular mechanisms underlying this effect and the relevance of the genetic predisposition on the biological functions of human neurons remain to be determined, given the difficulty of studying human live dopaminergic neurons.

Recent advances in stem cell technologies and genome editing approaches may allow circumventing these limitations and help to derive a suitable human model system of AUD. In fact, iPSCs and genome editing tools such as CRISPR/Cas9 enable the generation of human neurons in a dish to study specific genetic patterns, including single nucleotide polymorphisms (SNPs) and their role in alcohol consumption and alcohol abuse (Takahashi et al., 2007; Grobarczyk et al., 2015; Hockemeyer and Jaenisch, 2016; Slaymaker et al., 2016).

2. Aim of the study

The aim of my study was to generate an iPSC-based model system to investigate the toxic consequences of ethanol on human neurons, and to address ethanol-induced neurotoxicity in a quantitative and high-throughput amenable manner, with the potential to establish new drug treatment strategies for AUD.

Due to the involvement of dopaminergic neurons in the initiation of ethanol reinforcement and presumably also in the development of AUD, I focused on the effects of ethanol on neuronal cultures containing dopaminergic neurons.

For this purpose, my first goal was to generate human iPSC-derived neuronal cells containing dopaminergic neurons from AUD patients and controls. My second goal was to establish an HCA method to investigate the potential neurotoxic effects of acute and chronic ethanol exposure in human neurons. Finally, I wanted to investigate if the developed assay would be suitable to perform a compound screening to identify drugs that influence neurotoxicity upon ethanol exposure.

Furthermore, another goal was to generate an iPSC knockout line where the gene *KLB* was knocked out, which could enable to study the role of this gene in the context of alcohol consumption and dependence.

3. Material

3.1 Experimental models

3.1.1 Cells

Different cell lines were used in this study. The healthy control fibroblast CON2 was previously characterized in the lab, and established in our study (Lorenz et al., 2017). The background information of the fibroblasts used in this study are summarized in Table 3-A.

Table 3-A: Background information on fibroblasts

Name	Disease	Age	Gender	Source
CON2	Control	44	M	Dr. Stricker

hESCs and iPSCs used in this study are described in section 4.1.2 and are further specified in Table 3-B. The hESC line H1 was purchased from WiCell and was used in accordance with the German license of Alessandro Prigione issued by the Robert Koch Institute (AZ: 3.04.02/0077-E01). Control iPSCs were previously generated using episomal plasmids (Yu et al., 2011) and described as XM001 (Wang et al., 2018). Ethical approval to generate AUD patient derived iPSCs was approved by the ethic committee of the Charité-Universitätsmedizin Berlin (EA1/206/15). AUD iPSC lines were generated by the BIH StemCell Core Facility at Max Delbrück Center for Molecular Medicine (MDC) in Berlin (Sebastien Diecke).

Table 3-B :Background information on hESCs and iPSCs

Name	Disease	Age	Gender	Source
H1	Control	-	M	WiCell Research Institute
XM001	Control	47	F	Heicko Lickert
LR	Control	38	F	Markus Schülke, Charité
BIHi232 BIHi233 BIHi234 BIHi235 BIHi236	AUD	23-25	M	Josef Priller, Charité and Sebastian Diecke, MDC

3.1.2 iPSC-derived models

iPSC-derived NPCs and neurons were used in this study to model AUD. The generation and characterization of NPCs is explained in detail in section 4.1.3 and background information is summarized in Table 3-C. The generation and characterization of neurons is explained in section 4.1.4 and background information is summarized in Table 3-D.

Table 3-C: Background information on iPSC-derived NPC

Name	Disease	Gender	Source
H1	Control	M	Annika Zink
XM001	Control	F	Annika Zink
BIHi232 BIHi233 BIHi234 BIHi235 BIHi236	AUD	M	Annika Zink

Table 3-D: Background information on iPSC-derived neurons

Name	Disease	Gender	Source
H1	Control	M	Annika Zink
XM001	Control	F	Annika Zink
LR	Control	F	Annika Zink
BIHi232 BIHi233 BIHi234 BIHi235 BIHi236	AUD	M	Annika Zink and Josefin Conrad

3.2 Laboratory equipment

Relevant technical appliances are listed as follows:

Item	Product name	Supplier
Centrifuge	Universal 32 R	Hettich
	5810R	Eppendorf
	Heraeus Pico Microcentrifuge	Thermo Fisher Scientific
Cell culture bench	UVF	BDK Luft und Reinraum
	BDK-S	Technik GmbH
	Maxisafe 2020 TF	Thermo Fischer Scientific
Cell sorter	BD FACSAria TM III	BD Bioscience
HCA Platform	CellInsight CX7	Thermo Fisher Scientific
Electrophoreses	EPS 301	Amersham Bioscience
	Transiluminator TM-36	UVP Inc.
	GeneGenius Gel Imaging System	Syngene
	Electrophoreses chamber	BioRad
Fluorescent microscope	Imager Z1	Carl Zeiss GmbH
	Olympus IX70	OLYMPUS
Freezing container	Mr. Frosty	Nalgene
	CoolCell™	Corning
Freezer, -20	Comfort	Liebherr
Freezer, -80	Innova4725	New Brunswick
Hemocytometer	Neubauer Plus	Thermo Fisher Scientific

Incubator	Heraeus BBD 6220	Thermo Fisher Scientific
	Binder CB 160	Binder GmbH
Microcentrifuge	Biofuge pico	Heraeus
Microscope	Leica m80	Leica Microsystems
	Eclipse Ni-E Ts2	Nikon
Microscales		Sartorius
Pipettes (2-1000 µl)	Pipetman Classic	Gibson
Pipetaid/Serological pipettor	PIPETBOY acu 2	Integra Bioscience
Real-Time PCR System	ViiA 7	Thermo Fisher Scientific
Single channel electronic pipettes 0.5-10µl, 5-100µl, 20-300l, 50-1000µl	Research Pro	Eppendorf
Shaker	Rocky	LTF Labortechnik
	Orbital shaker (80rpm)	IKA
Spectrophotometer	NanoDrop 8000	Thermo Fisher Scientific
Thermal Cyclers	MJ Research PTC 200	MJ Research
	Simpli Amp Thermal cycler	Life Technologies
	Mastercycler X50s	Eppendorf
Thermomixer	Thermomixer comfort	Eppendorf
Vortexer	Vortex Genie 2	Scientific industries
Water bath	Isotemp 220	Thermo Fisher Scientific
	TW8 Water Bath	Julabo

3.3 Chemicals and Consumables

3.3.1 General consumables

General consumables and respective supplier used in this study are listed as follows:

Items	Supplier
13 mm Ø Coverslips	Thermo Fisher Scientific
48-well MEA plate	Axion Biosystems
96 Well Cell Culture Microplate, PS, F-Bottom, black, TC, µCLEAR®, 96-well black, clear bottom cell culture microplates	Greiner Bio-One
Cell culture multiwell plates (6-well, 12-well, 24-well)	Greiner Bio- One and Sarstedt AG & Co. KG
Cell spatula	TPP
Corning 60 mm Ultra-low attachment culture dish	Corning
Cryovials	Corning
Falcon polystyrene test tubes	BD Falcon
Falcon polystyrene test tubes with cell strainer	BD Falcon
Falcon tubes 15 ml, 50ml	BD Falcon
Glass pipettes	Sarstedt AG & Co. KG
MicroAmp™ Optical 384-well plates for qPCR	Thermo Fisher Scientific
Pasteur pipettes, glass, 150 mm	Applied Biosystems
PCR SingleCap 8er-SoftStrips 0.1ml	Biozym
Pipette tips (2 µl, 10 µl, 200 µl, 1000 µl)	Greiner Bio

Serological pipettes (2ml, 5ml, 10ml, 25ml)	Sarstedt AG & Co. KG
Reaction tubes (0.5 ml, 1.5 ml, 2 ml)	Sarstedt AG & Co. KG
Slides	Thermo Fisher Scientific
Vacuum filtration (250 ml, 500 ml, 1 L) 0.2 µM	Applied Biosystems

3.3.2 Cellular consumables

Item	Supplier
(+)-Sodium L-ascorbate Ascorbic Acid (Vitamin C)	Sigma Alddlrich
Antimycin A, 25 mM	Sigma Aldrich
B-27 supplement (50x) with and without Vitamin A	Gibco
Bambanker	NIPPON genetics
BDNF	MACS Miltenyi Biotec
CHIR-99021	Cayman Chemical
db-cAMP	Sigma Aldrich or StemCell
Dimethyl sulfoxide (DMSO), sterile filtered	Sigma Aldrich
DMEM, 4.5 g/l glucose	Gibco
DMEM/F12, HEPES	Gibco
Dorsomorphin	MACS Miltenyi Biotec
DPBS (without calcium and magnesium)	Thermo Fisher Scientific
FCCP, 25mM	Sigma Aldrich
Fetal Bovine Serum (FBS)	Life Technologies
FGF2	PeproTech
FGF8-a	MACS Miltenyi Biotec

Material

GDNF	MACS Miltenyi Biotec
Glucose	Sigma Aldrich
Hoechst 33342	Life Technologies
KnockOut-DMEM (KO-DMEM)	Thermo Fisher Scientific
KnockOut-Serum replacement (KO-SR)	Gibco
L-Glutamine	Lonza
Matrigel, Growth Factor Reduced	BD Bioscience
mTeSR™1	STEMCELL Technologies
MycoZap Plus-CL	Lonza
Mitomycin C	Sigma-Aldrich
N2-supplement (100x)	Gibco
Neurobasal® medium	Gibco
Non-essential amino acids (NEAA)	Gibco
Oligomycin	Sigma Aldrich
Opti-MEM, reduced serum media	Gibco
Pen/strep (10.000 U/ml)	Lonza
Purmorphamine	Millipore
ROCK inhibitor (RI), (Y-27632)	Enzo Life Sciences
SB-431542	Selleckchem
Sodium Pyruvate	Gibco
StemMACS iPS-Brew XF, human	Miltenyi Biotech
StemPro™ Accutase™ (Accutase)	Thermo Fisher Scientific
TGF-ß3	MACS Miltenyi Biotec
Trypsin-EDTA (0.05%), phenol red	Gibco

UltraPure 0.5M EDTA	Invitrogen

3.3.3 Molecular and chemical consumables

Item	Supplier
16% Paraformaldehyde (PFA)	Thermo Fisher Scientific
AmpliTaq Gold 360 DNA Polymerase	Thermo Fisher Scientific
BbsI	NEB
DNA Extension Ladder 100 bp and 1kb	Life Technologies
DNA Gel loading dye (6x)	Life Technologies
DNA Kit FlexiGene	Qiagen
DNase I	Invitrogen
Dnase/Rnase-free distilled water	Gibco
dNTP-Mix (10 mM) set	Thermo Fisher Scientific
Donkey normal serum	Gibco
DreamTaq DNA Polymerase	Thermo Fisher Scientific
Ethanol, 99,5% (v/v)	Carl Roth
Ethidium bromide (10 mg/ml)	Carl Roth
Immu-Mount Media	Thermo Fisher Scientific
Isopropanol, 100%	Carl Roth
Oligo(-dT) 12-18 Primer, 1µg/µl	Invitrogen
Polyethyleminine (PEI)	Sigma-Aldrich
Protease	Qiagen
Q5®High-Fidelity DNA Polymerase	NEB

RNase-Free Dnase Set (50)	Qiagen
SYBR-Green PCR mix	Applied Biosystem
Triton™- X-100	Sigma Aldrich
Tween-20	Sigma Aldrich

3.3.4 Kits

Kit	Source
AmpliTaq Gold™ 360 Master Mix	Thermo Fisher Scientific
Annexin-V FITC	MACS Miltenyi
Clone Jet PCR Cloning	Thermo Fisher Scientific
Cytotune®-iPS 2.0 Sendai Reprogramming Kit	Thermo Fisher Scientific
DNeasy blood and tissue kitx	QIAGEN
FlexiGene DNA Kit 250	QIAGEN
Infinium OmniExpressExome-8	Illumina
Lipofectamine 3000	Thermo Fisher Scientific
M-MLV Reverse Transcriptase	Invitrogen
NucleoBond Xtra Maxi Plus	MACHEREY-NAGEL GmbH & Co. KG
PCR Clean-Up System	Promega
Pure Yield Plasmid Miniprep System	Promega Corporation
Phire Animal Tissue Direct PCR	Thermo Fisher Scientific
QIAprep Spin Miniprep	QIAGEN
Qiagen RNeasy Mini kit (50)	QIAGEN
Wizard SV Gel and PCR Clean-Up System	Promega Corporation

3.3.5 Media

All media were sterile-filtered and pre-warmed to 37°C before usage. Maintenance and freezing media are listed below.

Table 3-E: Media for mouse embryonic fibroblasts (MEFs)

Medium	Component	Volume	Stock conc.	Final conc.
DMEM/ Fibroblasts	DMEM, 4.5 g/l glucose	500 ml	1x	1x
	FBS	50 ml	1 x	10 %
	NEAA	5 ml	100x	1x
	Pen/Strep	5 ml	10 mg/ml	0.1 mg/ml
	Pyruvate	5 ml	100 mM	1 mM
	Glutamine	5 ml	200 mM	2 mM

Table 3-F: Media for hESCs and iPSCs

Medium	Component	Volume	Stock conc.	Final conc.
iPS-Brew	iPS-Brew basal media	500 ml	1x	1x
	iPS-Brew supplement	10 ml	50x	1x
	MycoZap	1 ml	500x	1x
	Pen/Strep	5 ml	10 mg/ml	0.1 mg/ml

mTesR1	mTesR1 basal medium	400 ml	1x	1x
	mTeSR1 5x supplement	100 ml	5x	1x
	Pen/Strep	5 ml	10 mg/ml	0.1 mg/ml
	MycoZap	1 ml	500x	1x

Table 3-G: Media for NPCs

Medium	Components	Volume	Stock conc.	Final conc.
smEB$^-$ (base for medium 1 (M1))	KO-DMEM	40 ml	1x	1x
	KO-SR	10 ml	5x	1x
	Pen/Strep	500 µl	10 mg/ml	0.1 mg/ml
	Glutamine	500 µl	200 mM	2 mM
	NEAA	500 µl	100x	1x
	Pyruvate	500 µl	100 mM	1 mM
	MycoZap	100 µl	500 x	1x
sm$^-$ (base for M2 and sm$^+$)	DMEM/F12	240 ml	1x	0.5 x
	Neurobasal	240 ml	1x	0.5 x
	N2	2.5 ml	100x	0.5x
	B27 w/o vitamin A	5 ml	50x	0.5x
	Pen/Strep	5 ml	10 mg/ml	0.1 mg/ml
	Glutamine	5 ml	200 mM	2 mM
	MycoZap	1 ml	500 x	1x
Medium 1 (M1); day 0 – day 2	smEB$^-$	10 ml	1x	1x
	CHIR	5 µl	6 mM	3 µM
	SB	10 µl	10 mM	10 µM
	DM	2 µl	5 mM	1 µM
	PU	7.69 µl	0.65 mM	500 nM
Medium 2 (M2); day 2-day 4)	Sm$^-$	10 ml	1x	1x
	CHIR	5 µl	6 mM	3 µM
	SB	10 µl	10 mM	10 µM
	DM	2 µl	5 mM	1 µM
	PU	7.69 µl	0.65 mM	500 nM
sm$^+$ (maintenance of NPCs)	Sm$^-$	10 ml	1x	1x
	CHIR	5 µl	6 mM	3 µM
	PU	7.69 µl	0.65mM	500 nM
	Vit.C	7.5 µl	200 mM	150 µM

Table 3-H: Composition of freezing media.

Medium	Component	Volume	Final conc.
2x sm^+ freeze	sm^+	2 ml	20 %
	KO-SR	6 ml	60%
	DMSO	2 ml	20%

Table 3-I: Media for neurons

Medium	Components	Volume	Stock conc.	Final conc.
sm- + Vitamin A	Hams F/12	250 ml	1x	0.5x
	Neurobasal	250 ml	1x	0.5x
	N2	2.5 ml	100x	0.5x
	B27 + vitamin A	5 ml	50x	0.5x
	Pen/Strep	5 ml	10 mg/ml	0.1 mg/ml
	Glutamine	5 ml	200 mM	2 mM
	MycoZap	1 ml	500x	1x
Dsm+	sm- + vitamin A	10 ml	1x	1x
	FGF8-a	2 µl	500 µg/ml	100 ng/ml
	PU	15.38 µl	0.65 mM	1 µM
	Vitamin C	10 µl	200 mM	200 µM
Dsm2+	sm- + vitamin A	10 ml	1x	1x
	BDNF	10 µl	10 µg/ml	10 ng/ml
	GDNF	10 µl	10 µg/ml	10 ng/ml
	TGF-ß3	10 µl	1 µg/ml	1 ng/ml
	Vitamin C	10 µl	200 mM	200 µM
	db c-AMP	50 µl	100 mM	500 µM

	PU	7.69 µl	0.65 mM	0.5 µM
Dmsm+	sm- + vitamin A	10 ml	1x	1x
	BDNF	10 µl	10 µg/ml	10 ng/ml
	GDNF	10 µl	10 µg/ml	10 ng/ml
	TGF-ß3	10 µl	1 µg/ml	1 ng/ml
	Vitamin C	10 µl	200 mM	200 µM
	db c-AMP	50 µl	100 mM	500 µM

Table 3-J: FACS media

Media	**Component**	**Volume**	**Stock conc.**	**Final conc.**
Pre-FACS media	PBS	9,2 ml	1x	1x
	FBS	500 µl	1x	0.5x
	Pen/Strep	100 µl	10 mg/ml	0.1 mg/ml
	Gentamycin	100 µl	10 mg/ml	0.1 mg/ml
	EDTA	100 µl	200 mM	2 mM

3.3.6 Oligonucleotides and sequences

Table 3-K: Oligonucleotide sequences for qRT-PCR

Gene	Forward	Reverse
OCT4	GTGGAGGAAGCTGACAACAA	ATTCTCCAGGTTGCCTCTCA
NANOG	CCTGTGATTTGTGGGCCTG	GACAGTCTCCGTGTGAGGCAT
SOX2	GTATCAGGAGTTGTCAAGGCAGAG	TCCTAGTCTTAAAGAGGCAGCAAAC
DNMT3B	GCTCACAGGGCCCGATACTT	GCAGTCCTGCAGCTCGAGTTTA
DPP4	TGGTGTCAGGTGGTGTGTGG	CCAGGCTTGACCAGCATGAA
VIM	GGAGCTGCAGGAGCTGAATG	GACTTGCCTTGGCCCTTGAG
NESTIN	TTCCCTCAGCTTTCAGGAC	GAGCAAAGATCCAAGACGC
PAX6	GAATTCTGCAGACCCATGC	TCTCGTAATACCTGCCCAG
SOX1	TTGGCATCTAGGTCTTGGCTCA	CGGGCGCACTAACTCAGCTT
SOX2	GTATCAGGAGTTGTCAAGGCAGAG	TCCTAGTCTTAAAGAGGCAGCAAAC
OAZ1	GGATCCTCAATAGCCACTGC	TACAGCAGTGGAGGGAGACC
GAPDH	CTGGTAAAGTGGATATTGTTGCCAT	TGGAATCATATTGGAACATGTAAACC

Table 3-L: Oligonucleotides for CRISPR/Cas9

Name	Forward	Reverse
For Exon 3 sequencing	CTCTGCTTTCTTTTCTCTGT	GTTTCCGCTCTTTCTGTTT
Oligomer sequence Exon 3	CACCGATGCTTACACCATCCGCCG	GAGGGGATGAGAAAGAAG
gRNA Exon 3	GATGCTTACACCATCCGCCG	
KLB_1	GAGGGGATGAGAAAGAAG	GAGGGGATGAGAAAGAAG
KLB_3	AGAGGGGATGAGAAAGAA	GAGAGACCAGGCAGTATAA

Table 3-M: Mycoplasma analysis

Primer	Forward	Reverse
Myco 1	CGCCTGAGTAGTACGTTCGC	
Myco 2	CGCCTGAGTAGTACGTACGC	
Myco 3	TGCCTGAGTAGTCACTTCGC	
Myco 4	CGCCTGGGTAGTACATTCGC	
Myco 5	CGCCTGAGTAGTAGTCTCGC	
Myco 6	TGCCTGGGTAGTACATTCGC	
Myco r1		GCGGTGTGTACAAGACCCGA
Myco r2		GCGGTGTGTACAAAACCCGA
Myco r3		GCGGTGTGTACAAACCCCGA

3.3.7 Antibodies

Table 3-N: Primary antibodies for immunostaining analysis

Human antigen	Species	Source	Dilution	Marker
NANOG	Goat	R&D Systems	1:100	PSC
OCT4	Mouse	Santa Cruz Biotechnology	1:300	PSC
NESTIN	Mouse	Millipore	1:200	NPC
PAX6	Rabbit	Covance	1:200	NPC/Ectoderm
SOX2	Goat	Santa Cruz Biotechnology	1:100	PSC/NPC
DACH1	Rabbit	ProteinTech	1:100	NPC
β-III-tubulin	Mouse	Santa Cruz Biotechnology	1:1000	Neuronal
MAP2	Guinea pig	Synaptic Systems	1:1000	Neuronal
GFAP	Guinea pig	Synaptic Systems	1:500	Glial
NURR1	Rabbit	Sigma Aldrich	1:500	DA Neurons
TH	Rabbit	Millipore	1:300	DA Neurons
FOXA2	Rabbit	Sevenhills	1:100	DA Neurons
TRA-1-60	mouse	Millipore	1:200	PSC
SMA	mouse	DakotaCytomation	1:200	Mesoderm
Fibronectin	Rabbit	Sigma Aldrich	1:300	Mesoderm
SOX17	goat	R&D Systems	1:50	Endoderm

Table 3-O: Secondary antibodies for immunostaining analysis

Human antigen	Species	Source	Dilution
Alexa Fluor 488	Donkey anti-mouse	Invitrogen	1:300
Alexa Fluor 647	Donkey anti-mouse	Invitrogen	1:300
	Donkey anti-rabbit	Invitrogen	1:300
Cy2	Goat anti-mouse	Sigma Aldrich	1:300
	Donkey anti-rabbit	Sigma Aldrich	1:300
Cy3	Donkey anti-mouse	Merck Millipore	1:300
	Donkey anti-goat	Merck Millipore	1:300
	Donkey anti-guinea pig	Sigma Aldrich	1:300
Cy5	Donkey anti-mouse	Sigma Aldrich	1:300
	Donkey anti-goat	Sigma Aldrich	1:300

Table 3-P: Intracellular dyes for MNH assay

Stain	Localization	Target	Working conc.	Source
Hoechst 33342	Nucleus	DNA	1:10000	Life Technologies
TMRM	Mitochondria	MMP	0.5 nM	Life Technologies
Annexin-V FITC	Cytoplasm	Phosphatidylserine		MACS Miltenyi Biotec

3.3.8 Plasmids

Plasmid	Provider
pU6(BbsI)-CAG-Cas9-venus-bpA (#1)	Addgene ID 86986 Dr. Pawel Lisowski
eSpCas9 (1.1)	Addgene ID 71814 Slaymaker et al., 2016
pEF1-BCL-XL-wpre-polyA P1102	Dr. Xiao-Bing Zhang from State Key Laboratory of Experimental Hematology, Tianjin, China.

3.4 Software

Software	Source
Adobe Illustrator CS6	Adobe Inc.
AxioVision v4.6.3.0	Zeiss
BD FACSDiva Software v8.0.2	BD Bioscience
HCS Studio Cell Analysis Software v6-6-1	Thermo Fisher Scientific
FiJi version v1.52h	ImageJ
GraphPad Prism v5	GraphPad Software
ImageJ	NIH
Benchling online tool	Benchling
Excel	Microsoft
Adobe Photoshop CS6	Adobe Inc.

4. Methods[1]

4.1 Cell biology

4.1.1 Cell culture

Cells were maintained in standard culture media supplemented with appropriate amounts of small molecules and supplements to support the maintenance of the specific cell state or neural induction. All media were sterile-filtered and prepared under sterile conditions. Before usage, the media were pre-warmed to either 37°C or room temperature (20–22 °C). All media compositions as well as freezing media compositions are listed in section 3.3.5. Suppliers for cell culture media components, supplements and additional cell culture materials are listed in section 3.3.2 and 3.3.3.

[1] Parts of the methods section have been reused and modified from the published version: Zink A, Conrad J, Telugu NS, Diecke S, Heinz A, Wanker E, Priller J and Prigione A (2020) Assessment of Ethanol-Induced Toxicity on iPSC-Derived Human Neurons Using a Novel High-Throughput Mitochondrial Neuronal Health (MNH) Assay. Front. Cell Dev. Biol. 8:590540. https://doi.org/10.3389/fcell.2020.590540.

4.1.1.1 Cultivating conditions

Within this study different cell types were used which require different culture conditions. Cells were mostly cultured under feeder-free conditions except for stressful situations where cell survival was critical. Under both conditions, Matrigel (a membrane-like matrix, BD Bioscience) was used in a stock concentration of 5 mg/ml and final concentration of 200 µg/ml for pre-coating of the cell culture multiwell plates (Greiner Bio- One and Sarstedt). Matrigel was thawed overnight on ice in the cold room and diluted with cold Knock-Out Dulbecco's Modified Eagle Medium (KO-DMEM, Thermo Fisher Scientific), to 5 mg/ml and aliquoted. One aliquot was sufficient to coat 4 cell culture plates (200 µg/ml final concentration). Cell culture plates were pre-coated with Matrigel one day before and stored at +4°C overnight to ensure successful polymerization. For this, the 5 mg/ml Matrigel aliquot was dissolved in 30 ml cold KO-DMEM and 1.25 ml of the dissolved solution was added to each well of a 6 well plate. Different cultivation processes are described below corresponding to the specific cell type.

4.1.1.2 Thawing cells

Frozen cells were quickly but gently thawed in a 37°C prewarmed water bath, transferred into a 15 ml falcon tube set with 1 ml of the appropriate medium (section 3.3.5) and up to 10 ml pre-warmed PBS or media. Cell suspension was centrifuged at 120 rcf (relative centrifugal force) for 5 minutes for PSCs and 200 rcf and 3 minutes for NPCs. Afterwards, the supernatant was removed, the cell pellet was resuspended in the required

medium and seeded on previously prepared matrigel-coated culture plates (section 4.1.1.1). 10 µM Y-237632 ROCK-Inhibitor (RI, Enzo Life Sciences) was added to the corresponding media after thawing to support cell survival.

4.1.1.3 Cryopreservation and cell pellet preparation

Different passages of all cell lines and cell types, except neurons, were frozen frequently. For cryopreservation of PSCs, cells were enzymatically detached using 0.5 mM PBS/EDTA (section 4.1.1.4) and frozen in 1 ml Bambanker (serum-free cell freezing medium, NIPPON Genetics) in 2 ml cryovials. The vials were placed in a cryo-freezing container (Mr Frosty™ or CoolCell), which allows slow freezing at a rate of -1°C per minute and stored at -80°C overnight. For long term storage, the vials were kept in liquid nitrogen tanks. For cryopreservation of NPCs cells were dissociated using accutase (section 4.1.3). After centrifugation, cell pellets were resuspended in 50% freezing medium (see section 3.3.5) and 50% NPC culture medium and transferred into 2 ml cryovials. Vials were placed in a cryo-freezing container and stored at -80°C overnight. For long term storage, the vials were kept in liquid nitrogen tanks.

For cell pellet preparation, old media was removed, cells were washed 1x with PBS, harvested with a cell spatula (TPP) in 1.5 ml PBS and transferred into 1.5 ml tubes (Sarstedt). Cell suspension was centrifuged at 13.000 rpm for 5 minutes. After discarding the supernatant, the cell pellet was shock-frosted in liquid nitrogen and stored at -80°C until further use.

4.1.1.4 Cultivation of iPSCs

Under normal conditions, hESCs and iPSCs were cultured under feeder-free conditions in either mTeSR^{TM}1 (mTESR; Stem Cell Technologies) or StemMACS iPS-Brew XF, human (iPS Brew; Miltenyi Biotec). Media was changed daily, and cells were split regularly once or twice a week in a splitting ratio of up to 1:4 either mechanically or up to 1:8 using 0.5 mM PBS/EDTA (UltraPure 0.5M ETDA, Invitrogen). For passaging using PBS/EDTA, cells were washed twice with PBS devoid of Ca^{2+} and Mg^{2+} and incubated with 0.5 mM EDTA in PBS at 37°C and 5% CO_2. After 3-5 minutes, cells were almost detached from the culture dish bottom and the PBS/EDTA was carefully discarded without destroying the almost detached cell cluster. Cell cluster were carefully resuspended in fresh iPS-Brew or mTESR and seeded out on pre-coated matrigel plates with 10 µM RI and a final volume of 2 ml each 6-well.

4.1.1.5 Generation of mouse embryonic feeder cells

Even though PSCs were cultured under feeder-free conditions, cultivation on mouse embryonic fibroblasts (MEFs) after fluorescence-activated cell sorting (FACS) showed to increase cell survival. MEFs were obtained from 2-week-old mouse embryos (strain CF1), plated on petri dishes, and maintained in Dulbecco's Modified Eagle Medium (DMEM)-medium (see Table 3-E) with medium changes every 2–5 days. At 80–90 % confluency, cells were passaged using Trypsin (Gibco). After sufficient expansion, usually after 2–3 passages, the MEFs were mitotically inactivated by incubation with mitomycin C (Sigma-Aldrich) for 2 hours at 37°C. Afterwards, cells were counted with a Neubauer hemocytometer (Thermo Fisher Scientific) and frozen as aliquots of 1.3 x10^6

cells/vial for one 6-well-plate or $2.6x10^6$ cells/vial for two 6-well plates. For supported cultivation of PSCs, plates containing MEFs were prepared one day before. MEFs were quickly thawed in a 37°C water bath, transferred into a 15 ml falcon and 5–10 ml pre-warmed DMEM-medium was added. Cell suspension was centrifuged for 4 minutes at 120 rcf, the supernatant discarded, and the pellet re-suspended in 9 ml of DMEM-medium. Cells were equally distributed to each well of the 6-well plate, pre-coated with matrigel (Corning, 200 µg/ml) and filled up to 2 ml with DMEM-medium. MEFs were kept at 37°C, 5% CO_2 overnight to ensure attachment of the cells before PSCs were added on top.

4.1.2 iPSC generation

Patient peripheral blood mononuclear cells were obtained after informed consent and under ethical approved regulations (EA1/206/15). The patient PBMCs were reprogrammed using the Cytotune®-iPS 2.0 Sendai Reprogramming Kit (Thermo Fisher Scientific) according to the manufacturer's instructions by the Stem Cell Core Facility in the lab of Sebastian Diecke (for details on contributions see chapter 7). The hESC line H1 was purchased from WiCell and was used in accordance with the German license of Alessandro Prigione issued by the Robert Koch Institute (AZ: 3.04.02/0077-E01). Control iPSC lines were previously generated using episomal plasmids (Yu et al., 2011) and described as XM001 (Wang et al., 2018). All pluripotent stem cells (PSCs) were cultivated on matrigel-coated plates using StemMACS iPS-Brew XF medium, supplemented with Pen/Strep (Thermo Fisher Scientific) and MycoZap (Lonza). We routinely monitored against mycoplasma contamination using PCR (see section 4.2.2). 10 µM RI was added after splitting to promote survival. PSC cultures were kept in a

humidified atmosphere of 5% CO_2 at 37°C and 5% oxygen. All other cultures were kept under atmospheric oxygen condition. Pluripotency of the generated lines was confirmed following previously published procedures (Prigione et al., 2010) using *in vitro* embryoid bodies (EB)-based differentiation. Karyotype analysis was performed by the MDC Stem Cell Core Facility (for details on contributions see chapter 7**)**. Briefly, DNA was isolated using the DNeasy blood and tissue kit (Qiagen). SNP karyotyping was assessed using the Illumina platform and the OMNI-EXPRESS-8v1.6 Chip (Illumina). The Analysis was done using Karyostudio 1.3 (Illumina).

4.1.3 Generation and cultivation of NPCs

NPCs were generated based on a previous report using small molecules (Reinhardt et al., 2013). Briefly, PSCs were detached from matrigel-coated plates using StemPro™ Accutase (Accutase, Thermo Fisher Scientific) and the collected sedimented cells were transferred into ultra-low attachment culture dishes (Corning) or uncoated 6-well plates and kept for two days in ES-based medium (smEB) without FGF2 (PeproTech), supplemented with 0.5 µM purmorphamine (PU; Millipore), 3 µM CHIR 99021 (CHIR; Caymen Chemical), 10 µM SB-431542 (SB; Miltenyi Biotech) and 1µm dorsomorphin (Sigma Aldrich). From day 2 to day 4, the media was switched to N2B27 media consisting of Neurobasal:DMEM/F12 [1:1, Gibco], N2 [1:200, Gibco], B27 without vitamin A [1:100, Gibco] with the addition of 0.5 µM PU, 3 µM CHIR, 10 µM SB and 1 µM dorsomorphin. On day 4 the media was switched to the final maturation media containing N2B27 supplemented with 3 µM CHIR, 0.5 µM PU and 150 µM vitamin C (Sigma Aldrich). On day 6, the suspended cells were transferred onto matrigel-coated well plates

and kept in the maturation media with media exchange every 2 days. NPCs were maintained on this media without RI and used for experiments between passage 7 and 30. NPCs were cultured on matrigel-coated 6-well plates in sm+ medium containing N2B27 supplemented with CHIR, PU and vitamin C. Medium was changed every second day. Cells were enzymatically split into single cells at ratios between 1:4 up to 1:12 using pre-warmed accutase for 5–10 min at RT (until cells detach) and centrifuged at 200 rcf for 3 minutes. The cells were re-suspended in fresh sm+ medium and plated on matrigel-coated 6-well plates. Summary of the media compositions are depicted in section 3.3.5.

4.1.4 Generation and cultivation of neurons

For neuronal differentiation, NPCs between passage 7 and 13 were used. To initiate the differentiation, the media was changed to the N2B27 based media consisting of Neurobasal:DMEM/F12 [1:1], N2 [1:200], B27 with vitamin A [1:100], and the addition of 200 µM vitamin C, 100 ng/mL FGF8 (R&D Systems) and 1µM PU. After 8 days, the media condition was replaced by N2B27 based media with the addition of 200 µM vitamin C, 0.5 µM PU, 500 µM cAMP (StemCells), 10 ng/mL BDNF (MACS Miltenyi Biotech), 10 ng/mL GDNF (MACS Miltenyi Biotech) and 1 ng/mL TGFbeta3 (MACS Miltenyi Biotech). On day 9, cells were split with accutase and seeded on Matrigel-coated plates in N2B27 based media with the addition of 200 µM vitamin, 500 µM cAMP, 10 ng/mL BDNF, 10 ng/mL GDNF, and 1 ng/mL TGFbeta3. The media was changed every 3–4 days and the differentiated cells were kept in culture for 4 weeks up to 8 weeks. General passaging of neurons was not necessary because of their post-mitotic nature. Splitting of neurons was performed to re-plate the neurons on the Matrigel-coated

96-well assay plate or for immunostaining on 24-well plates containing coverslips and coated with matrigel. For this, the old culture media was removed, the cells were gently washed 1x with pre-warmed PBS before incubation with accutase for 3–5 minutes at RT. Accutase activity was diluted using either PBS or culture media and cells were gently centrifuged at 60 rcf. Supernatant was removed and cells were resuspended in culture media, counted using a Neubauer hemocytometer and seeded according to the wanted density in culture media supplemented with 10 µM RI. RI was always added after splitting to promote survival. For analysis, 4- to 8-week-old-neurons were used. Summary of the media compositions are depicted in section 3.3.5.

4.1.5 Microelectrode Array recordings

Microelectrode array (MEA) recordings were conducted using the Maestro system from Axion BioSystems. A 48-well MEA plate with 16 electrodes per well was precoated with 1 mg/ml polyethyleminine (PEI, Sigma-Aldrich) for 1 hour at RT, washed three times with sterile H_20 and air-dried overnight in the cell culture hood. Afterwards, the plate was pre-coated with matrigel by placing a 7 µl drop of matrigel (200 µg/ml) into the center of the well (on top of the electrodes) and incubated for 1 hour at 37°C, 5% CO_2. Remaining coating solution was removed and 80,000–120,000 neurons per well were seeded on the electrodes in each well of the MEA plate by preparing a cell suspension of 7 µl and applying a droplet directly into the center of each well of the MEA plate. Following an incubation of 1 hour at 37°C, 5% CO_2 to ensure settlement of the neurons, 300 µl maturation media was slowly added to each well. Half of the media was refreshed every two days. Two weeks after plating, spontaneous activity was recorded at a sampling rate of 12.5 kHz under controlled conditions (37°C and 5% CO_2) for 10 minutes on

different days. Using Axion Integrated Studio (AxIS 1.4.1.9), a digital low pass filter of 4 kHz and high pass filter of 200 Hz cut off frequency and a threshold of 5.5x the standard deviation was set to minimize false-positives detections. Raw data was analyzed using the Neural Metric Tool (Axion BioSystems) to analyze spikes. Electrodes that measured more than 5 spikes per minute were considered active.

4.2 Molecular biology

4.2.1 Real-Time Quantitative Reverse Transcription PCR (qRT-PCR)

Gene expression analysis was performed by quantitative real-time RT-PCR (qRT-PCR) using SYBR Green PCR Master Mix (Applied Biosystems) according to the manufacturers description and the ViiA™ 7 Real-Time PCR System (Applied Biosystems). RNA isolation and conversion into complementary DNA (cDNA) was performed as described in section 4.2.5.1. For each target gene, cDNA samples and negative controls (100 ng of original total RNA equivalents per 12 µl PCR reaction) were measured in triplicates using 384-Well Optical Reaction Plates (Applied Biosystems). Cycling conditions are depicted in Table 4-A. Relative transcript levels of each gene were calculated based on the $2^{-\Delta\Delta CT}$ method. Data were normalized to the housekeeping genes *GABDH* or *OAZ1* and are presented as mean LOG2 ratios in relation to control cell lines. Primers were for OCT4 F: GTGGAGGAAGCTGACAACAA and R: ATTCTCCAGGTTGCCTCTCA, for NANOG F: CCTGTGATTTGTGGGCCTG and R: GACAGTCTCCGTGTGAGGCAT, for SOX2 F: GTATCAGGAGTTGTCAAGGCAGAG and R: TCCTAGTCTTAAAGAGGCAGCAAAC, for DNMT3B F: GCTCACAGGGCCCGATACTT and R: GCAGTCCTGCAGCTCGAGTTTA, for DPP4 F: TGGTGTCAGGTGGTGTGTGG and R: CCAGGCTTGACCAGCATGAA, for VIM F: GGAGCTGCAGGAGCTGAATG and R: GACTTGCCTTGGCCCTTGAG, for NESTIN F: TTCCCTCAGCTTTCAGGAC and R: GAGCAAAGATCCAAGACGC, for PAX6 F: GAATTCTGCAGACCCATGC and R TCTCGTAATACCTGCCCAG, for SOX1 F: TTGGCATCTAGGTCTTGGCTCA and R: CGGGCGCACTAACTCAGCTT, for SOX2 F:

GTATCAGGAGTTGTCAAGGCAGAG and R: TCCTAGTCTTAAAGAGGCAGCAAAC. qPCR cycler program is depicted in Table 4-A. The list of primers is summarized in Table 3-K.

Table 4-A: qPCR-cycle program

STEP	TEMP	TIME
Hold stage	50°C	120 seconds
Initial Denaturation	95°C	10 minutes
40 Cycles	95°C	15 seconds
	62°C	30 seconds
	72°C	30 seconds/kb
Final Extension	72°C	10 minutes
Melt curve stage	95°C	15 minutes
	62°C	30 seconds
	72°C	30 seconds
	95°C	15 seconds

4.2.2 Mycoplasma test

For mycoplasma testing a PCR based method was used. 9 primers (6 forward, 3 reverse) were used to amplify the 6 most common mycoplasma strains. Supernatant directly taken from the well was used as PCR template, without further isolation of mycoplasma DNA. Supernatant from a contaminated cell line was used as a positive control (provided by AG Kühn, MDC). Following primers were used:

Myco 1 F: CGCCTGAGTAGTACGTTCGC; Myco 2 F: CGCCTGAGTAGTACGTACGC; Myco 3 F: TGCCTGAGTAGTCACTTCGC; Myco 4 F: CGCCTGGGTAGTACATTCGC; Myco 5 F: CGCCTGAGTAGTAGTCTCGC; Myco 6 F: TGCCTGGGTAGTACATTCGC; Myco r1 R: GCGGTGTGTACAAGACCCGA; Myco r2 R: GCGGTGTGTACAAAACCCGA; Myco r3 R: GCGGTGTGTACAAACCCCGA.

The protocol for PCR mix is depicted in Table 4-B and the cycle program in Table 4-C.

Table 4-B: Mycoplasma-PCR reagents and volumes

Mycoplasma-PCR reagent	Volume [µl]
Sample supernatant	2
10x dream tag buffer	2.5
5 mM dNTPs	0.5
DreamTaq DNA Polymerase	0.25
Primer mix	0.5
Nuclease-free water	19.25

Table 4-C: Mycoplasma-PCR cycle program

Temperature [°C]	Time [sec]	cycles
95	180	
95	20	
65	30	x29
72	60	
72	240	
16	∞	

4.2.3 Immunostaining

For Immunocytochemistry, cells were harvested, depending on the cell type, as described before either by enzymatic digestion using accutase for NPCs and neurons or PBS/EDTA for PSCs, plated on matrigel-coated 24-well plates containing cover slips (Thermo Fisher Scientific) until they reached about 70% confluency. Subsequently, the

cells were fixed with 4% PFA (Thermo Fisher Scientific) in PBS for 20 min at RT followed by three washing steps with PBS. To assess the expression of marker proteins the cells were first treated with blocking solution (10% donkey serum [Merck], 1% Triton X-100 [Sigma-Aldrich] in PBS with 0.1% Tween 20 [Sigma-Aldrich]) for 1 hour at RT to permeabilize the fixed cells before incubation with the primary antibodies. The primary antibodies were diluted in blocking solution over night at 4°C. Primary antibodies were used as follows: NANOG (R&D Systems, 1:100), OCT4 (Santa Cruz, 1:300), NESTIN (Millipore, 1:200), PAX6 (Covance, 1:200), SOX2 (Santa Cruz, 1:100), DACH1 (ProteinTech, 1:100), TUJ-1 (Sigma-Aldrich,1:1000), GFAP (Synaptic Systems, 1:500), NURR1 (Sigma Aldrich, 1:500), TH (Millipore, 1:300), FOXA2 (Sevenhills, 1:100), TRA-1-60 (Millipore, 1:200), MAP2 (Synaptic System, 1:1000). The primary antibodies were removed the next day and washed 3 x with PBS-T for 5 minutes on a shaker (60–80 rpm) before applying the corresponding secondary antibodies (Invitrogen, Alexa Fluor, 1:300 in blocking solution; Cy2, Cy3, Cy5 Sigma Aldrich, Merck Millipore, 1:300 in blocking solution) and cell nuclei marker Hoechst 33342 (Thermo Fisher Scientifics, diluted 1:2500 in blocking solution) for 1 hour at RT in the dark. Finally, cells were washed three times with PBS-T for 5 min on a shaker and stored in PBS at 4°C. Plates were protected from light and the fluorescence was detected under the inverted microscope Olympus IX70. For further images, the coverslips were mounted in mounting medium (IMMU-MOUNT ™, Thermo Scientific) and visualized with the Zeiss Axio Imager Z1 confocal microscope in combination with AxioVision V4.6.3.0 software (Zeiss). Images were merged and further processed using Adobe Photoshop CS6. A list of the primary and secondary antibodies used in this study are depicted in Table 3-N and Table 3-O.

4.2.4 CRISPR/Cas9 Genome Editing

For genome editing a CRISPR/Cas9 plasmid vector containing specific guide RNA (gRNA) targeting the *KLB* gene to induce *KLB* gene knockout was designed. Plasmid preparation and cloning was performed by Tobias Hahn (Master student) and guided by Dr. Pawel Lisowski. Transient transfection of the control iPSC line (XM001) was performed by Josefin Conrad with the help of either Tobias Hahn or me. Cell harvesting and seeding of the cells after fluorescence-activated cell sorting (FACS) was performed by me. The FACS sorting itself was performed with the help of the FACS core facility at MDC. Details on contribution are depicted in section 7.

First, we designed the oligos based on gRNA sequences designed by Feng Zhangs laboratory (Sanjana et al., 2014) as a pair of complementary sequences whose orientation matched that of the DNA target. We annealed the oligomers and cloned them into the pU6-(BbsI)sgRNA_CAG-eCas9-venus-bpA plasmid (Addgene ID 86986) encoding the enhanced specificity variant eSpCas9 (eSpCas9(1.1) plasmid; Addgene ID 71814) (Slaymaker et al., 2016) with reduced off-target effects and robust on-target cleavage, sgRNA, and a fluorescent Venus reporter by BbsI restriction enzyme overhangs with N1–N20 of the selected eCas9 target sequence under the expression of the sgRNAs by the human U6-promoter.

The sgRNA was cloned into the pU6-(BbsI) sgRNA_CAG-eCas9-venus-bpA plasmid by ligation using T4 Ligase (4 µl vector [~100 ng], 1.5 µl annealed oligos. 1.5 µl 10x ligation buffer, 1.5 µl T4 Ligase and filled up to 15 µl with nuclease-free water).

To increase iPSC survival after eCas9-induced double-strand break (DSB) cleavage transient BCL-XL overexpression was applied. Components of BCL-XL plasmid was kindly provided by Dr. Xiao-Bing Zhang from State Key Laboratory of Experimental

Hematology, Tianjin, China. Cloning of BCL-XL plasmid was kindly provided by Dr. Pawel Lisowski. Primer and oligonucleotide sequences are depicted in Table 3-L. Background information on the plasmids used is depicted in section 3.3.8.

4.2.4.1 Transient transfection of iPSC line XM001

Transient transfection of corresponding plasmids was performed on the iPSC-line XM001. Cells were grown in feeder-free conditions in iPS-Brew in a 6-well culture plate. One day before transfection, cells were dissociated using accutase and seeded in a concentration of ~ 1 x 10^5 cells per well on a matrigel-coated 6-well plate as single cells or small clumps in iPS-Brew supplemented with 10µM RI. Lipofection was performed using the Lipofectamine 3000 kit according to the manufacturer's protocol (Thermo Fisher Scientific). Plasmids were diluted to 2 mg DNA in 125 ml of Opti-MEM reduced serum medium (Gibco). The DNA-lipid complex was dropwise added to one well of a 6-well plate with the addition of 5 µM RI to the culture medium and incubated overnight at 37°C, 5% CO_2. Media was changed the following day and cells were kept until fluorescence-activated cell sorting.

4.2.4.2 FACS sorting of transfected iPSCs

Cells were dissociated with accutase, washed with 1x PBS, and resuspended in FACS media (section 3.3.5). Cells were filtered using polystyrene test tubes with cell strainer (falcon). FACS-based cell sorting using FACSAria III (BD) was performed with the help of the MDC FACS Facility. Venus-positive cells were sorted and recovered in mTESR supplemented with 1x Penicillin-Streptomycin (P/S) (Invitrogen) and 10 µM RI.

Cells were plated on matrigel-coated 6-well plates containing MEFs. Once the sorted cells recovered, cells were seeded in low density (500-1000 cells/well) under feeder-free conditions to assure single colony formation.

4.2.4.3 Single cell seeding, colony formation and colony picking

FACS sorted cells were dissociated using accutase and seeded in low density on matrigel coated 6-well plates (500-1000 cells/well) and cultured until small colonies formed. Small colonies were picked under the microscope (Leica M80) before merging with neighboring colonies and transferred into a new well of a 24-well plate coated with matrigel containing fresh mTESR and 10 µM RI. Single colonies were further cultured in mTESR and once reaching ~60–80% confluency, half of the colony was removed under the microscope by simple scratching and prepared for Sanger Sequencing.

4.2.5 Sanger Sequencing

Sample preparation for Sanger sequencing was performed using either DNARelease additive (Phire Animal Tissue Direct PCR Kit, Thermo Scientific) and a modified protocol (collect supernatant, centrifuge at 1000g for 3 min, wash with 1 ml PBS, centrifuge at 1000g for 3 min, dilute in 20 µl dilution buffer and add 0.5 µl DNARelease additive, incubate for 3 min at RT, incubate 2 min at 98°C and run the PCR or store at -20°C for later use) or the FlexiGene DNA-isolation Kit (Qiagen) according to the manufacturer's guidelines. PCR for genomic DNA was performed using AmpliTag Gold® 360 Master Mix (Thermo Fisher Scientific) according to manufacturer's

guidelines. The protocol for PCR reaction mix is depicted in table Table 4-D and the PCR-cycle program is depicted in Table 4-E.

Table 4-D: AmpliTag Gold PCR reaction mix

Component	Volume per 25 µl reaction	Final concentration
PCR-grade water	variable	
360 GC enhancer	1 µl	N/A
Primer F	1.25 µl	0.5 µM
Primer R	1.25 µl	0.5 µM
AmpliTag Gold® 360 Master Mix	12.5 µl	1X
DNA	variable	50-100 ng
Total PCR volume	25 µl	

Table 4-E: PCR-cycle program

Stage	Step	Temp.	Time
Holding	Activation of AmpliTag Gold® 360 Master Mix	95°C	10 min
35 cycles	Denature	95°C	30 sec
	Anneal	55°C	30 sec
	Extend	72°C	60 sec/kb
Holding	Final extension	72°C	7 min

Holding	Final hold	4°C	pause

Samples were screened for positive bands (1028bp) and sent for sequencing containing 11 µl of DNA sample (100 ng/µl) and primer (10 µM/µl). Primers for KLB-KO sequencing are summarized in Table 3-L.

4.2.5.1 RT-PCR for KLB expression in PSCs and PSC-derived neurons

Total RNA from the control embryonic stem cell line H1, human liver (clontech # 636531) and PSC-derived neurons was isolated using the RNeasy Mini Kit (Qiagen) and quality-checked by Nanodrop analysis (Nanodrop Technologies). cDNA was generated using the Moloney Murine Leukemia Virus (M-MLV) Reverse Transcriptase kit (Thermo Fisher) according to the manufacturers protocol. Briefly, RNA (1 µg) of each sample was diluted in 9 µl of RNase-free water and mixed with 1 µl of oligo-dT-primer (0.5µg/µl; 15mer) to a final volume of 11 µl and incubated for 5 min. at 65°C. For subsequent reverse transcriptase, 9 µl of the RT-PCR master mix (Table 4-F) was added to the RNA-oligo-dT mix (11 µl) and incubated at 37°C for 60 minutes. To inactivate the reaction, samples were heated at 70°C for 5 minutes. Synthesized cDNA was stored at -20°C for subsequent PCR.

Table 4-F: Master Mix for RT-PCR

Reagent	Volume [µl]
5X Reaction Buffer	4µl
RiboLock RNase Inhibitor (20 U/µl)	1µl
dNTP Mix (10mM)	2µl
M-MLV-RT (20 U/µl)	2µl

The protocol for PCR mix using Q5 High-fidelity DNA polymerase (NEB) is depicted in Table 4-G, and the cycle program in Table 4-H. The following primer were used for PCR and are additionally depicted in Table 3-L:

KLB_1 F: GAGGGGATGAGAAAGAAG;
KLB_1 R: GAGGGGATGAGAAAGAAG;
KLB_3 F: AGAGGGGATGAGAAAGAA;
KLB_3 R: GAGAGACCAGGCAGTATAA.

Table 4-G: Reaction setup for one reaction (25µl volume)

COMPONENT	25 µl REACTION
5X Q5 Reaction Buffer	5 µl
10 mM dNTPs	0.5 µl
10 µM Forward Primer	1.25 µl
10 µM Reverse Primer	1.25 µl
Template DNA	variable
Q5 High-Fidelity DNA Polymerase	0.25 µl
Nuclease-Free Water	Fill up to 25 µl

Table 4-H: PCR-cycle program

STEP	TEMP	TIME
Initial Denaturation	98°C	30 seconds
	98°C	10 seconds
35 Cycles	55°C	30 seconds
	72°C	30 seconds/kb
Final Extension	72°C	2 minutes
Hold	4°C	

4.3 Mitochondrial Neuronal Health (MNH) assay

HCA-based quantification of mitochondrial membrane potential and neuronal profiling was assessed using the CellInsight CX7 high-content analysis (HCA) platform (CellInsight CX7, Thermo Fisher Scientific) and the HCS Studio™ Cell Analysis Software with integrated BioApplications (Thermo Fisher Scientific). Briefly, 4-8-week-old neurons were split using accutase and seeded at a density of 10,000–20,000 cells/ on matrigel-coated 96 well plates with black-wall and clear-bottom (µClear, Corning). The cells were live-stained with 0.5 nM TMRM (ThermoFisher) for 30 minutes at 37°C and 5% CO_2 and counterstained with 1:10,000 Hoechst (Thermo Fisher). Staining solution was removed and neurons were washed three times gently with 1x PBS before corresponding phenolred-free media was applied and cells were measured at the CellInsight CX7. Images were obtained using the CellInsight CX7 and analyzed using the HCS Studio Cell Analysis Software and the "Cellomics CellHealthProfiling v4 BioApplication" quantifying the TMRM signal which accumulates in active mitochondria as a result of the MMP.

Afterwards, neurons were fixed with 4% PFA for 15 minutes at RT, stained with TUJ1 antibody and counter-stained with Hoechst (see section 4.2.3). The morphological changes of TUJ1-postive cells were quantified using the HCS Studio Cell Analysis Software and the "Cellomics Neuronal Profiling v4 BioApplication" (Thermo Fisher Scientific).

4.3.1 Protocol parameters for HCA-based MNH assay

Assay data were acquired on the CellInsight CX7 with a 10x and 20x objective and software autofocus configured for fully automated plate scanning. Eight fields were acquired per well. All images were automatically analyzed using the HCS Studio Cell Analysis Software to identify nuclei, MMP and neurite segments.

For MMP quantification the protocol parameters were set as follows: primary object detection (cell nuclei) was based on Hoechst staining, captured in channel 1. Detection of the cellular region of interest, captured in channel 2, was based on TMRM staining which accumulates in active mitochondria as a result of the MMP. Changes in TMRM intensity within the region of interest (ring region with adjusted threshold) were quantified using the "Cellomics CellHealthProfiling v4 BioApplication" using the feature "MeanTargetAvgIntensityCh2". For neuronal profiling quantification the protocol parameters were set as follows: primary object detection (cell nuclei) was based on Hoechst staining, captured in channel 1. Detection of the region of interest (neurites) was based on TUJ1 staining, captured in channel 2. The morphological changes of TUJ1-postive cells were quantified using the "Cellomics Neuronal Profiling v4 BioApplication" Features obtained with the BioApplication used for evaluation of the neuronal branching complexity were:

"NeuriteTotalCountPerNeuronCh2," "NeuriteTotalLengthPerNeuronCh2," and "BranchPointTotalCountPerNeuronCh2". Further information on cellular targets, channels, staining method, and emission spectra can be seen in Table 4-I. Furthermore, cell properties and BioApplication features corresponding to the cellular target are depicted in Table 4-J, and a more detailed description of the features is described in Table 4-K.

Table 4-I: Cellular targets and dyes used for HCA-based MNH assay.

Cellular target	Channel	Dye /antibody	Fluorophore emission
Nucleus	1	Hoechst 3342	Blue (350 nm)
Mitochondrial transmembrane potential (MMP)	2	TMRM	Red-orange (574 nm)
Neurites	2	Primary antibody: TUJ1 Secondary antibody: Alexa Fluor 647	Far-red (663 nm)

Table 4-J: HCA-based cell properties and BioApplication for MNH assay.
Adapted from Cell Health Profiling V4 and Neuronal Profiling V4 – BioApplication Guide

Cellular target	Properties	Cell Health Profiling Feature
Nucleus	Detect primary object – quality control and acute toxicity	Valid object count
MMP	Determine average intensity of mitochondria labelled with TMRM that accumulates in mitochondria as a result of the MMP Detection of moderate toxicity	MEANTargetAvgIntenCh2 (measurement region= Ring)
Neurites	Detect neurite -count, -length, branch points, % of TUJ1	ValidNeuronCount NeuriteTotalCountperNeuron NeuriteTotalLengthperNeuron BranchPointTotalCountperNeuron

Table 4-K: HCA-based BioApplication features for MNH assay.
Adapted from Cell Health Profiling V4 and Neuronal Profiling V4 – BioApplication Guide

Target	Feature	Description
Nucleus	CellHealthProfiling: ValidObjectCount	Number of valid objects identified in the well (based on Ch1 – Hoechst)
MMP	CellHealthProfiling: Mean_TargetAvgIntenCh2	Average intensity of TMRM of all pixels within target mask (ring)
Neurite count	NeuronalProfiling: NeuriteTotalCountPerNeuronCh2	Total number per neuron of all neurites selected for analysis in the field
Neurite length	NeuronalProfiling: NeuriteTotalLengthPerNeuronCh2	Total length per neuron (in micrometers) of all neurites selected for analysis in the field
Branch points	NeuronalProfiling: BranchPointsTotalCountPerNeuron	Total number per neuron of all branch points belonging to all neurites selected for analysis in the field

Methods

Z-factors were calculated using the formula:

$$z - factor = 1 - \frac{3(\sigma p + \sigma n)}{|\mu p - \mu n|},$$

where σ represents the means and μ the standard deviations of the positive (p) and negative (n) controls. For calculating the Z-factor, oligomycin-treated wells were used as positive controls and FCCP together with antimycin A-treated wells as negative controls.

4.3.2 Ethanol exposure and treatment of neurons

FCCP and Ant.A, or Oligomycin were applied to 4- to 8-weekold neurons together with the staining solution (0.5 nM TMRM and 1:10,000 Hoechst) and incubated for 30 min at 37°C, 5% CO_2. Staining solution containing FCCP and Ant.A, or Oligomycin was removed and neurons were washed three times gently with 1x PBS before corresponding phenolred-free media was applied and cells were measured at the CellInsight CX7. Exposure to ethanol was performed 5 days after re-plating 4-8-week-old neurons on black-wall, round bottom 96-well plates (μClear, Corning). 99.5% ethanol (v/v; Roth) was prediluted in culture media as 5 M stock solution freshly before use. Accordingly, 10 mM–2.5 M ethanol was further diluted in phenolred-free culture media and administered to the neurons. For the chronic ethanol exposure, freshly prepared culture media containing ethanol was changed every other day at the same time for 7 days including one day of withdrawal. Evaporation of alcohol following daily media changes in unsealed culture plates may provide a pattern of exposure more similar to alcohol consumption observed in human daily heavy drinkers. After 7 days of ethanol exposure, neurons were stained with 0.5 nM TMRM and 1:10,000 Hoechst. Following the removal of the staining

solution, media containing ethanol was reapplied and incubated again for 1 hour before assessment of the mitochondrial neuronal health using the CellInsight CX7.

For the acute ethanol exposure, neurons were first stained with 0.5 nM TMRM and 1:10,000 Hoechst before freshly prepared phenolred-free culture media containing ethanol was administered to the neurons for 1 hour at 37°C, 5% CO_2. After the incubation time, neurons where immediately processed at the CellInsight CX7. Drug treatment (flavoxate, disulfiram, baclofen and lithium) was performed on 4- to 8-week-old neurons with incubation overnight at 37°C, 5% CO2. The next day, staining solution containing 0.5 nM TMRM and 1:10,000 Hoechst was added to the media for 30 min at 37◦C, 5% CO2.

4.3.2.1 Apoptosis/ Annexin V

The Annexin V intensity as indicator for apoptosis was assessed using the CellInsight CX7 and the integrated "CellHealthProfiling" BioApplications. Briefly, 4-8-week-old neurons were split using accutase and seeded at a density of 10,000–20,000 cells/well on matrigel-coated 96 well plates with black-wall and clear-bottom (µClear, Greiner). The cells were live-stained with 5 µl Annexin V per 10^6 cells for 30 minutes at 37°C and 5% CO_2 and counterstained with 1:10,000 Hoechst. Images were obtained with the CellInsight CX7 and quantified using the HCS Studio Cell Analysis Software. For quantification of the Annexin V intensity the protocol for quantifying TMRM intensity (see section 4.3.1) was modified according to the Annexin V staining.

4.3.3 Compound screening – MNH assay

For the proof-of-concept compound screening, 48 compounds were selected from a library of 700 FDA-approved drugs based on their use for neurological diseases (Selleckchem- z65122, Table 9-A) and 5 drugs were added, used in the context of AUD treatment. Briefly, 10,000–20,000 neurons/well were plated on 96-well plates (Corning) 5 days before adding the compounds overnight. The compounds were used in a final concentration of 0.5 µM diluted in culture media. The DMSO concentration was diluted down below 0.05%. The second day, neurons were stained with 0.5 nM TMRM together with 1:10,000 Hoechst diluted in phenol red-free culture medium for 30 min at 37°C, 5% CO_2 by adding the staining solution into the media containing the drugs. After removal of the staining solution, compounds together with 1 M ethanol were applied to the neurons and incubated for 1 hour at 37°C, 5% CO_2. Control wells included neurons kept untreated as well as neurons treated with 1 M ethanol only. Image acquisition was conducted with the HCA platform CellInsight CX7 and analyzed using the “Cell Health Profiling” and “Neuronal Profiling” BioApplications. The same screening was repeated twice, and the values shown in Fig. 23 represent the mean values of the two runs (mean, +/- SD). The list of compounds is depicted in the supplementary Table 9-A.

5. Results[2]

5.1 Generation of human neurons from hESCs and iPSCs for the evaluation of ethanol-induced neuronal toxicity

In order to obtain human neurons from iPSCs, I first generated small molecule neural progenitor cells (NPCs) following a small molecule-based protocol through the formation of embryoid bodies (EBs) (Reinhardt et al., 2013) (Fig. 8A). NPCs are multipotent stem cells that can efficiently differentiate into central nervous system cell types, including neurons and glia (oligodendrocytes and astrocytes). The use of only small molecules for self-renewal and expansion of NPCs enables the generation of large amounts of NPCs with reduced cost. The NPC approach thus is beneficial for following HCA applications.

I obtained NPCs from a control iPSC line XM001, which was derived from female fibroblasts using episomal reprogramming (Helmholtz Zentrum München, IDR) (Wang et al., 2018), and a control hESC line H1 (Thomson et al., 1998), which was obtained from a male donor and purchased from WiCell (WiCell, USA) and used according to the German law (license from Robert Koch Institute AZ: 3.04.02/0077-E01).

[2] The text and figures of the results section have been reused with modifications from the published version: Zink A, Conrad J, Telugu NS, Diecke S, Heinz A, Wanker E, Priller J and Prigione A (2020). Assessment of Ethanol-Induced Toxicity on iPSC-Derived Human Neurons Using a Novel High-Throughput Mitochondrial Neuronal Health (MNH) Assay. *Front. Cell Dev. Biol*. 8:590540. https://doi.org/10.3389/fcell.2020.590540.

Results

To initiate neural induction in EBs, the bone morphogenic protein (BMP) inhibitor dorsomorphin (DM), and the transforming growth factor ß (TGFß)-signaling inhibitor SB43152 (SB) were supplemented to the basic media (sm-, see section 3.3.5). At the same time, purmorphamine (PU) and CHIR99021 (CHIR) were added to the media to stimulate the sonic hedgehog (SHH) signaling pathway, inhibit the glycogen synthase kinase-3 (GSK3), and activate the canonical WNT signaling (Chambers et al., 2009; Kim et al., 2010). After the first days in the induction medium, EBs formed neuroepithelial structures (Fig. 8B). EBs were gently dissociated and seeded on Matrigel-coated plates for further differentiation and purification. NPC morphology was homogenous after 4-6 passages post neural induction (Fig. 8B). NPCs expressed the neural progenitor markers NESTIN, PAX6, and DACH1, as well as the multipotent neural stem cell marker SOX2, the pan-neuronal marker TUJ1, and traces of MAP2, a protein primarily present in the human brain (Fig. 8C). Even though weak expression of MAP2 in NPCs is often observed, high values are more likely associated with more mature neurons (Izant and McIntosh, 1980; Dehmelt and Halpain, 2004). Hence, the cells which are MAP2 positive may indicate a differentiation towards mature neurons. TUJ1 can more likely be defined as an early pan-neuronal marker instead of an indicator for terminally differentiated neurons. Hence, expression of TUJ1 is not necessarily an indicator for a differentiation towards neurons. NPCs retained their multipotent identity over multiple passages (>30) as well as after freezing and thawing without changes in cell morphology. It was possible to use NPCs between passage 7 and 30.

Quantitative real-time RT-PCR (qRT-PCR) confirmed the relative gene expression of NPC markers *SOX1*, *SOX2*, *NESTIN* and *PAX6*, which were stably expressed in NPCs starting around passage 10 (Fig. 8D). Importantly, the pluripotency markers *OCT4*,

NANOG, *DNMT3B,* and *DPPA4* were downregulated in NPCs compared to the original iPSCs at the undifferentiated level.

Differentiation into neurons was induced in NPCs between passage 7–20 and at around 80% of confluence. Neural induction was induced by PU together with FGF8 for 8 days to activate the SHH and stimulate the formation of ventral midbrain cells including midbrain dopaminergic neurons. After 8 days the media was exchanged to N2B27 containing PU, ascorbic acid (vitamin C), the TGFß, dibutyryl cyclic adenosine monophosphate (dbcAMP), and the neurotrophic factors brain-derived neurotrophic factor (BDNF) and glial cell line-derived neurotrophic factor (GDNF). Starting from day 10, PU was removed, and the maturation medium was exchanged every 2-3 days containing vitamin C, BDNF, GDNF, TGFß and dbcAMP (Fig. 8A). Detailed media formulations can be found in section 3.3.5. Changes in cell morphology became visible within the first 10 days of differentiation. Neurons were kept in the maturation medium for up to 8 weeks. Immunostainings confirmed the expression of the pan-neuronal marker TUJ1, the neuronal marker MAP2, as well as the dopaminergic markers TH, NURR1, and FOXA2 (Fig. 8F). Neurons were stable over at least 8 weeks in culture without the addition of glial cells, suggesting the presence of a mixed culture. From a previous study (Inak-Girrbach, 2019, dissertation), we know that the neurons derived using our small molecule-based protocol also include glial cells and NPCs (data not shown). Quantitative analysis of the percentage of generated neurons using the CellInsight CX7 HCA platform (Thermo Fisher) showed that overall 75% of the cells were TUJ1-positive and around 20% expressed TH (Fig. 8E). Neurons were robust enough to tolerate enzymatic splitting using Accutase® (accutase), which enabled the transfer of cells into various plate types for numerous approaches.

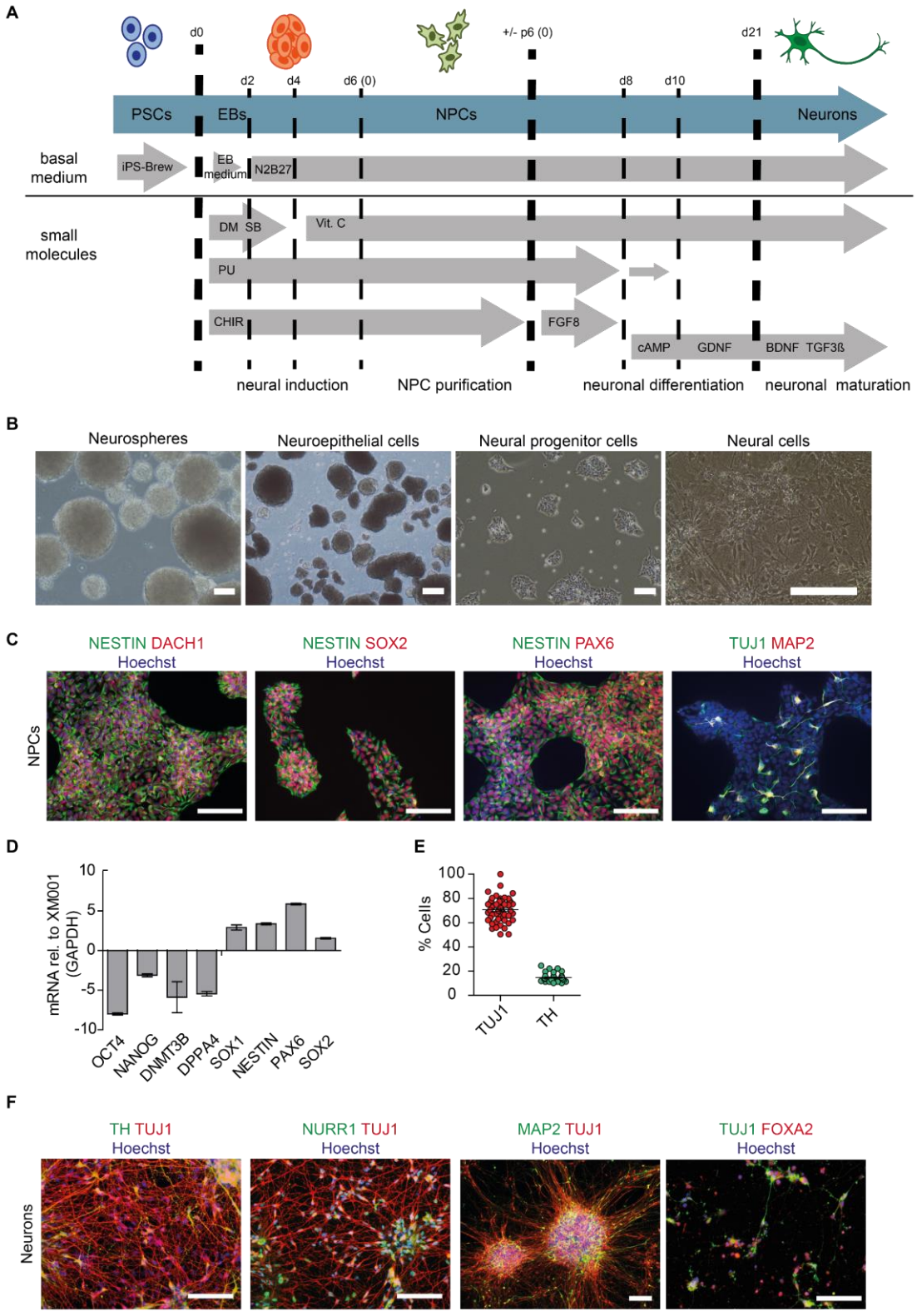

Fig. 8: Generation and characterization of NPCs and neurons.
(A) Schematic of the protocol for the generation of small molecule-based neural progenitor cells (NPCs) and neurons. **(B)** Microscopic images of the different stages starting from neurospheres and neuroepithelial cells over neural progenitor cells into neurons. **(C)** Immunocytochemistry of

NPCs stained for neural progenitor associated markers NESTIN, DACH1, PAX6 and SOX2, the pan-neuronal marker TUJ1 and the neuronal marker MAP2. Scale: 100µm. **(D)** Quantitative real-time reverse transcription PCR (qRT-PCR) of neural progenitor markers including *SOX1, NESTIN, PAX6 SOX2* and the pluripotency markers *OCT4, NANOG, DNMT3B* and *DPPA4*. Transcription levels in NPCs were normalized to the housekeeping gene *GAPDH* (mean=SD +/- ; n= 3 technical replicates) and compared to the expression in undifferentiated iPSCs (XM001). **(E)** HCA-based quantification of TUJ1 and TH percentage (%) of the overall culture. **(F)** Immunocytochemistry of neurons expressing TUJ1, TH, NURR1, MAP2 and FOXA2 counterstained with Hoechst. Scale: 100µm.

To assess neuronal functionality, I aimed to establish the microelectrode array (MEA) scan analysis (Axion BioSystems). For this, 4-8-week-old neurons were plated on the MEA-plate and spontaneous activity was measured on different days for 10 minutes each under controlled conditions (37°C, 5%, CO_2). Since this system was not yet established in the lab, different densities of neurons ranging from 80,000 cells to 200,000 cells per MEA well were tested (Fig. 9A). Neurons plated at a density of 100,000 cells gave the most promising results. Nevertheless, results for the mean firing rate varied between different wells of the MEA plate (Fig. 9B). Several batches of neurons were measured, and spontaneous activity (mean firing rate) could be observed in some wells (Fig. 9C and Fig. 9D). The batch-to-batch variability might also be explained by the fact that neurons left in the MEA plates for several weeks started to partially detach from the plates. Nevertheless, we are confident that the derived neurons were functionally active, since whole-patch-clamp recordings performed by colleagues demonstrated the presence of action potentials and post-synaptic currents (Inak-Girrbach, 2019, dissertation).

Results

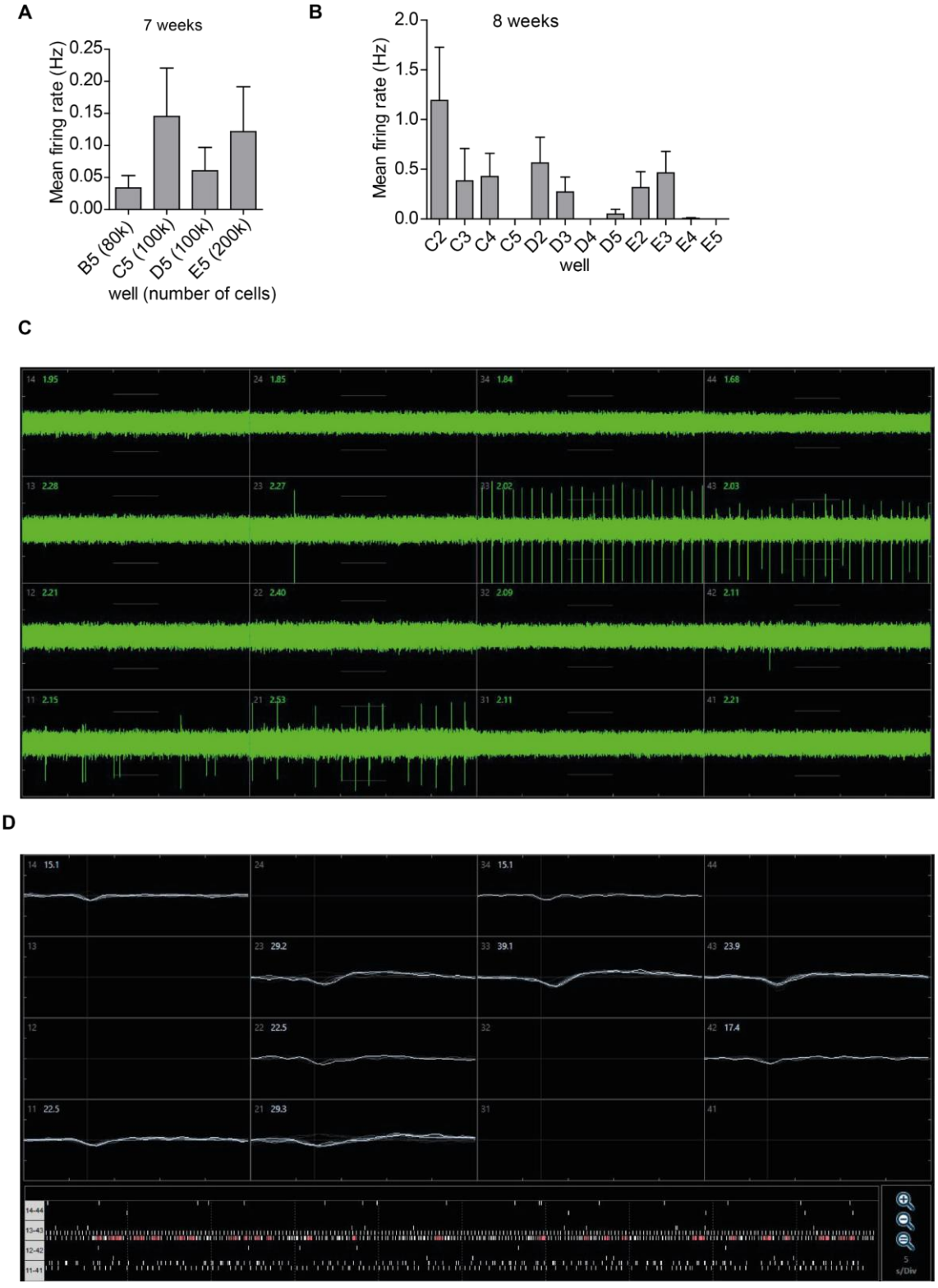

Fig. 9: MEA recordings of 7-8-week-old neurons from control iPSCs (XM001).
(A) MEA recordings of mean firing rate (Hz) of 7-week-old neurons derived from control iPSCs (XM001) seeded in different cell densities (80,000, 100,000 and 200,000). **(B)** Exemplary MEA recoding of mean firing rate of 8-week-old neurons derived from control iPSCs (XM001). Graph shows values obtained from different wells (wells C, D and E). **(C-D)** Representative recordings

of spike plot (**C**) and wave plot (**D**) of network-based electrophysiological properties of control neurons after 8 weeks in culture using MEA.

5.2 Establishment of the Mitochondrial Neuronal Health (MNH) assay

In the publication from Lorenz et al. 2017, I performed a compound screening on iPSC-derived NPCs obtained from patients with Leigh syndrome (Lorenz et al., 2017). The screening was based on HCA of the MMP. For this current study, I set out to optimize the MMP assay and adapt it on neurons as possible readout for the evaluation of neuronal health following ethanol exposure. To reach this goal, I combined the HCA assay evaluating MMP with another HCA assay measuring neuronal growth complexity. We dubbed the multiplexed HCA assay as mitochondrial neuronal health (MNH) assay.

To carry out the MHN assay, I used the CellInsight CX7 HCA platform from ThermoFisher Scientific. The platform combines fluorescence microscopy, image processing, and automated cellular measurements, thereby enabling the quantitative analysis of physiological processes within cells in a high-throughput manner. Image processing is based on the HCS Studio™ Cell Analysis Software using BioApplications. For the evaluation of the MMP, the "Cell Health Profiling" BioApplication was used (Cellomics® Cell Health ProfilingV4, BioApplication, Thermo Scientific). For the evaluation of neuronal health, the "Neuronal Profiling" BioApplication was used (Cellomics® Neuronal Profiling V4, BioApplication, Thermo Scientific).

5.2.1 Neuronal branching

To enable a reliable quantification of neuronal branching complexity, I observed that neurons must be sufficiently sparse to allow discriminating each cell body and its

respective neurites. Keeping the neurons rather sparse also reduced the possibility of clump formation which also affects the detection of cell bodies (Fig. 10).

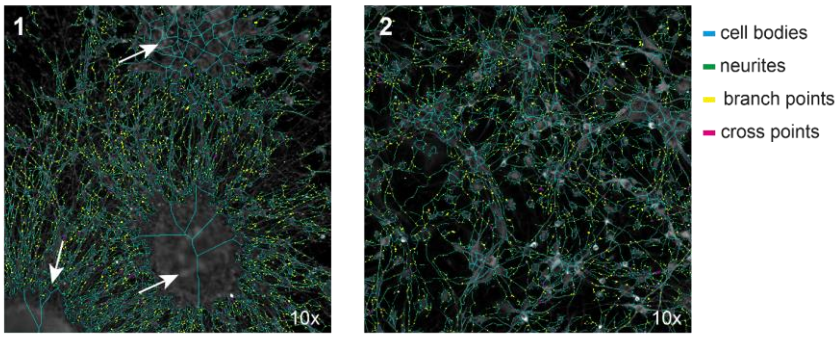

Fig. 10: Neurite detection using the Cellomics® Neuronal Profiling V4.
(A) Image 1, very dense neurons tend to form cluster (white arrows), which disable the algorithm to discriminate between different cell bodies and fails to assign the neurites to a single cell body. Image 2, sufficiently sparce neurons allow the discrimination of each cell body and its respective neurites. Cell bodies were detected based on the Hoechst signal and neurites based on staining with the antibody TUJ1. Images were taken with the CellInsight CX7 microscope with 10x magnification. Cell bodies are depicted in blue, neurites in green, branch points in yellow and cross points in magenta.

When neurons are plated very densely, the software cannot distinguish the boarders of the cell body correctly, and thus it cannot assign the neurites to a defined cell (Fig. 10, white arrows). On the other hand, when neurons were plated too sparsely, the neuronal survival was dramatically affected. I experimentally determined that neurons should be between 10,000–20,000 cells per well to generate reliable results.

Neurons were kept for 4-8 weeks before starting analysis. Within the first days after neuronal induction of the NPCs, cells strongly proliferated. This made it difficult to predict the final density after 4 up to 8 weeks in the assay plate. Therefore, neurons were cultured in 6-well plates coated with matrigel during the neuronal induction, and re-plated on the 96-well assay plate (black wall, clear bottom, Greiner) only after the maturation

stage. To determine the time-point for the measurement after re-plating, the neurons were re-plated after 4 weeks, and then fixed after 1 day or after 5 days (Fig. 11A).

I then sought to validate whether the neurite outgrowth assay could distinguish between cells that form neurites, like mature neurons, and cells that do not form neurites, like NPCs. NPCs and neurons were stained with Hoechst 33342 (Hoechst, Molecular Probes) to mark the nuclei, and with the antibody tubulin beta III (TUJ1) to identify neuronal processes (Fig. 11B). TUJ1 plays a role in neuronal cell differentiation and is present in the cell body, dendrites, axon, and axonal terminations (Memberg and Hall, 1995). The HCA images were obtained with the CellInsight CX7 microscope and analyzed using the "Neuronal Profiling" BioApplication. Neuronal and non-neuronal cells were identified in channel 1 based on the cell nuclear stain Hoechst (Fig. 11B, above). Information gained from channel 1 included nuclear features, such as size, shape, and intensity. Neurons and neuronal-like cells were identified in channel 2 by indirect immunofluorescence using the primary antibody TUJ1, and Alexa Fluor 647 (Molecular Probes) as secondary antibody (Fig. 11B, below). The TUJ1 staining provided information about cell body features, such as size, shape, and intensity, as well as about neurite features, such as count, size, intensity, branch, and cross point counts. Since TUJ1 does not enable the discrimination between dendrites and axons, any projection from the cell body was simply considered as neurites (without connotations related to dendrites or axons).

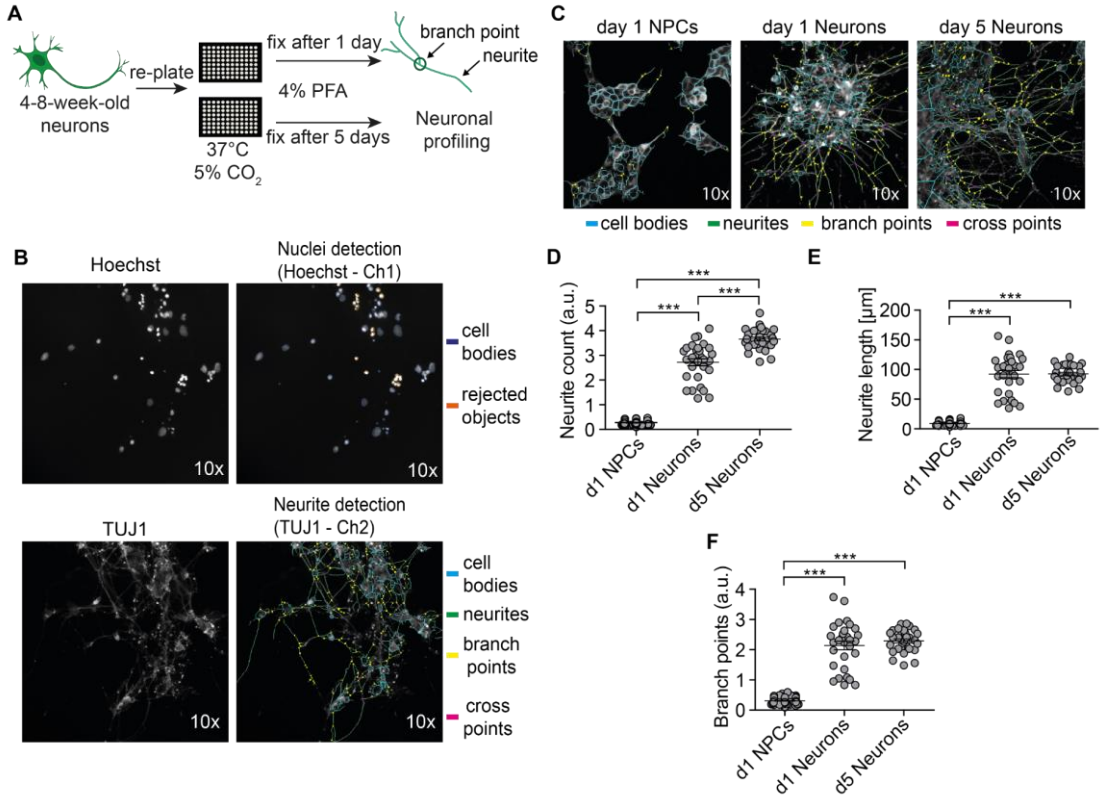

Fig. 11: HCA-based quantification of neuronal branching.
(A) Schematic workflow for the quantitative evaluation of neuronal profiling. **(B)** Representative images of nuclei detection and neurite detection using the "Neuronal Profiling" BioApplication. Cell bodies depicted in dark blue (channel 1), rejected objects in orange, cell bodies in light blue (channel 2), neurites in green, branch points in yellow and cross points in magenta. Images were taken at 10x magnification using the CellInsight CX7. **(C)** Representative images of NPCs and 4-8-week-old neurons fixed after day 1 and neurons fixed after day 5. Cell bodies depicted in blue, branch points in yellow, neurites in green and cross points in magenta. All images were taken at 10x magnification using the CellInsight CX7. **(D-F)** HCA-based quantification of neurite count (**D**), neurite length (**E**) and branch points (**F**) from NPCs and 4-8-week-old neurons 1 and 5 days (d) after re-plating on the assay plate. n= 1 independent experiment with 30 replicates for neurons and 60 replicates for NPCs). Each dot represents the value obtained from one well (mean +/- SEM; ***p< 0.001; one-way ANOVA followed by Dunnett`s multiple comparison test).

Day 5 NPCs were excluded from the measurement since they overgrew the plate and images could not be processed with the protocol in a meaningful way. NPCs kept for one day after re-plating (day 1 NPCs) showed no or only short neurites (marked in green) and no branch points (yellow) or cross points (magenta) compared to neurons kept for one day (day 1 Neurons) and five days (day 5 Neurons) after re-plating (Fig. 11C).

Quantitative analysis using the "Neuronal Profiling" BioApplication confirmed the observed findings (Fig. 11D-F). Day 1 NPCs had almost no neurites, whereas day 1 neurons exhibited around 2-3 neurites per neuron (Fig. 11D). NPCs also showed only very short or no neurites (values below 10 µm), while day 1 neurons and day 5 neurons formed neurites with around 100 µM neurite length per neuron in average (Fig. 11E). These experiments confirmed that the HCA-based neuronal outgrowth assay can determine the number and size of neurites and can identify mature neuronal populations. I then analyzed the differences in the neuronal population at day 1 and day 5 (Fig. 11D-F**)**. Neurons showed in average 2 branch points per neuron at both day 1 and day 5 (Fig. 11F). At day 5, neurons exhibited around 3-4 neurites per neuron (Fig. 11D). Compared to day 1 neurons, day 5 neurons formed more neurites and longer neurites, and exhibited more branch points. Moreover, the values obtained for day 5 neurons on neurite count (Fig. 11D), neurite length (Fig. 11E), and branch points (Fig. 11F) were less variable and more homogenous compared to day 1 neurons. This suggested that neurons required more than one day after re-plating to form a homogenous culture. In fact, day 5 neurons showed more robust features of neuronal maturity. For this reason, I performed all further measurements with neurons kept for at least five days after re-plaiting before analysis.

5.2.2 Mitochondrial membrane potential (MMP)

To assess MMP changes, I used the potentiometric fluorescent dye tetramethylrhodamine methyl ester (TMRM, Thermo Fisher Scientific), which accumulates in active mitochondria of living cells. The TMRM signal diminishes during MMP depolarization, an effect which can be seen for example during apoptosis.

Results

MMP modulators, carbonylcyanide p-trifluoromethoxyphenylhydrazone (FCCP), antimycin A (Ant.A) and oligomycin, were used to test the sensitivity of the assay. Depolarization of the MMP was induced using the mitochondrial oxidative phosphorylation uncoupler FCCP together with antimycin A (Ant.A), an inhibitor of mitochondrial respiration. FCCP increases the proton permeability across the intermembrane matrix (IMM) and disconnects the electron transport chain from the formation of ATP (Dispersyn et al., 1999). Ant.A blocks the respiratory chain complex III and therefore prevents oxidation of NADH (Campo et al., 1992). Collectively, the drugs disrupt the MMP and lead to a depolarized state. Oligomycin in turn acts by blocking the F0 subunit of the ATP synthase, leading to the reduction of the electron flow across the electron transport chain (Symersky et al., 2012).

To quantify changes in MMP upon stimulation with FCCP+Ant.A and oligomycin, 4-8-week-old neurons were re-plated on the assay plate (matrigel-coated 96-wp; black wall, clear bottom, Greiner). The neurons were kept for 5 days before the assay to ensure homogenous branch formation. On the day of the assay, neurons were live-stained with a non-quenching concentration of 0.5 nM TMRM (Perry et al., 2011) for 30 minutes at 37°C, and counterstained with 1:10,000 Hoechst. At the same time, the modulators FCCP+Ant.A or oligomycin in different concentrations were added to the cells (0.005–200 µM) (Fig. 12A). The staining solution containing the MMP modulators was removed, and neurons were washed 1x with PBS before measurement. Images were obtained and quantified with the CellInsight CX7 in a high-content manner. Exemplary images of staining with 0.5 nM TMRM showed decrease in TMRM intensity after exposure to 200 µM FCCP+200 µM Ant. A, and an increase in TMRM intensity after exposure to 200 µM oligomycin (Fig. 12B). To quantify the changes in TMRM intensity, the HCA-

platform CellInsight CX7 was used (Fig. 12**C**). Accordingly, cell bodies were identified based on Hoechst staining. To exclude potential debris and dead cells from the measurement, the threshold for cell identification was set to reject very small objects, big objects and objects that appeared very bright. A region of interest (ROI, purple circles, Fig. 12C) was defined by setting a ring around the cell nuclei. Within the ROI, the average intensity of the TMRM signal accumulating in the mitochondria was measured based on a defined threshold. Quantification of the TMRM intensity was conducted based on the "Cell Health Profiling" BioApplication using the feature "MEANTargetAvgIntenCh2". This feature enables to determine the average intensity of TMRM accumulating in mitochondria depending on the MMP.

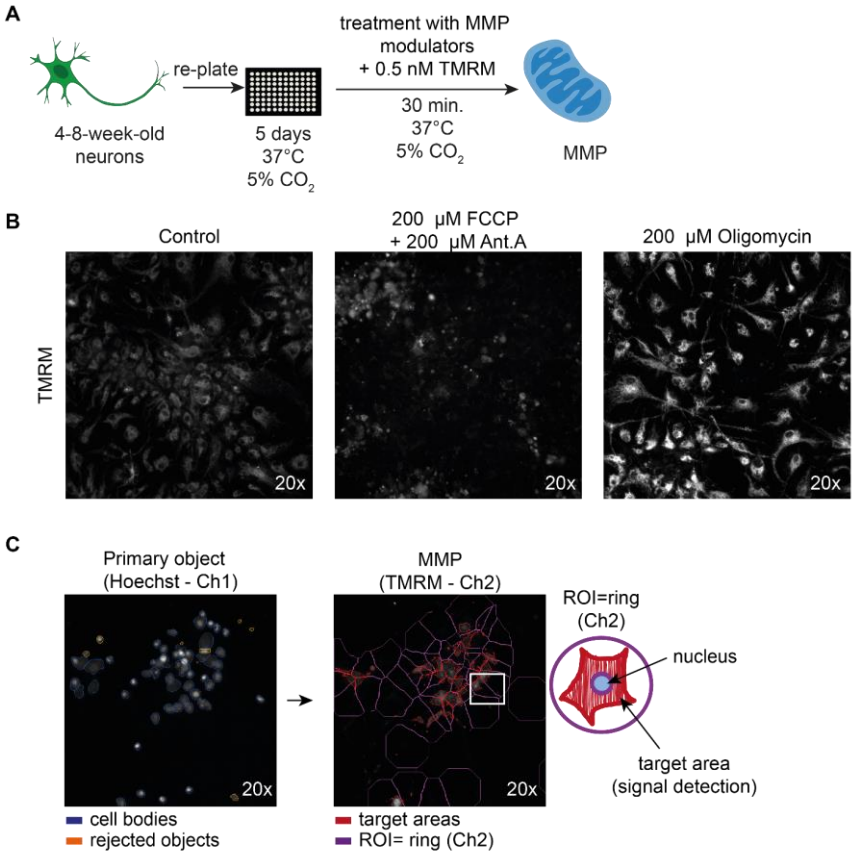

Fig. 12: HCA-based quantification of MMP.

(A) Schematic of the workflow to quantitatively measure MMP in 4-8-week-old neurons upon exposure to MMP modulators. **(B)** Exemplary images of neurons stained with 0.5 nM TMRM and treated with either 200 µM FCCP + 200 µM antimycin A (FCCP+Ant.A) or 200 µM oligomycin. Images were taken using the CellInsight CX7 with 20x magnification. **(C)** Exemplary images showing the detection principle of the primary objects and the MMP using the "Cell Health Profiling" BioApplication. Cell bodies are depicted in blue based on Hoechst staining detected in channel 1 (Ch1), rejected objects are depicted in orange. The target areas, based on TMRM signal are detected in channel 2 (Ch2) and depicted in red. The region of interests (ROI), defined using the ring feature, are depicted in purple.

5.2.3 The MNH assay

HCA-based quantification of MMP of 4-8-week-old neurons treated with different concentrations of FCCP+Ant.A confirmed their depolarizing properties. The drugs provoked a decrease in the MMP in a dose-dependent manner, with significant values starting at 1 µM FCCP+Ant.A (Fig. 13A). Conversely, the adenosine triphosphatase (ATPase) inhibitor oligomycin caused an expected increase in MMP, which became hyperpolarized in a dose-dependent manner starting at 10 µM (Fig. 13B). The MMP modulating effects of the mitochondrial modulators are in line with previous publications (Kalbáčová et al., 2003; Li et al., 2014). The results indicate that the assay can detect changes in the MMP upon stimulation in a dose-dependent manner.

A statistical indicator for HT bioassays regarding reproducibility and robustness is defined by the z-factor. A bioassay is considered marginal if the z-factor is below 0.5 and excellent if between 0.5 and 1 (Zhang et al., 1999). At 200 µM FCCP+Ant.A versus 200 µM oligomycin the assay suggests excellent features with a z-factor of 0.747 (Fig. 13B). The z-factor is defined as:

$$z - factor = 1 - \frac{3(\sigma p + \sigma n)}{|\mu p - \mu n|}$$

μ_p represents the mean values of the positive control (oligomycin) and μ_n represents the mean values of the negative control (FCCP+Ant.A). σ_p is the standard deviation of the positive control, and σ_n the standard deviation of the negative control.

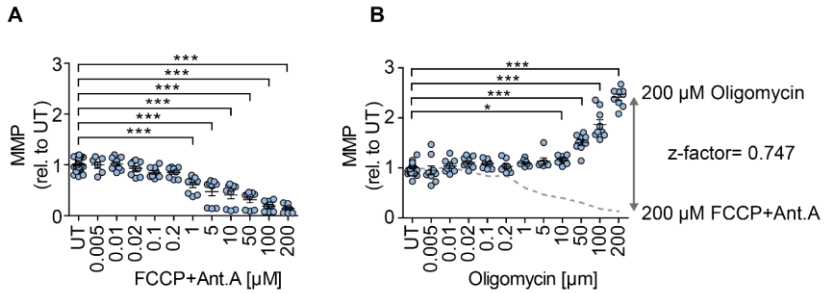

Fig. 13: HCA-based quantification of MMP after exposure to modulators.
(A) HCA-based quantification of MMP in 4-8-week-old neurons from control hESC (H1) treated with increasing concentrations of FCCP and antimycin A (FCCP+Ant.A; 0.005 µM – 200 µM; mean +/- SEM; ***p<0.001; one-way ANOVA followed by Dunnett`s multiple comparison test). Each dot represents values obtained from one well (n= 3 independent experiments), normalized to the corresponding untreated control (UT) exposed to the assay media only. **(B)** HCA-based quantification of MMP in 4-8-week-old neurons from control hESC (H1) treated with increasing concentrations of oligomycin (0.005 µM – 200 µM; mean +/- SEM; *p<0.05, ***p<0.001; one-way ANOVA followed by Dunnett`s multiple comparison test). Each dot represents values obtained from one well (n= 3 independent experiments), normalized to the corresponding untreated controls (UT) exposed to the assay media only. Assessment of the z-factor of 0.747 obtained at 200 µM FCCP and 200 µM Ant.A versus 200 µM oligomycin suggesting an excellent assay.

After live-staining with TMRM, neurons were fixed with 4% paraformaldehyde (PFA) for 15 minutes and immunostained with TUJ1 to measure the neuronal health during exposure to the uncouplers FCCP+Ant.A or oligomycin (Fig. 14A). The neurite count, neurite length, and branch points remained unchanged during exposure to increasing concentrations of oligomycin (Fig. 14E-G). Exposure to FCCP+Ant.A only led to shortening of the neurites (Fig. 14C) and reduction of branch points (Fig. 14D) starting at 200 µM. Neurite count remained unchanged (Fig. 14B).

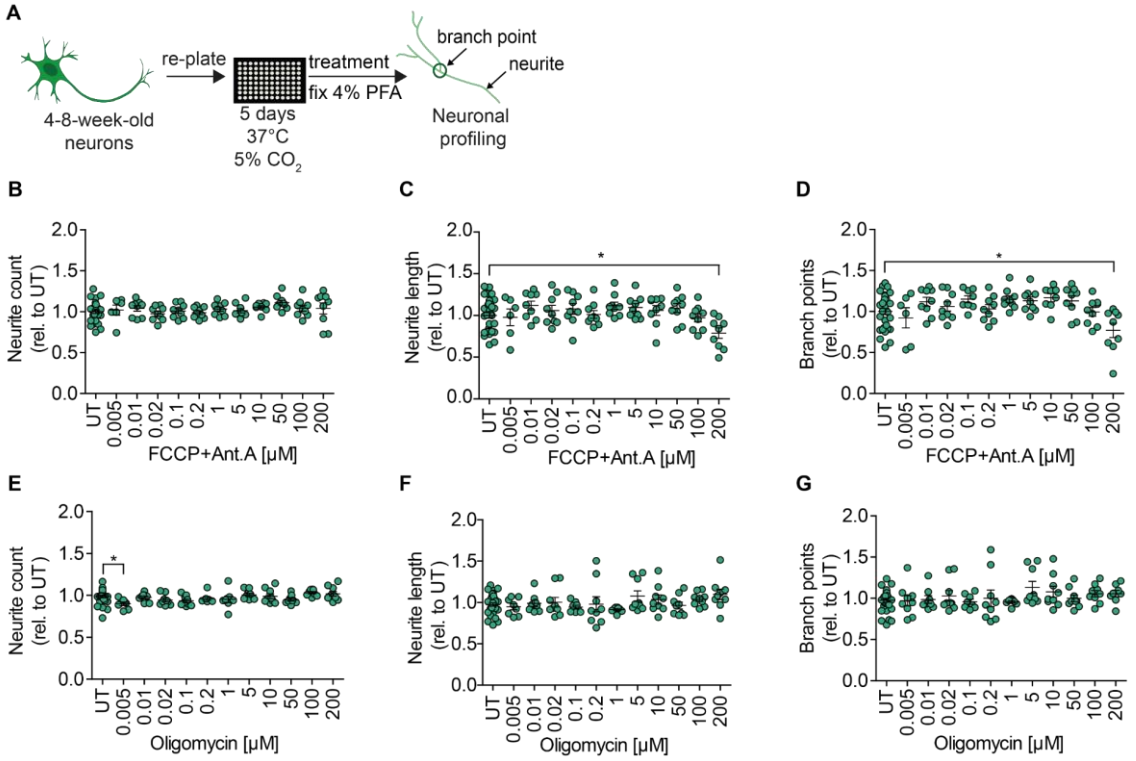

Fig. 14: HCA-based quantification of neuronal branching after exposure to modulators. **(A)** Schematic of the assay workflow for the quantification of the neuronal profiling. **(B-D)** HCA-based quantification of neuronal profiling including neurite count (**B**), neurite length (**C**) and branch points (**D**) in 4-8-week-old neurons from control hESC (H1) treated with increasing concentrations of FCCP and antimycin A (FCCP+Ant.A; 0.005 – 200 µM; mean +/- SEM; *p<0.05). Each dot represents values obtained from one well (n= 3 independent experiments), normalized to the corresponding untreated controls (UT) exposed to the assay media only. **(E-G)** HCA-based quantification of neuronal profiling including neurite count (**E**), neurite length (**F**) and branch points (**G**) in 4-8-week-old neurons from control hESC (H1) treated with increasing concentrations of oligomycin (0.005 – 200 µM; mean +/- SEM; *p<0.05). Each dot represents values obtained from one well (n= 3 independent experiments), normalized to the corresponding untreated controls (UT) exposed to the assay media only.

Overall, it was possible to quantitatively identify changes in the MMP and neuronal outgrowth using the MNH assay. The data suggest that changes in the MMP can be quantified based on the intensity of TMRM accumulating in active mitochondria. Together with the neuronal branching outgrowth, the evaluation of the MMP may serve as features to determine the overall health of neurons, where the MMP may serve as early indicator for cell death.

Fig. 15 summarizes the final workflow of the HCA-based MNH assay, which combines live-cell measurement of MMP with quantification of neuronal outgrowth. The MNH assay can be divided into 5 main parts.

1. Generation of neurons starting from PSCs. After maturation, neurons are plated on the HCA assay plate. The ideal plate is a black wall, clear bottom plate, which ensures optimal conditions for image acquisition and enables the possibility to check the morphology of the neurons.

2. Live-cell staining with TMRM and Hoechst. The staining can be performed either before treatment, simultaneously, or after the treatment, depending on the experimental settings. In the experiments (Fig. 12, Fig. 13 and Fig. 14) for stimulation with FCCP+Ant.A or oligomycin, the exposure to the modulators was performed simultaneously to the TMRM staining.

3. Image acquisition and quantification at the CellInsight CX7 HCA platform. After washing and removal of the TMRM dye, the plates are loaded into the HCA platform and image acquisition on live-cells is started. The images are quantified using the "Cell Health Profiling" BioApplication either simultaneously with the image acquisition or afterwards.

4. Staining with TUJ1. After the live-cell image acquisition, neurons are fixed with 4% PFA and immunostained with TUJ1 antibody and counterstained with Hoechst.

5. Image acquisition and quantification at the CellInsight CX7 HCA platform. After washing and removal of the antibody staining, the plates are loaded into the HCA platform and image acquisition on fixed cells is started. The images are quantified using the "Neuronal Profiling" BioApplication either simultaneously with the image acquisition or afterwards.

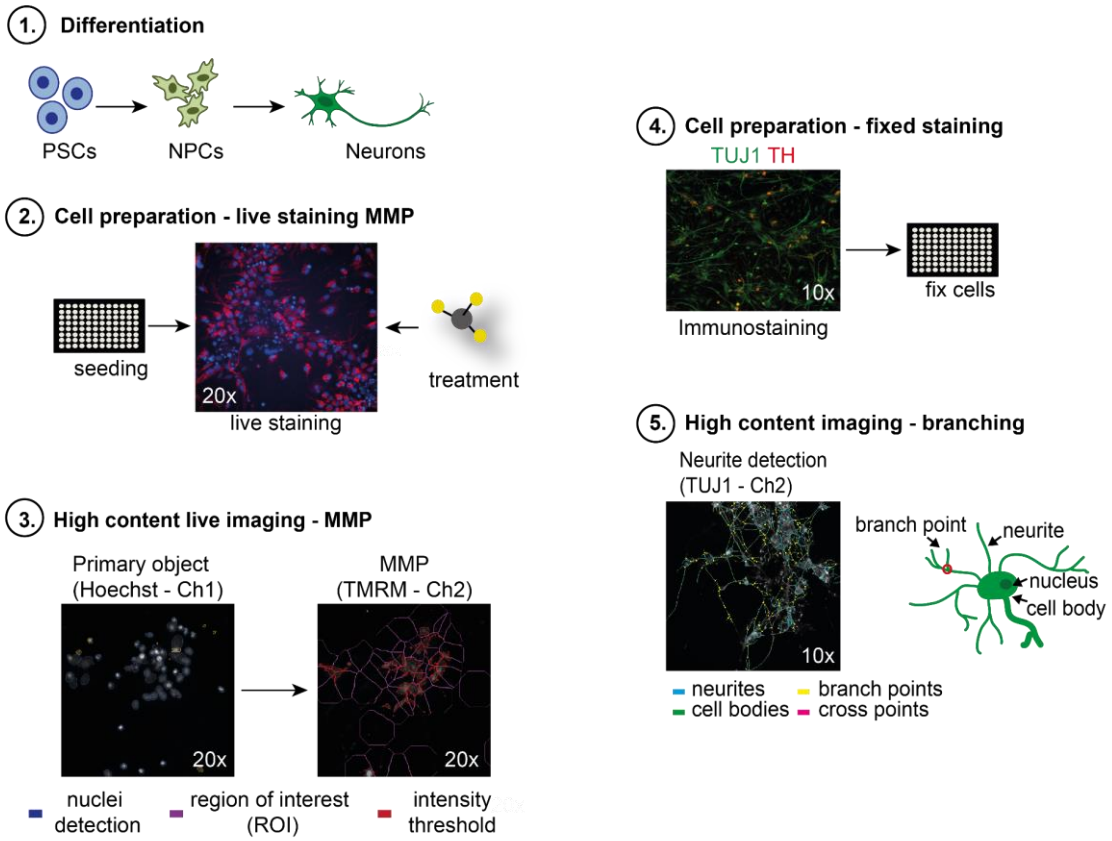

Fig. 15: Schematic workflow of the MNH assay
1. PSCs are differentiated into NPCs and neurons; 2. Neurons are live-cell stained with TMRM and exposure to modulators or treatment with compounds can be performed; 3. HCA-based quantification of the MMP using the "Cell Health Profiling" BioApplication; 4. Fixation of the neurons with 4% PFA and subsequent staining with TUJ1; 5. HCA-based quantification of the neuronal branching complexity using the "Neuronal Profiling" BioApplication.

5.3 Applying the MNH assay to quantify the effects of ethanol on human neurons

Using the MNH assay, I was able to assess the uncoupling effect of FCCP+Ant.A on MMP in a dose dependent manner, and to monitor the neuronal branching complexity. I therefore aimed to apply the MNH assay to investigate the effects of ethanol on human neurons.

For the assessment of ethanol toxicity on human neurons, I used 4-8-week-old neurons derived from the control iPSC line XM001. Neurons were plated on the assay plates and kept for 5 days before analysis with media changes every 2 days. Neurons were exposed to increasing doses of ethanol for either 7 days, to mimic chronic ethanol intake, or only 1 hour, to mimic acute ethanol intake.

A wide range of ethanol concentrations was picked to evaluate the effects of different concentrations starting from 10 mM to 2.5 M. The presumed physiological range of ethanol for *in vitro* studies is 10–100 mM, while the addition of ethanol to cell cultures has been reported in the 1 to 500 mM range (Dolganiuc and Szabo, 2009). As mentioned in the introduction, ethanol-related effects on brain function can occur already at blood alcohol concentrations (BAC) below 10 mM. However, values of BAC higher than 300 mM have been reported in AUD individuals (Johnson et al., 1982). In the following experimental setting, ethanol evaporation may occur inside the incubator during the exposure. This means that the final ethanol concentration on the neurons may be lower than the one measured before the exposure.

Ethanol was pre-diluted into the cell media as a 5 M stock concentration starting from 99.5% ethanol (v/v, Carl Roth) freshly before each experiment, and further diluted in media accordingly. Old media was aspirated completely and exchanged with fresh media containing ethanol in the indicated concentration. Image acquisition and quantification was performed using the CellInsight CX7 without temperature and CO_2 control. The total image acquisition time for the plate in the CellInsight CX7 did not exceed 30 minutes.

5.3.1 MNH assay-based quantification of the effects of chronic ethanol exposure

It is known that long-term ethanol exposure has detrimental effects on neuronal and glial function (Nath et al., 2012). To model chronic ethanol exposure on neurons, 4-8-week-old neurons were treated with increasing ethanol concentrations ranging from 10 mM–2.5 M for 7 days with media changes every 24 hours.

Neurons were cultured for 4-8 weeks, re-plated on the assay plates, and kept for 5 days prior to the assay. 5 days after re-plating, neurons were treated with ethanol for 7 days, with full media exchange for 6 days. On the day of the assay, neurons were stained with TMRM for MMP and Hoechst for nuclei determination. Afterwards, ethanol was added to the neuronal cultures. In this manner, ethanol remained present during the image acquisition with the CellInsight CX7 microscope. After assessment of the MMP, neurons were fixed and stained using an antibody against the pan-neuronal marker TUJ1 (Fig. 16A). This staining allowed to quantify neuronal branching growth and complexity.

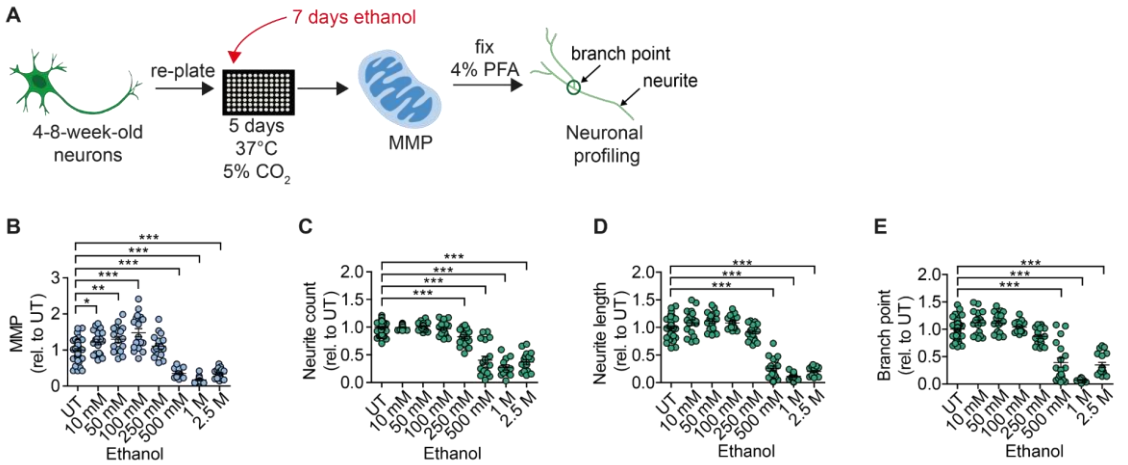

Fig. 16: MNH assay-based quantification of neuronal health after chronic ethanol exposure. **(A)** Schematic of the MNH assay workflow for chronic (7 days) ethanol exposure. **(B)** MNH assay-based quantification of the MMP in 4-8-week-old neurons from control iPSC (XM001) treated for 7 days (chronic) with increasing concentrations of ethanol (10 mM–2.5 M; mean +/- SEM; *p<0.05, **p<0.01, ***p<0.001; one-way ANOVA followed by Dunnett`s multiple comparison test). Each dot represents values obtained from one well (n= 3 independent experiments), normalized to the corresponding untreated controls (UT) exposed to the assay

media only. **(C-E)** MNH assay-based quantification of the neuronal profiling including neurite count (**C**), neurite length (**D**), and branch points (**E**) in 4-8-week-old neurons from control iPSC (XM001) treated for 7 days (chronic) with increasing concentrations of ethanol (10 mM–2.5 M; mean +/- SEM; ***p<0.001; one-way ANOVA followed by Dunnett`s multiple comparison test). Each dot represents values obtained from one well (n= 3 independent experiments), normalized to the corresponding untreated controls (UT; exposed to the assay media only).

After the 7-day exposure to ethanol, I observed that the MMP increased in neurons exposed to increasing doses of ethanol between 10 mM up to 100 mM (Fig. 16B). However, MMP collapsed for ethanol doses equal or higher than 500 mM. This suggested that at 500 mM ethanol concentration, neurons started to experience toxicity and loss of cellular health. Concentrations below 250 mM did not change the branching complexity (Fig. 16C-E). Instead, ethanol concentrations of 250 mM and above modulated the branching complexity significantly, leading to a decrease in the neurite count starting at 250 mM (Fig. 16C). Shortening of neurite length (Fig. 16D) and reduction in neurite branch points (Fig. 16E) became evident starting at 500 mM ethanol. The decrease in branching complexity at ethanol concentrations of 500 mM ethanol and above is in line with the response observed for MMP. This may suggest that ethanol concentrations starting at 500 mM over 7 days negatively modulate mitochondrial neuronal health.

Taken together, the MNH assay showed that neurons undergo morphological and functional changes in response to chronic ethanol exposure starting at 500 mM ethanol concentrations.

5.3.2 MNH assay-based quantification of the effects of acute ethanol exposure

Following the observed MMP stress response after chronic ethanol exposure for 7 days, I aimed to determine whether a toxicity effect of ethanol could occur already after

acute (1 hour) exposure. Healthy control neurons derived from one iPSC line (XM001) and one hESC line (H1) were cultured for 4-8 weeks, re-plated on the assay plates, and kept for 5 days prior to the assay. On the day of the assay, neurons were stained with TMRM for MMP, and Hoechst for nuclei detection. The neurons were treated for 1 hour with different ethanol concentrations supplemented into the media. MMP was quantified using the CellInsight CX7. After assessment of MMP, neurons were fixed and stained using TUJ1 antibody to quantify neuronal branching (Fig. 17A).

After acute exposure to different ethanol concentrations, a small upregulation of MMP for 10 mM ethanol in hESC-derived neurons was observed (Fig. 17G). Ethanol concentrations of 500 mM and above led to a dose-dependent reduction of the MMP in iPSC- and hESC derived neurons (Fig. 17C and Fig. 17G**)**. Additionally, NPCs generated from XM001 were exposed for 1 hour to ethanol and screened for changes in MMP (Fig. 17K). A dose-dependent MMP decrease was also observed in NPCs, starting at 1 M ethanol (Fig. 17L).

Neurite count exhibited a dose-dependent decreased upon exposure to ethanol concentrations starting at 250 mM and above for iPSC-derived neurons (Fig. 17D) and starting at 500 mM and above for hESC-derived neurons (Fig. 17H). A dose-dependent decrease of the neurite length was observed starting at 500 mM ethanol for iPSC- and hESC-derived neurons (Fig. 17E and Fig. 17I). The number of branch points decreased starting at 500 mM ethanol for iPSC-derived neurons (Fig. 17F), and from 1 M ethanol for hESC-derived neurons (Fig. 17J).

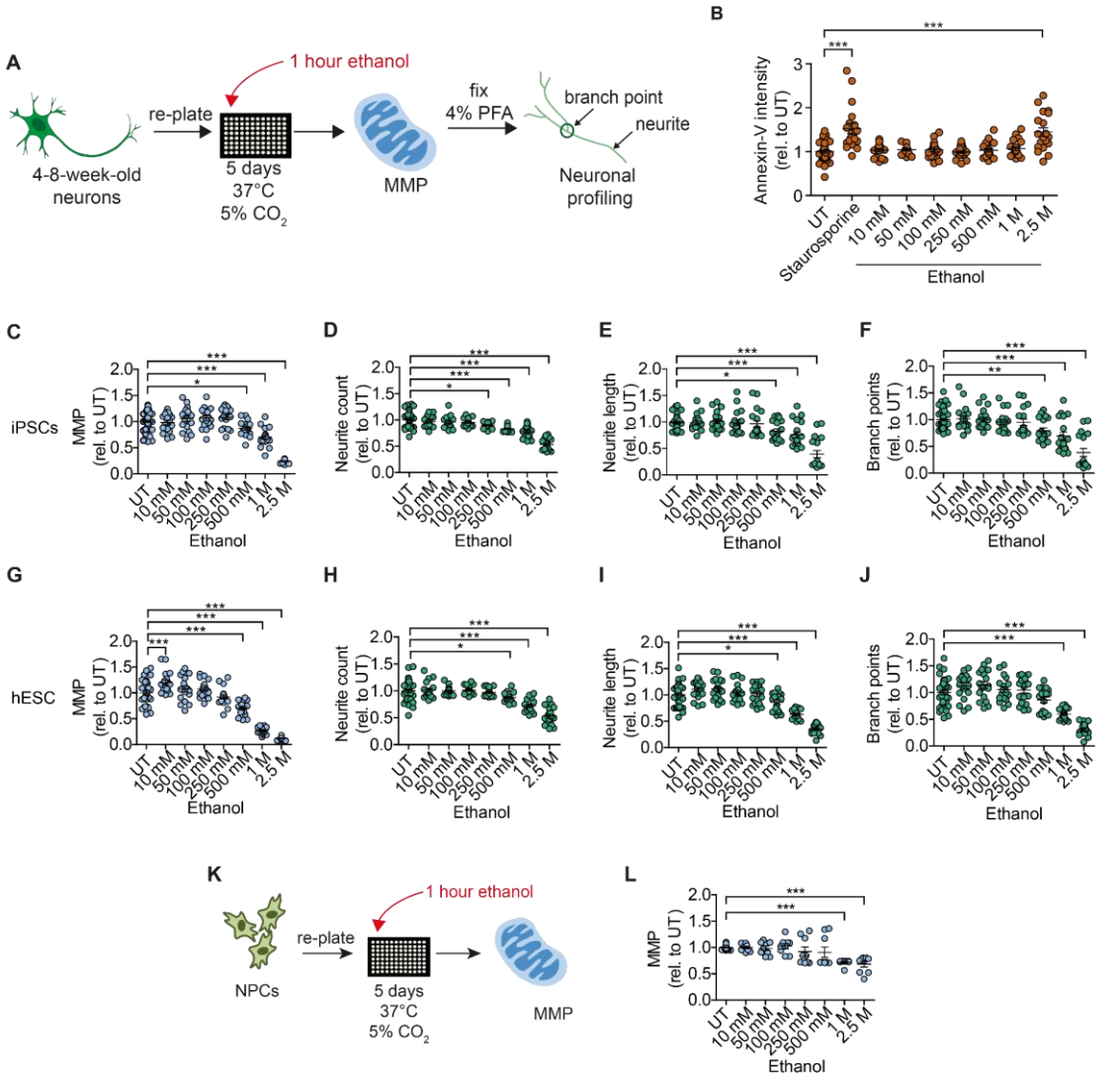

Fig. 17: MNH assay-based quantification of neuronal health after acute (1 hour) ethanol exposure.

(A) Schematic of MNH assay workflow for acute (1 hour) ethanol exposure on neurons. **(B)** Quantification of the Annexin V intensity of 4-8-week-old neurons from control iPSCs (XM001) exposed to ethanol for 1 hour (mean +/- SEM ***p<0.001; one-way ANOVA followed by Dunnett`s multiple comparison test). Control wells included untreated neurons (UT) and neurons treated with 1 µM staurosporine for 1.5 hours. Each dot represents values obtained from one well (n= 4 independent experiments) normalized to UT controls exposed to the assay media only. **(C)** MNH assay-based quantification of MMP in 4-8-week-old neurons from control iPSC (XM001) treated for 1 hour (acute) with increasing concentrations of ethanol (10 mM–2.5 M). Each dot represents values obtained from one well (n= 3 independent experiments; mean +/- SEM; *p<0.05, ***p<0.001; one-way ANOVA followed by Dunnett`s multiple comparison test), normalized to the corresponding untreated controls (UT) exposed to the assay media only. **(D-F)** MNH assay-based quantification of neuronal profiling including neurite count (**D**), neurite length (**E**) and branch points (**F**) in 4-8-week-old neurons from control iPSC (XM001) treated for 1 hour with increasing concentrations of ethanol (10mM–2.5M). Each dot represents values obtained from one well (n= 3 independent experiments; mean +/- SEM; *p<0.05, **p<0.01, ***p<0.001;

one-way ANOVA followed by Dunnett`s multiple comparison test), normalized to the corresponding untreated controls (UT) exposed to the assay media only. **(G)** MNH assay-based quantification of MMP in 4-8-week-old neurons from control hESC (H1) treated for 1 hour with increasing concentrations of ethanol (10mM–2.5M). Each dot represents values obtained from one well (n= 3 independent experiments, mean +/- SEM; ***p<0.001; one-way ANOVA followed by Dunnett`s multiple comparison test), normalized to the corresponding untreated controls (UT) exposed to the assay media only. **(H-J)** MNH assay-based quantification of neuronal profiling including neurite count (**H**), neurite length (**I**) and branch points (**J**) in 4-8-week-old neurons from control hESC (H1) treated for 1 hour with increasing concentrations of ethanol (10 mM–2.5 M). Each dot represents values obtained from one well (n= 3 independent experiments, mean +/- SEM; *p<0.05, ***p<0.001; one-way ANOVA followed by Dunnett`s multiple comparison test), normalized to the corresponding untreated controls (UT) exposed to the assay media only. **(K)** Schematic of MNH assay workflow of acute (1 hour) ethanol exposure on NPCs. **(L)** MNH assay-based quantification of MMP in NPCs from control iPSCs (XM001) treated for 1 hour with increasing concentrations of ethanol (10 mM–2.5 M). Each dot represents values obtained from one well (n= 3 independent experiments mean; +/- SEM; ***p<0.001; one-way ANOVA followed by Dunnett`s multiple comparison test), normalized to the corresponding untreated controls (UT) exposed to the assay media only.

Overall, the MMP and branching after acute ethanol exposure recapitulated observations made after chronic exposure, with a dose-dependent decrease in MMP polarization for 500 mM–2.5 M ethanol, and a dose-dependent decrease in branching capacity for 500 mM–2.5M ethanol for iPSC and hESC lines.

To evaluate the rate of apoptosis upon ethanol exposure on neurons, the Annexin V intensity was quantified using HCA. Annexin V is an intracellular protein that can bind to phosphatidylserine (PS) in the presence of physiological calcium concentrations. PS is found on the intracellular leaflet of the plasma membrane in healthy cells. During apoptosis, PS translocates to the external leaflet and Annexin V can bind. Annexin V staining does not enable to discriminate between apoptosis and necrosis. 4-8-week-old neurons were re-plated on the assay plate and kept for 5 days before applying the Annexin V dye. Control wells were treated with 1 µM staurosporine for 1.5 hours before staining with Annexin V. Staurosporine is a protein kinase inhibitor that induces cell death through

intrinsic apoptotic pathways (Hingorani et al., 2011). For detection of the Annexin V intensity, the protocol for TMRM-intensity used in the MNH assay was modified accordingly. Exposure to 1 µM staurosporine for 1.5 hours significantly increased the Annexin V intensity compared to untreated control neurons, and apoptotic cell death, based on Annexin V intensity only occurred in neurons exposed to 2.5 M ethanol concentration (Fig. 17B). Hence, in the experimental settings neurons retained their viability even after exposure of relative high concentrations of ethanol.

Taken together, neurons derived from PSCs consistently showed a dose-dependent decrease in MMP polarization and branching complexity upon ethanol exposure. Importantly, the changes observed after chronic ethanol exposure could be recapitulated after acute ethanol exposure. Moreover, negative modulations in MMP and branching complexity occurred for lower ethanol concentrations than necessary to initiate widespread apoptotic cell death. This suggest that the negative effects of ethanol on mitochondrial and neuronal health in human neurons may occur rapidly. Overall, the MNH assay enables to capture early stages of toxicity that may still be revertible.

5.4 Generation of AUD-iPSCs and differentiation into NPCs and neurons

After having observed a dose-dependent decrease of MMP in hESC-derived and iPCS-derived neurons exposed to 1 M ethanol, I sought to determine whether neurons derived from individuals suffering from AUD would show similar susceptibility to ethanol exposure.

For this purpose, iPSCs from 5 individuals (age 23-25) diagnosed with AUD according to ICD-10 were obtained. The iPSC lines BIHi232, BIHIi233 BIHi234, BIHi235, and BIHi236 were kindly generated by the BIH Stem Cell Core Facility (headed by Dr.

Sebastian Diecke) using Sendai virus-based reprogramming of patient-derived PBMCs (Fig. 18A). After receiving the AUD-iPSCs, I characterized the lines with the help of Ms. Josefin Conrad (details on contributions can be found in section 7).

We first confirmed that AUD-iPSCs showed homogenous and typical PSC morphology (Fig. 18C). We then determined that AUD-iPSCs had a normal karyotype (Fig. 18D). Karyotyping was performed using Illumina platform and the OMNI-EPRESS-8v1.6 Chip by the BIH Stem Cells Core Facility. Validation of pluripotency and stemness was based on immunostainings and qRT-PCR. The pluripotent state of AUD-iPSCs was confirmed using qRT-PCR by comparing transcription levels of iPSCs to the fibroblast control line CON2. Transcription levels compared to fibroblasts demonstrated upregulation of the pluripotency-associated genes *OCT4*, *NANOG*, *SOX2*, *DNMT3B* and *DPPA4*, and downregulation of the fibroblast-associated marker *VIM* in all 5 AUD-iPSC lines (Fig. 18B). Immunostainings confirmed the expression of the pluripotency markers OCT4 and TRA 1-60 in all AUD-iPSC lines (Fig. 18C).

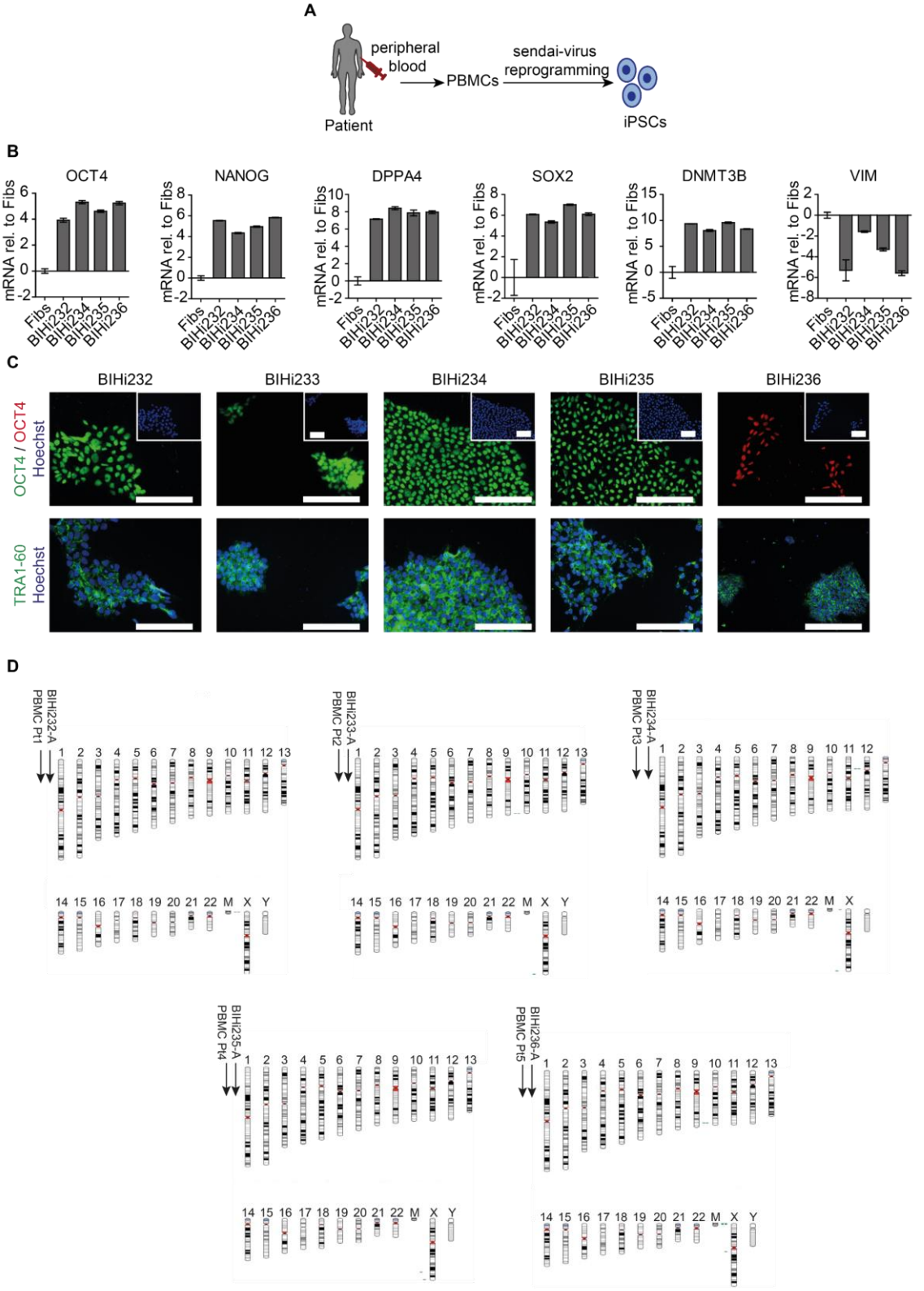

Fig. 18: Characterization of AUD-iPSCs.

(A) Schematic of the iPSC generation starting from PBMCs. **(B)** Quantitative real-time RT-PCR of pluripotency in AUD patient iPSCs (BIHi232, BIHi233, BIHi234, BIHi235, BIHi236) relative to fibroblast (Fibs) line CON2. Relative transcript levels of each gene were calculated based on

the 2-ΔΔCT method. Data were normalized to the housekeeping gene *GAPDH* and are presented as mean LOG2 ratios in relation to fibroblasts (CON2; mean +/- SD). **(C)** Representative images of the pluripotency-associated protein markers OCT4 and TRA1-60 counterstained with Hoechst in AUD-patient derived iPSCs (BIHi232, BIHi233, BIHi234, BIHi235 and BIHi236). Scale bar: 100 µm. **(D)** Single nucleotide polymorphism (SNP)-based virtual karyotype of AUD patient-derived iPSCs (BIHi232, BIHi233, BIHi234, BIHi235 and BIHi236). The karyotype of the iPSCs was compared to the corresponding parental cells (PBMCs). No larger areas of insertions or deletions were detected. Green: area with genomic gain; red: with genomic loss; gray: area with loss of heterozygosity. Pt= patient.

5.4.1 Differentiation of AUD-iPSCs into NPCs and neurons

To evaluate the susceptibility of neurons derived from individuals suffering from AUD to different ethanol doses, AUD-iPSCs were differentiated into neurons as described for control iPSCs (chapter 5.1). AUD-iPSCs from 5 different patients were successfully differentiated into NPCs expressing the neural progenitor associated markers PAX6 and NESTIN (Fig. 19A). NPCs from all AUD-lines also expressed the pan-neuronal marker TUJ1 and MAP2, indicating the presence of immature neurons within the NPC culture. This is a characteristic feature of all NPC lines generated within this study and suggest that AUD-NPCs may have the capability to differentiate and give rise to fully mature neurons. Expression of the glial marker GFAP was absent in AUD-NPCs and control NPCs. Transcriptional profiling (relative to the iPSC line XM001) confirmed that NPCs expressed neural progenitor-associated genes such as *NESTIN*, *PAX6*, *SOX1*, and *SOX2* (Fig. 19B).

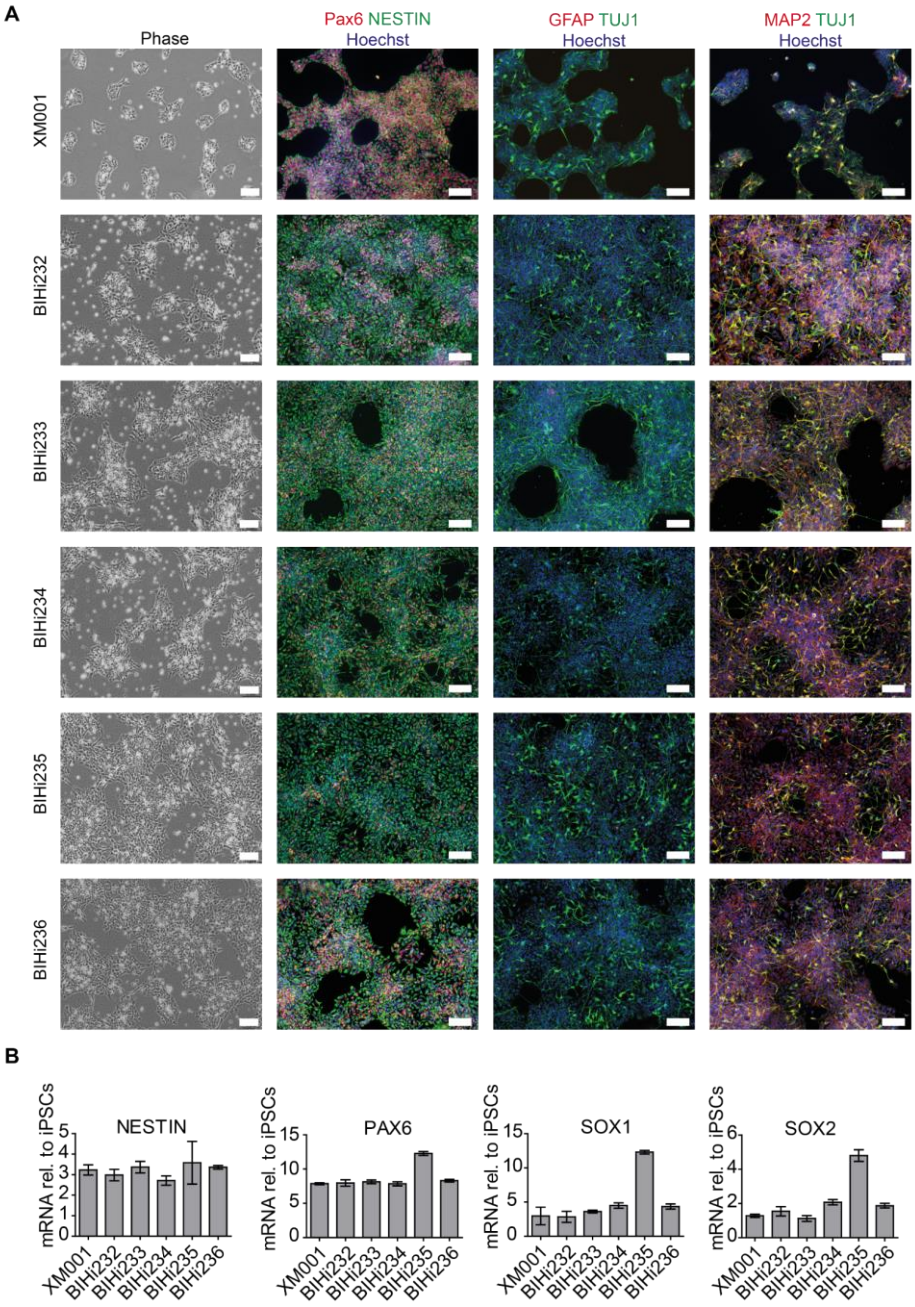

Fig. 19: Characterization of NPCs differentiated from AUD patient iPSCs.
(A) Representative images of the NPC-associated protein markers NESTIN and PAX6 counterstained with Hoechst of NPCs differentiated from AUD-patient derived iPSCs (BIHi232, BIHi233, BIHi234, BIHi235 and BIHi236) and the control NPC from the line XM001 including brightfield images. Scale bar: 100 µm. **(B)** Quantitative real-time RT-PCR analysis of the NPC-associated protein markers *NESTIN*, *PAX6*, *SOX1* and *SOX2* in AUD patient-derived NPCs (BIHi232, BIHI233, BIHi234, BIHi235, BIHi236). Relative transcript levels of each gene were calculated based on the 2-ΔΔCT method. Data were normalized to the housekeeping gene ornithine decarboxylase antizyme 1 (*OAZ1)* and are presented as mean LOG2 ratios (mean +/- SD) in relation to control iPSCs (XM001).

AUD-patient NPCs were further differentiated into neurons, as described for control NPCs (chapter 5.1.). After 10 days of differentiation, neuron-specific morphology was visible and neurons expressed the pan-neuronal marker TUJ1, as well as the dopaminergic neuron-associated markers FOXA2 and TH (Fig. 20).

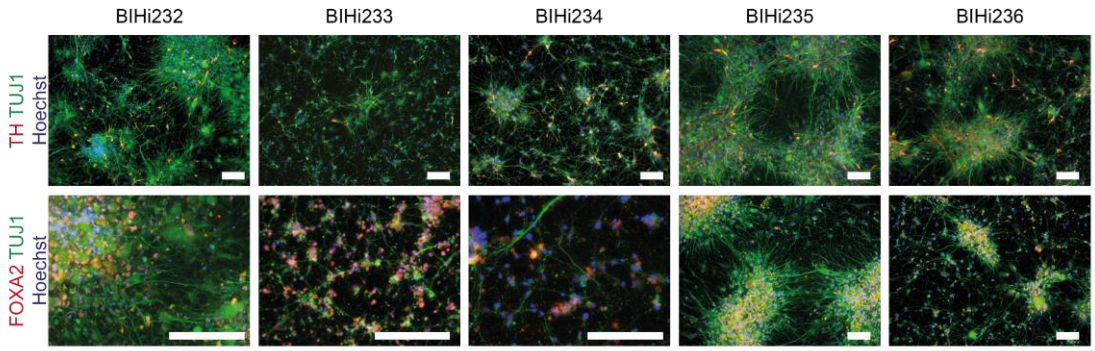

Fig. 20: Characterization of neurons differentiated from AUD-patient iPSCs.
Representative images of neurons differentiated from AUD-patient derived iPSCs (BIHi232, BIHi233, BIHi234, BIHi235 and BIHi236) expressing the neuronal-associated protein marker TUJ1 and the dopaminergic-neuron associated protein markers FOXA2 and TH. Neurons were counterstained with Hoechst. Scale bar: 100 µm.

Taken together, the 5 AUD-iPSCs were successfully differentiated into NPCs as demonstrated by immunostainings and qRT-PCR analysis. Furthermore, all 5 AUD-NPCs were successfully differentiated into neuronal cultures containing dopaminergic neurons as demonstrated by immunostainings.

5.4.2 MNH assay-based quantification of ethanol effects on AUD-neurons

To evaluate the ethanol susceptibility of neurons derived from individuals with AUD, I used the MNH assay in the acute setting (exposure to ethanol for 1 hour). 4-8-week-old neurons were seeded 5 days before the assay on the assay plate. On the day of the assay, ethanol was diluted in the media, and added to the neurons for 1 hour. The

MMP and branching complexity was quantified using the MNH assay (Fig. 21A). AUD-neurons showed a decrease in MMP starting at 1 M ethanol for BIHi232 (Fig. 21B), BIHi233 (Fig. 21C), and BIHi236 (Fig. 21F). Interestingly, AUD-neurons from lines BIHi234 (Fig. 21D) and BIHi235 (Fig. 21E) showed less susceptibility to ethanol toxicity, as their MMP decreased only after exposure to 2.5 M ethanol. Their response curves appear overall flatter compared to the other AUD-neurons and control neurons (see Fig. 17C and Fig. 17G). It should be noted that experiments on neurons derived from BIHi232 (Fig. 21B), BIHi234 (Fig. 21D), BIHi235 (Fig. 21E) and BIHi236 (Fig. 21F) were performed up to five times, but for BIHi233 (Fig. 21E) only twice.

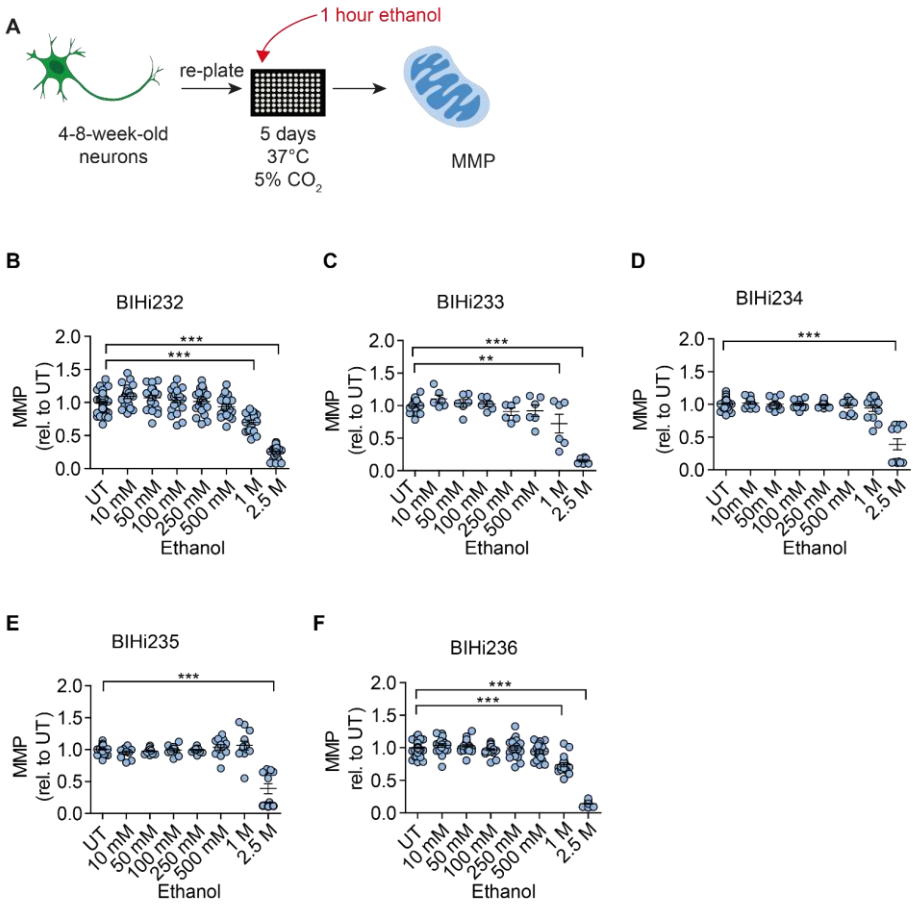

Fig. 21: MNH assay-based quantification of MMP in AUD patient-derived neurons exposed to acute ethanol.

Results

(A) Schematic of the MNH assay workflow to quantify MMP after acute (1 hour) ethanol exposure of neurons derived from AUD-iPSCs. **(B-F)** MNH assay-based quantification of MMP in 4-8-week-old neurons from AUD patients (BIHi232, BIHi233, BIHi234, BIHi235 and BIHi236) treated for 1 hour with increasing concentrations of ethanol (10 mM–2.5 M). Each dot represents values obtained from one well (BIHi236 n=5; BIHi232, BIHi234 and BIHi235 n=4; BIHi233 n=2; mean +/- SEM; **p<0.01, ***p<0.001; one-way ANOVA followed by Dunnett`s multiple comparison test), normalized to the corresponding untreated controls (UT) exposed to the assay media only.

After measuring MMP, neurons were fixed and stained with TUJ1 to quantify neuronal profiling (Fig. 22A). In terms of branching outgrowth, AUD-neurons showed responses similar to control neurons, with a significant decrease in neuronal branching complexity (Fig. 22B-M). Unfortunately, the dataset for neurons derived from BIHi233 is missing due to loss of the neurons during the staining procedure. Moreover, for neurons derived from BIHi234 only one round was performed (Fig. 22E-G). Nevertheless, the tendency in all 5 AUD lines was comparable. For all AUD-neurons, neurite count decreased significantly starting from 1 M ethanol (Fig. 22B; Fig. 22E; Fig. 22H; Fig. 22K). A similar decrease was observed for neurite length with a decrease starting from 500 mM ethanol for BIHi232 (Fig. 22C**)** and BIHi236 (Fig. 22L**)**, and starting from 1 M for BIHi234 (Fig. 22F**)** and BIHi235 (Fig. 22I). The number of branch points decreased starting from 500 mM ethanol for BIHi232 (Fig. 22D**)**, BIHi234 (Fig. 22G), and BIHi236 (Fig. 22M), and starting from 1 M for BIHi235 (Fig. 22J).

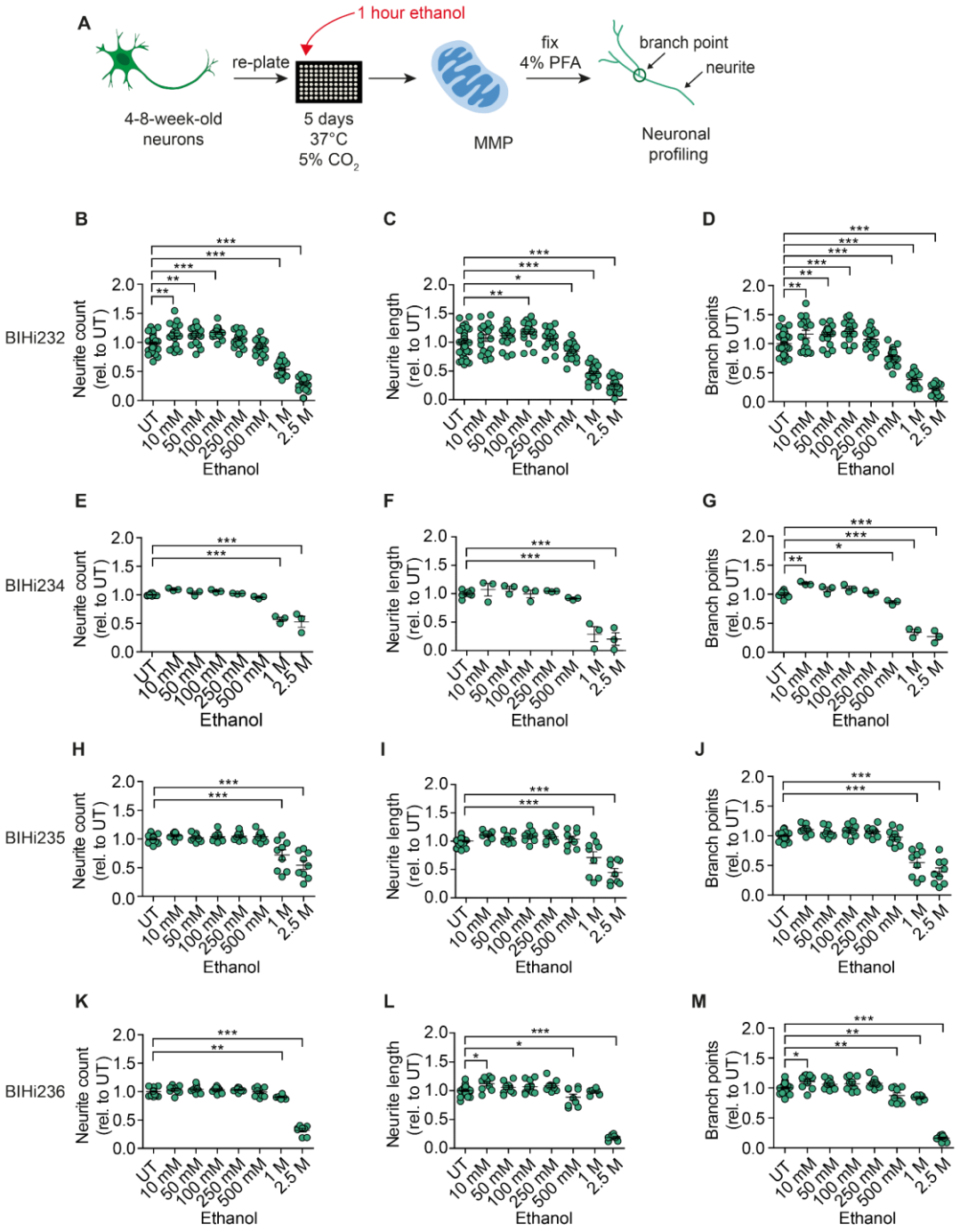

Fig. 22: MNH assay-based quantification of neuronal branching in AUD-neurons after acute ethanol exposure.

(A) Schematic of the MNH assay workflow for acute (1 hour) ethanol exposure of neurons from AUD patients. **(B-M)** MNH assay-based quantification of neuronal branching (neurite count, neurite length and branch points) in 4-8-week-old AUD-neurons treated for 1 hour with increasing concentrations of ethanol (10 mM–2.5 M). Each dot represents values obtained from one well (BIHi232 and BIHi235 n=3; BIHi236 n=2; BIHi234 n=1; mean +/- SEM; *p<0.05, **p<0.01, ***p<0.001; one-way ANOVA followed by Dunnett`s multiple comparison test), normalized to the corresponding untreated controls (UT) exposed to the assay media only. Graphs divided as follows: BIHi232: neurite count (**B**), neurite length (**C**) and branch point (**D**); BIHi234: neurite

count (**E**), neurite length (**F**) and branch point (**G**); BIHi235: neurite count (**H**), neurite length (**I**) and branch point (**J**); BIHi236: neurite count (**K**), neurite length (**L**) and branch point (**M**).

Taken together, acute ethanol exposure negatively affected mitochondrial neuronal health in neurons derived from AUD patients. AUD-neurons recapitulated the pattern of neurotoxicity detected in neurons derived from control subjects. Nonetheless, some AUD-neurons appeared less susceptible to ethanol neurotoxicity.

5.5 Proof-of-concept compound screening for modulators of ethanol-induced human neurotoxicity

The MNH assay allowed to quantify changes in mitochondrial polarization and neuronal outgrowth in a quantitative and robust manner. The changes induced by ethanol exposure were significant and could be confirmed in neurons derived from seven different PSC lines, including control iPSCs, hESCs, and 5 patient iPSCs. Moreover, the determined z-factor of 0.747 (Fig. 13B and chapter 5.2.3) makes the assay suitable for high-throughput drug discovery applications. Hence, I aimed to assess whether the MNH assay could be used to carry out a compound screening to identifying modulators of ethanol-induced human neurotoxicity following acute exposure to 1 M ethanol. I used a library of compounds from Selleckchem (z65122) that contains 700 drugs already approved by the FDA for safe clinical use. Among these drugs, 48 compounds were pre-selected based on their clinical use in the context of neurological and psychiatric diseases (compound number 1-48; Fig. 23B-D; Table 9-A). Additionally, I included in the screening 5 AUD drugs: disulfiram, chlomethiazole, acamprosate, naltrexone and baclofen. These drugs are commonly employed for clinical use in AUD patients (compound number 49-53; Fig. 23B-D; Table 9-A). The AUD drugs are used to treat either withdrawal symptoms (chlomethiazole) or alcohol dependence (disulfiram, baclofen, naltrexone and acamprosate) (see Table 1-A). However, no previous studies investigated the effects of any of these drugs in the context of ethanol-induced neurotoxicity on iPSC-derived neurons.

For the proof-of-concept compound screening, 4-8-week-old neurons derived from control iPSCs (XM001 line) were used under the settings of acute ethanol exposure. Neurons were seeded on the assay plate and kept for 5 days before starting the MNH

assay (Fig. 23A). All compounds were used at 0.5 µM concentration and were dissolved in Dimethyl sulfoxide (DMSO). The compounds were diluted down to a final DMSO concentration below 0.25% in media to minimize a possible causative effect by DMSO. The compounds were added to the neurons overnight (ON) and diluted in fresh culture media (24 hours in total). To ensure similar conditions in all samples, media was changed at the same time for both untreated neurons and for neurons treated with the compounds. MMP and neuronal profiling was quantified using the MNH assay. On the day of the assay, staining for MMP detection was performed by adding TMRM (0.5 nM final concentration) and Hoechst without changing the media. After the incubation time of 30 minutes at 37°C, 5% CO_2, the staining solution and cell media was aspirated, neurons were washed once with PBS, and phenol red-free media containing 1 M ethanol together with 0.5 µM compound was applied. Untreated control neurons were exposed to phenol-red free media without any further supplementation. Images were immediately taken with the CellInsight CX7 and simultaneously quantified using the "Cell Health Profiling" BioApplication. Afterwards, neurons were fixed with 4% PFA, immunostained with TUJ1, and images were taken and quantified using the "Neuronal Profiling" BioApplication. The same compound screening was repeated twice in two different biological replicate experiments. The MMP and branching complexity of neurons treated with compounds overnight and exposed to ethanol for 1 h were compared to neurons that were only exposed to ethanol for 1 h.

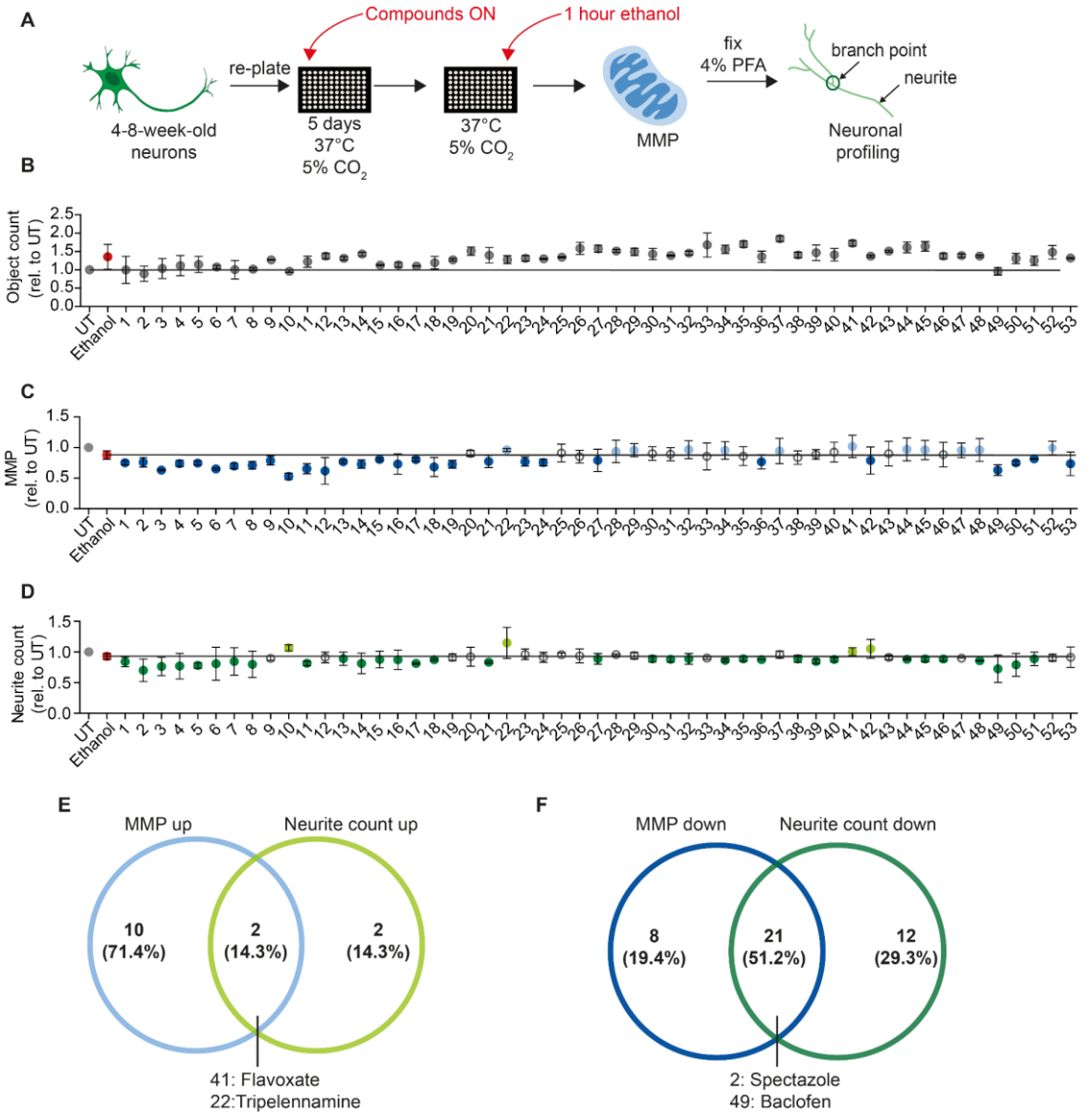

Fig. 23: Proof-of-concept compound screening in human neurons exposed to ethanol.
(A) Schematic MNH assay workflow for compound screening. **(B)** MNH assay-based quantification of object count of neurons from control iPSCs (XM001 line) after overnight (ON) treatment with 48 FDA-approved drugs (Selleckchem, z65122) and 5 AUD drugs with subsequent exposure to 1 M ethanol for 1 hour (acute exposure; mean +/- SD; n= 2 independent experiments). Values from each experiment were normalized to the corresponding UT controls. The black line marks the mean of UT control. **(C-D)** MNH assay-based quantification of MMP (**C**) and neuronal profiling (**D**; neurite count) after ON treatment with 48 FDA-approved drugs out of the Selleckchem library (z65122) and 5 AUD drugs with subsequent exposure to 1 M ethanol for 1 hour (acute exposure). Values from each experiment were normalized to the corresponding UT controls (mean +/- SD; n= 2 independent experiments). The black line marks the mean value of 1 M ethanol exposure (red dot). Grey circles mark the compounds that displayed no change in MMP or neurite counts. Light blue dots in (**C**) mark positive hit compounds that increased MMP of more than 0.5 times the SD of neurons only exposed to ethanol. Dark blue dots in (**C**) mark negative hit compounds that decreased the MMP more than 0.5 times the SD of neurons only

exposed to ethanol. Light green dots in (**D**) mark positive hit compounds that increased neurite count of more than 0.5 times the SD of neurons only exposed to ethanol. Dark green dots in (**D**) mark negative hit compounds that decreased neurite count of more than 0.5 times the SD of neurons only exposed to ethanol. **(E)** Venn diagram for the compounds that increased MMP ("MMP up") and increased neuronal outgrowth ("neurite count up"). **(F)** Venn diagram for the compounds that decreased the MMP ("MMP down") and/or the neuronal outgrowth ("neurite count down") in neurons exposed to ethanol.

Overall, object count, obtained by quantifying the Hoechst-based nuclei count, showed no overt changes in the cell number following the compound treatments (Fig. 23B). This suggested that the compounds in the used concentration of 0.5 µM were not toxic. Therefore, it was possible to confidently compare treated neurons to untreated neurons. As baseline for comparisons, I used neurons exposed to 1 M ethanol for 1 hour that were not treated with compounds (red dots) (Fig. 23B-D). In line with the previous experiments (Fig. 16 and Fig. 17), 1 M ethanol caused a decrease in MMP (Fig. 23C, red dot) and neurite count (Fig. 23D, red dot) compared to neurons that were not exposed to ethanol (UT, grey dots).

A compound was defined as a positive hit for MMP or neurite count when the compound led to values that were at least 0.5 times higher than the standard deviation (SD) of neurons that were only exposed to ethanol (Fig. 23C-D, light blue dots, and light green dots). A compound was defined as a negative hit for MMP or neurite count when the compound led to values that were at least 0.5 times lower than the SD of neurons that were only exposed to ethanol (Fig. 23C-D, dark blue dots, and dark green dots).

12 positive hit compounds were found to increase the MMP in the presence of ethanol (Fig. 23C, light blue dots). 4 positive hit compounds increased the number of neurites in the presence of ethanol (Fig. 23D, light green dots). 2 positive hit compounds, tripelennamine and flavoxate ameliorated both MMP and neurite count (Fig. 23E). 29

negative hit compounds decreased MMP further than observed for 1 M ethanol alone (Fig. 23C, dark blue dots). 33 negative hit compounds decreased neurite count further than observed for 1 M ethanol alone (Fig. 23D, dark green dots). 21 negative hit compounds decreased both MMP and neurite count. (Fig. 23F). Among these 21 negative hit compounds baclofen, a drug used in the context of AUD treatment, appeared to worsen both parameters in the presence of ethanol (Compound number 49 in Fig. 23D).

Overall, the MNH assay-based proof-of-concept compound screening demonstrated the possibility to identify drugs modulating the MMP and branching complexity in a high-throughput manner in iPSC-derived neurons. This approach led to the identification of potential hit compounds positively modulating ethanol-induced human neurotoxicity. Furthermore, the negative hit compounds suggest enhanced neurotoxicity in addition to ethanol toxicity. Further in-depth validations of the identified hit candidates are required to confirm their ability to affect ethanol-induced neurotoxicity positively or negatively.

5.5.1 Assessment of hit compound candidates

Using the MNH assay, it was possible to identify hit compounds modulating human neuronal health. Among the tested compounds, 21 hit compounds suggested increased neurotoxicity. Based on those findings, I was interested in determining whether the negative hit compounds already have a neurotoxic effect in the absence of ethanol.

From the identified hit candidates, I selected 2 compounds that negatively modulated the MNH and are commonly employed in the context of AUD: baclofen (compound number 49, Table 9-A) and disulfiram (compound number 53, Table 9-A). Moreover, I selected flavoxate (compound number 41; Table 9-A) which positively modulated the MMP and neurite count simultaneously. In the compound screening, disulfiram negatively

modulated MMP but not neurite count and baclofen appeared to negatively affect MMP and neurite count in neurons exposed to ethanol (Fig. 23).

For the assessment of neuronal toxicity in the absence of ethanol, 4-8-week-old neurons were re-plated and kept for 5 days before overnight treatment with different concentrations of either disulfiram (Fig. 24A) or baclofen (Fig. 24F). Control neurons were kept in media only as well as in the highest corresponding DMSO concentration (0.2%) since disulfiram and baclofen were dissolved in DMSO. Disulfiram negatively affected MMP (Fig. 24B) and neurite count (Fig. 24C) at concentrations of 10 µM disulfiram in the absence of ethanol. Neurite length (Fig. 24D) decreased when exposed to 0.5 µM and starting at 5 µM disulfiram overnight. Number of branch points (Fig. 24E) decreased when exposed to 0.5 µM and 10 µM disulfiram overnight.

Baclofen also negatively affected MMP in the absence of ethanol at concentrations of 1 µM and 10 µM (Fig. 24G). Moreover, neuronal branching complexity (neurite count: Fig. 24H; neurite length: Fig. 24I; branch points: Fig. 24J) was also significantly reduced following overnight treatment with 0.5 µM–10 µM baclofen.

The data suggest that disulfiram and baclofen may negatively modulate neuronal health in the absence of ethanol.

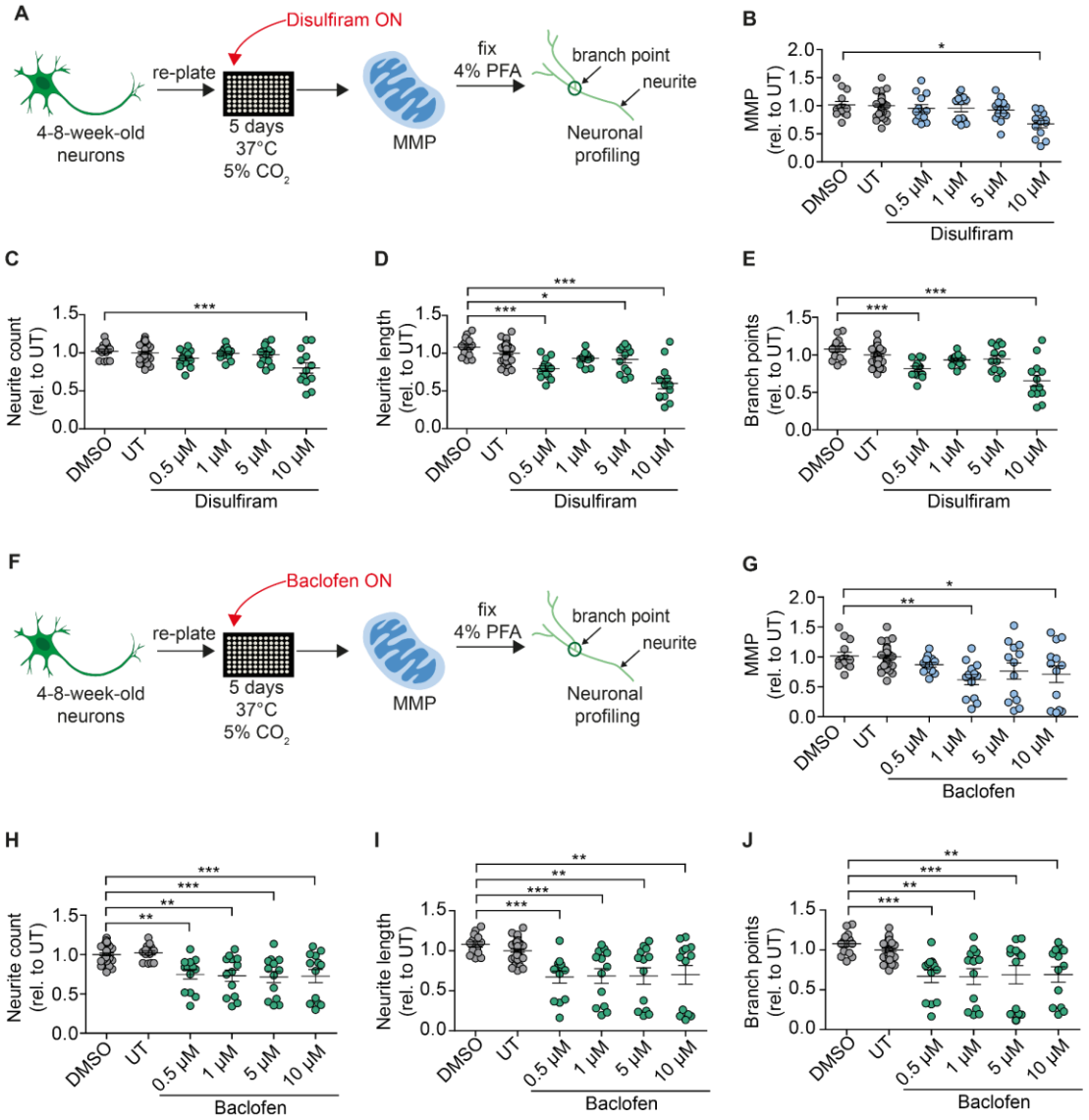

Fig. 24: MNH assay-based quantification of disulfiram and baclofen on iPSC-derived neurons.

(A) Schematic of the MNH assay workflow of overnight (ON) treatment with disulfiram. **(B-E)** MNH assay-based quantification of MMP (**B**) and neuronal branching including neurite count (**C**), neurite length (**D**) and branch points (**E**) from control iPSC-derived neurons (XM001) after overnight treatment with different concentrations of disulfiram (0.5–10 µM). Each dot represents values obtained from one well (n= 3 independent experiments; mean +/- SEM; *p<0.05, **p<0.01, ***p<0.001; one-way ANOVA followed by Dunnett`s multiple comparison test), normalized to DMSO (0.2%). **(F)** Schematic of the MNH assay workflow of overnight (ON) treatment with baclofen. **(G-J)** MNH assay-based quantification of MMP (**G**) and neuronal branching including neurite count (**H**), neurite length (**I**) and branch points (**J**) from control iPSC-derived neurons (XM001) after overnight treatment with different concentrations of baclofen (0.5–10 µM). Each dot represents values obtained from one well (n= 3 independent experiments; mean +/- SEM; *p<0.05, **p<0.01, ***p<0.001; one-way ANOVA followed by Dunnett`s multiple comparison test), normalized to DMSO (0.2%).

Results

Since the MNH assay appeared suitable for the evaluation of neurotoxicity as observed following the exposure to baclofen and disulfiram, I aimed to study lithium in absence of ethanol to evaluate its effect on cellular health. As mentioned above, lithium is used in the treatment of bipolar disorder and has been suggested for the treatment of AUD (see chapter 1.6).

I assessed the effects of increasing concentrations of lithium on mitochondrial neuronal health. Briefly, 4-8-week-old neurons were re-plated and kept for 5 days prior to the assay. On the day of the assay, different concentrations of lithium were supplemented into the media for 1 hour and 4-8-week-old neurons were measured using the MNH assay (Fig. 25A). Lithium negatively modulated the MNH of control iPSC-derived neurons starting from 2 mM concentration where 1 mM lithium is in the range of clinical use (Young, 2009). A significant decrease of the MMP was observed for 5 mM lithium (Fig. 25B). Moreover, 2 mM and higher decreased neuronal length (Fig. 25D) and number of branch points (Fig. 25E). No changes in neurite count were observed (Fig. 25C). Results so far are in line with published data reporting neurotoxicity of lithium in some individuals (Lang and Davis, 2002; Mignarri et al., 2013; Shah et al., 2015).

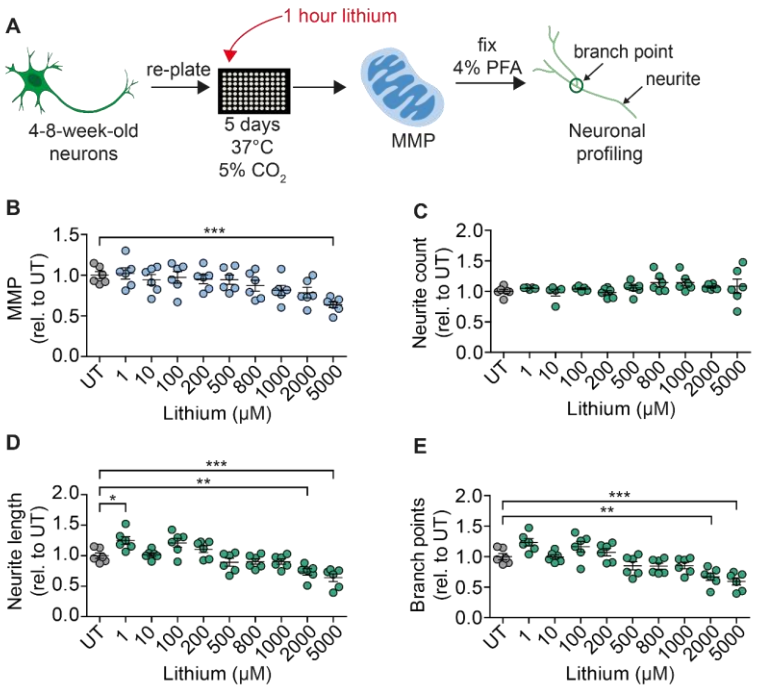

Fig. 25: MNH assay-based quantification of 4-8-week-old neurons exposed to lithium.
(A) Schematic workflow of MNH assay on 4-8-week-old neurons exposed to lithium for 1 hour. **(B-E)** MNH assay-based quantification of MMP (**B**) and neuronal profiling including neurite count (**C**), neurite length (**D**) and branch points (**E**) on control iPSC-derived 4-8-week-old neurons (XM001) after treatment with different concentrations of lithium (1 µM–5 mM) for 1 hour. Each dot represents values obtained from one well (n= 2 independent experiments; mean +/- SEM; *p<0.05, **p<0.01, ***p<0.001; one-way ANOVA followed by Dunnett`s multiple comparison test), normalized to untreated controls (UT) exposed to the assay media only.

As a positive hit compound from the proof-of-concept screening I picked flavoxate and further assessed the effect of 1 µM flavoxate in the absence of ethanol using the MNH assay. For this, 4-8-week-old neurons were re-plated and kept for 5 days before overnight treated with 1 µM flavoxate (Fig. 26A). Control neurons were kept in the corresponding DMSO concentration. Overnight treatment with 1 µM flavoxate increased MMP (Fig. 26B) and neurite arborization (Fig. 26C-E) compared to neurons treated only with DMSO. These results indicate a potentially positive effect of flavoxate on the MNH.

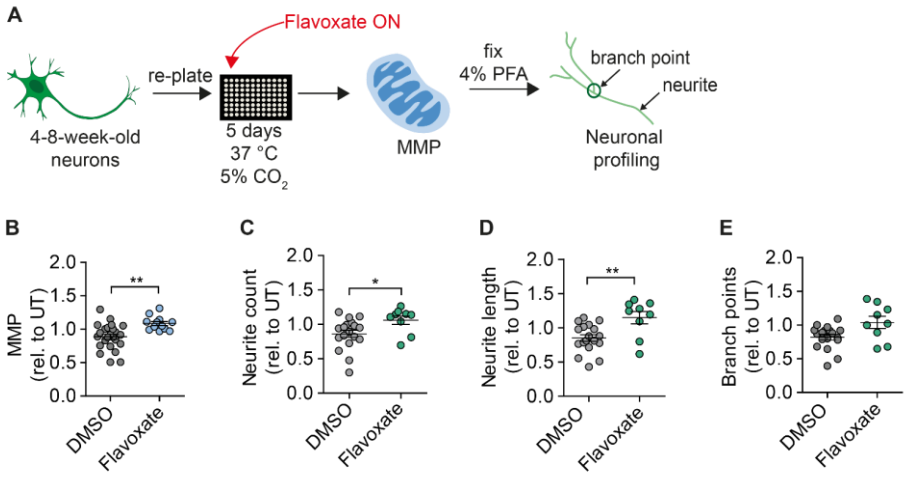

Fig. 26: MNH assay-based quantification of 4-8-week-old neurons exposed to flavoxate. **(A)** Schematic workflow of MNH assay on 4-8-week-old neurons exposed to flavoxate overnight (ON). **(B-E)** MNH assay-based quantification of MMP (**B**) and neuronal profiling including neurite count (**C**), neurite length (**D**), and branch points (**E**) after ON treatment of 4- to 8-week-old neurons from control iPSCs (XM001) with 1 µM flavoxate (n = 3 independent experiments; mean ± SEM; *< 0.05, **p<0.01; one-way ANOVA followed by Dunnett's multiple comparison test).

Overall, using the MNH assay it was possible to evaluate neuronal health and toxicity independent of ethanol as seen for the two AUD drugs baclofen and disulfiram as well as for lithium and flavoxate, making the MNH assay potentially relevant for assessing the health and toxicity of human neurons. Moreover, the results suggest that by identifying compounds counteracting neurotoxicity, it may be possible to discover general modulators of MNH in humans.

5.6 Genome editing using CRISPR/Cas9

To dissect the possible role of KLB in AUD and possibly identify novel treatment strategies, a gene knockout using CRISPR/Cas9 strategy was aimed. Since restricted expression of KLB to specific areas has not been demonstrated so far, I first investigated the expression of KLB using RT-PCR in hESCs (H1) and neurons derived from iPSCs (mDANLR) and hESCs (mDANH1). I used human liver samples (clontech # 636531) as positive control. Expression of KLB mRNA could be observed in all samples (Fig. 27).

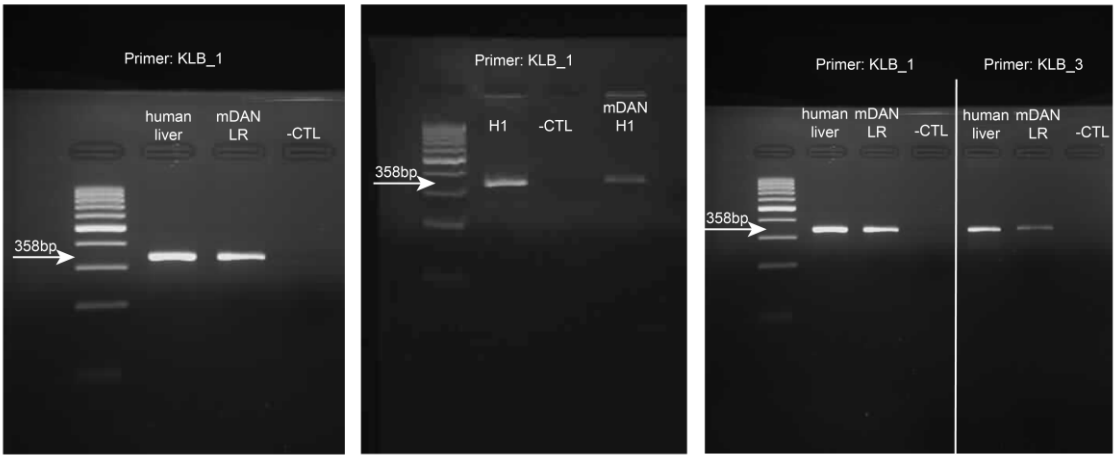

Fig. 27: KLB expression in ESCs and hPSC-derived neurons.
RT-PCR based KLB gene expression using two different primer sets (KLB_1 and KLB_3) on the ESC line H1, PSC-derived neurons from LR (mDANLR) and H1 (mDANH1), and human liver as positive control. Water was used as blank for quality control (-CTL).

5.6.1 CRISPR/Cas9 vector construction and design

To generate KLB-KO iPSCs, control iPSCs (XM001 line) were transfected with the pU6(BbsI)sgRNA-CAG-eCas9-venus-bpA vector encoding the guide RNA (gRNA), a high efficiency version (eCas9) of the Cas9 designer nuclease, which generates less off-target effects compared to Cas9, and a venus reporter. The eCas9 and gRNAs sequences,

which uniquely targeted the human *KLB*, were taken from Zhang's laboratory (Broad Institute, Boston) (Sanjana et al., 2014; Slaymaker et al., 2016). Chosen gRNAs were picked to target Exon 3 of *KLB* (Fig. 28B).

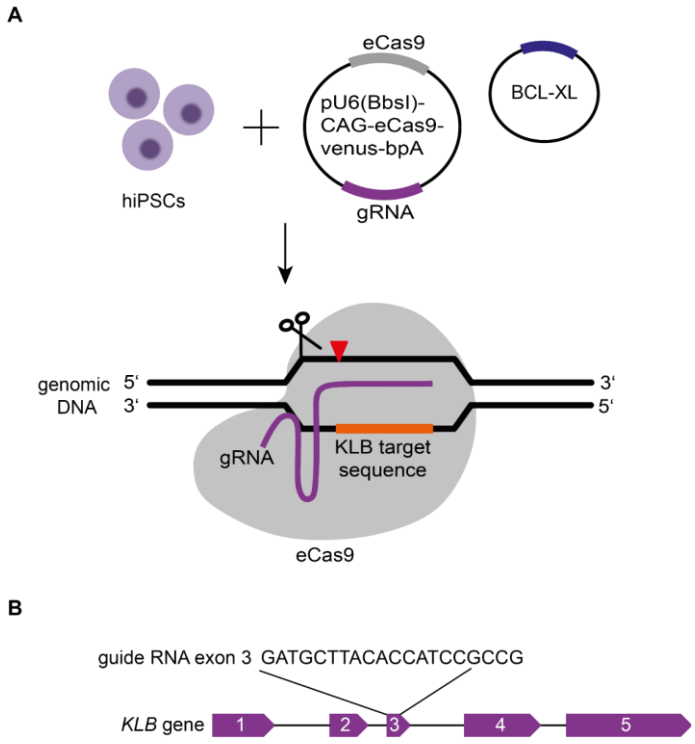

Fig. 28: Genome editing strategy.
(A) Schematic overview of the gene editing strategy using eCas9 and plasmid expressing BCL-XL to support cell survival. **(B)** Schematic of the *KLB* gene with the guide RNA sequences targeting exon 3.

The gRNA was cloned into the eCas9 plasmid vector. Like other cells, stem cells have two different DNA repair mechanisms to repair double strand breaks (DSB), the homology directed repair (HDR) and the non-homologous end joining (NHEJ). While HDR is more precise, NHEJ is rapid but error-prone (Weeden and Asselin-Labat, 2018). To increase iPSC survival after eCas9-induced DSB cleavage a plasmid expressing BCL-XL (Li et al., 2018) was also included into the transfection protocol (Fig. 28A). Further

information on the gRNA sequences and plasmids used are listed in section 3.3.6. Corresponding plasmids were transiently transfected into the control XM001 iPSC line using Lipofectamine 3000 according to the manufacturer's protocol.

5.6.2 Screening for the corrected clones

The vector pU6-(BbsI)-sgRNA_CAG-eCas9-venus-bpA encodes a fluorescent Venus reporter (positive-green). Hence, three days after transfection, cells were sorted by FACS against Venus with the help of the FACS facility at MDC (headed by Dr. Hans-Peter Rahn) and plated in low density (500 – 1000 cells per 6 well) on MEF plates to support cell growth. Following the transfection and fluorescence sorting, single colonies were picked and transferred into Matrigel-coated 24-well plates. Clones were screened for KLB-KO by extraction of genomic DNA according to manufacturer's protocol (FlexiGene DNA-isolation Kit from Qiagen) for subsequent Sanger sequencing (Fig. 29A).

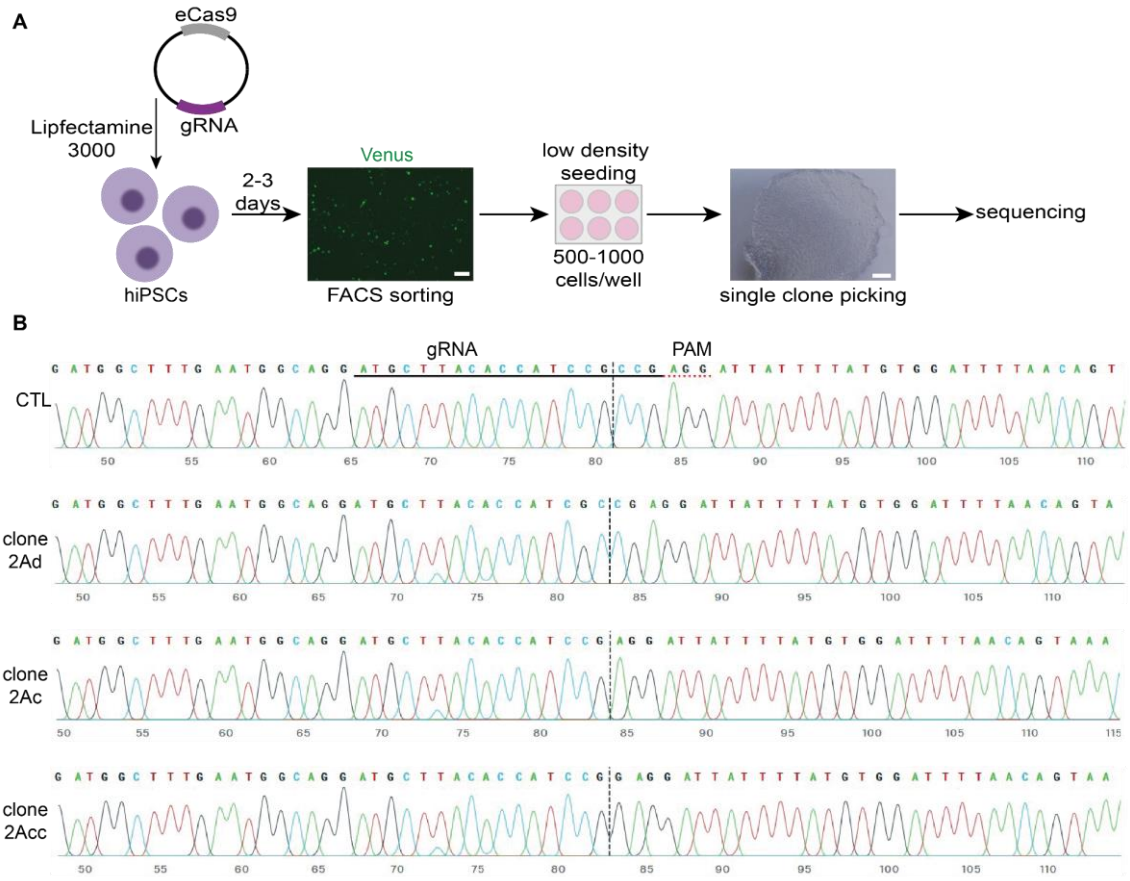

Fig. 29:Screening of potential clones.
(A) Schematic workflow of the genome editing strategy to knock out the *KLB* gene in iPSCs (XM001 line) using the CRISPR/Cas9 system. Scale FACS: 100 µm; scale picking: 300 µm. **(B)** Sanger sequencing of edited (clone) and wild-type (CTL) clones showing the region around the guide sequence. The horizontal black underlined region represents the guide sequence (gRNA). The red dotted underline is the protospacer adjacent motif (PAM) site. The vertical black dotted line represents the predicted cut site.

Sequencing results of the set of screened clones indicated single or multiple nucleotide deletions within the region of detection (Fig. 29B**)**. In the presented clones (2Ad, 2Ac and 2Acc) the deletions occurred approximately 3 bp upstream of the protospacer adjacent motif (PAM) sequence (AGG), which is consistent with the predicted Cas9 cut site (Wu et al., 2014).

Overall, the groundwork for a possible KLB-KO line was set but further functional validation should be conducted to demonstrate differences in mRNA transcript levels and protein expression.

6. Discussion

Although many researchers have studied the pathophysiology of drug abuse, the neurotoxicity induced by those drugs still requires extensive attention. Neurotoxicity is considered a major cause of neurodegenerative disorders. Most drugs of abuse, including alcohol, have significant neurotoxic effects (Mohammad Ahmadi Soleimani et al., 2016). The exact mechanisms underlying ethanol-induced toxicity in the human brain cells remain unknown, which is partly due to the lack of suitable human cell-based model systems. Hence, understanding the level of neurotoxicity caused by ethanol may enable the development of protective drugs to reduce the risk of developing neurodegenerative decline due to excessive alcohol consumption like in AUD. Mitochondria may play an essential role during ethanol intoxication, where the MMP may serve as an indicator for viable cells. Even though some recent studies demonstrated the potential of iPSC-technology to uncover the genetic and cellular mechanisms of AUD (Lieberman et al., 2012, 2018; De Filippis et al., 2016), the effect of ethanol on neuronal mitochondrial function and neurite outgrowth in human-iPSC-derived neurons remained not investigated. In this study, I developed an HCA-based mitochondrial neuronal health (MNH) assay to assess the cellular health of induced pluripotent stem cell-derived neurons. I used the MNH assay to study the effect of ethanol on neuronal cultures containing dopaminergic neurons and furthermore employed the MNH assay as potential tool for drug screenings.

Altogether, using the MNH assay I was able to capture ethanol-induced neurotoxicity in control human hESC- and iPSC-derived neurons as well as neurons derived from AUD iPSCs, and employ a possible screening tool for the assessment of neurotoxicity.

Discussion

6.1 Generation of iPSC-derived NPCs and neurons

Chronic alcohol consumption is associated with central nervous system changes. Ethanol causes damage to the structure and function of the brain (Bates et al., 2002) including direct effects on dopaminergic neurons, resulting in increased extracellular dopamine mainly in the striatum (Charlet et al., 2011). The assessment of possible toxic effects of substances and compounds is of high importance in the hazard assessment and drug development process. To date, neurotoxicity testing still relies on expensive, time consuming and often ethically debated *in vivo* animal studies which make them virtually unsuitable for HT toxicity screenings. Overall, there is an emerging need for reliable *in vitro* test systems capable of detecting early toxicity observed in human cells.

In this study, I used iPSC-derived neurons as a model system to assess the effect of ethanol on mitochondrial neuronal health. For the generation of NPCs from iPSCs I used a protocol based solely on small-molecules (Reinhardt et al., 2013). As described in the results the protocol led to the generation of homogenous cultures with highly proliferative NPCs, which made it possible to generate a vast number of NPCs. These were two prerequisites that had to be met to provide sufficient cells in high quality for performing HCA. Hence, the generated NPCs represent a robust tool for large-scale disease modeling as well as compound screenings.

Next, I differentiated the iPSC-derived NPCs into neurons. Again, I used the protocol of Reinhardt et al. (Reinhardt et al., 2013). I aimed for the generation of midbrain dopaminergic neurons since they seem to play a main role in the reinforcing effect of ethanol on the brain and may also be affected through ethanol-induced neurotoxicity. Results indicate successful generation of neurons with a change in morphology compared to NPCs. The results showed that the protocol used to generate dopaminergic neurons

seems to lead to the generation of a mixed culture. Therefore, further characterization of the cell culture composition should be conducted to define the present cell types. In a study performed by my colleague Gizem Inak-Girrbach, a closer evaluation of the culture components revealed the presence of glial cells as well as neuronal progenitor cells (Inak-Girrbach, 2019, dissertation). To further dissect the functionality of the dopaminergic neurons, it would be necessary to measure their ability to release the neurotransmitter dopamine. This could be achieved by measuring dopamine levels in the supernatant for example through a commercially available ELISA kit suitable for cell culture samples or through quantification using HPLC.

In this study, I focused on the detection of ethanol toxicity on one specific cell type whereas in the brain various cell types may differentially be affected by ethanol. Hence, in the experimental setting it would have been interesting to determine the proportion of glial to neurons before and after chronic ethanol exposure, which may help to better understand if or to which extend alcohol exposure affects different cell populations. As already mentioned, the human iPSC-derived neurons used in this study consisted of neurons and presumably glia cells, more specifically astrocytes. In the brain, astrocytes are the most abundant glia cells involved in a broad spectrum of functions. Those include water and ion homeostasis, the contribution to the BBB maintenance, uptake of neurotransmitters such as glutamate and GABA, they perform immune functions, synthesize and release neurotrophic factors, and play a role in the formation of neural scars following injury (Matias et al., 2019). Glial cell dysfunction is believed to play a role in neurological and psychiatric disorders including AUD (Erickson et al., 2019). Neurons depend on the interaction with several types of glial cells to ensure maintenance, survival and normal activity (Barres, 2008). Hence, if alcohol consumption damages glial

cells or disrupts their activity, this could also negatively affect neuronal function (Miguel-Hidalgo, 2018).

To understand AUD pathology, the effect of ethanol on single cell types as well as on cell populations and whole organs are of interest. In fact, due to ethanol's multisystemic action on various tissue and organs, it would be interesting to additionally test the effects of ethanol under more complex physiological conditions found in human tissue such as cell-cell interaction, which influence fundamental cellular behaviors including proliferation, differentiation, apoptosis and gene expression (Duval et al., 2017).

Recent improvements in the development of human iPSC-derived three-dimensional (3D) organoids allow to mimic *in vivo* tissues and organs in a more physiological manner compared to two-dimensional (2D) models (Kelava and Lancaster, 2016; Renner et al., 2020). Organoids contain several cell types with self-organizing properties, reflecting some aspects of the specialized functions of the organ to be modeled (Lancaster and Huch, 2019). Though organoids are powerful tools for modeling human diseases, many hurdles remain such as the lack of vascularization which increases the risk for necrosis, or the limited reproducibility due to their self-organizing nature. However, several research groups focus on the optimization of protocols for the generation of reproducible 3D structures that consistently exhibit similar traits - shape, size, and cellular composition - under the same experimental conditions (Wang, 2018; Lancaster and Huch, 2019).

In a very recent study from 2020, iPSC-derived cerebral organoids were used for the first time to model alcohol-induced neurotoxicity (Arzua et al., 2020). The group showed that alcohol exposure for 6 hours resulted in changes observed at cellular, subcellular, bioenergetic metabolism, and gene expression levels, as well as mitochondrial dysfunction and metabolic stress. These results are in accordance with the findings on

mitochondrial dysfunction made in this study, as well as previous findings *in vivo* and *in vitro* reporting for example increased ROS production (Reddy et al., 2013), altered mitochondrial respiration (Haorah et al., 2013; Reddy et al., 2013), impaired ATP production (Bustamante et al., 2012; Jung, 2015), and increased cell death (Lamarche et al., 2013).

Overall, iPSC-based model systems, including 2D and 3D culture systems, appear to be a suitable tool for the assessment of ethanol's effect on cellular functions and for the evaluation of ethanol-induced toxicity.

6.2 Assessment of ethanol toxicity in iPSC-derived neuronal cultures using the MNH assay

iPSC-derived neurons allow to investigate the effect of ethanol alone or in combinations with diverse other pharmacological or naturally derived substances. Using the newly developed MNH assay, I could show that acute and chronic ethanol exposure caused a reduction in mitochondrial neuronal health in control hESC- and iPSC-derived neurons, iPSC-derived NPCs as well as in AUD-derived neurons, suggesting ethanol-induced neurotoxicity. Nevertheless, the AUD-patient derived neurons showed slight variances in the response to ethanol. This suggests a potential individual variability in the toxic effects of acute ethanol exposure and a possible decrease in the ethanol susceptibility in the case of individuals with AUD. These findings may potentially explain why healthy subjects experience negative consequences after acute alcohol ingestion, while AUD individuals would require higher doses of ethanol to experience similar negative consequences.

Discussion

I performed a proof-of-concept screening on control iPSC-derived neurons using the MNH assay and identified possible modulators of the overall neuronal health following exposure to ethanol as well as independently of ethanol. The screening comprised 48 FDA-approved compounds, which were selected from a compound library based on their application in neurological diseases, and 5 drugs used in the treatment of AUD. The results observed for baclofen are in line with current clinical observations where its use for the treatment of AUD is still debated partly due to concerns about safety (de Beaurepaire et al., 2019). Moreover, several case reports presented patients who developed neurological symptoms after disulfiram therapy for alcohol, pointing out a neurotoxic effect of disulfiram (Torre et al., 2010; Heung et al., 2018).

Additionally, the toxicity on the mitochondrial neuronal health observed for lithium, another drug that has been suggested for the treatment of AUD, is in accordance with the literature (Lang and Davis, 2002; Mignarri et al., 2013; Shah et al., 2015). Among the FDA-approved drugs I found flavoxate, a spasmolytic drug which is mainly used to treat overactive bladder (Arcaniolo et al., 2015), to positively modulate neuronal health by increasing the MMP and neurite arborization (Fig. 26). Further studies should be conducted to confirm the results and determine the mode of action of the positive hit candidates in relation to ethanol as well as the pharmacokinetic and pharmacodynamic properties.

Overall, the data on AUD drugs raise concerns about the potentially increased toxicity of drugs when used in conjunction with alcohol consumption. Hence, there is still the need for appropriate hazard assessment of drugs used for the treatment of AUD to warrant safety and reduce the risk for neurotoxicity and subsequent neurodegeneration.

Usually, for *in vitro* studies the 10–100 mM ethanol range is considered physiological, whereas supplementation of cell culture ranging from 1–500 mM is reported in the literature (Dolganiuc and Szabo, 2009). In fact, for the chronic ethanol exposure hyperpolarization was observed at physiological ethanol concentrations of 50–100 mM and MMP depolarization was observed starting from 500 mM. These results are in line with previously reported results on human retina cells where cells showed hyperpolarization at low concentrations up to 50 mM for 24 hours and the collapse of the mitochondrial membrane potential starting from 400 mM (Bonet-Ponce et al., 2015).

To further study the ethanol-induced neurotoxicity I aimed to measure apoptosis. For this the Annexin V-FITC kit from MACS Miltenyi was used, which is described for the use in flow cytometry. The Annexin V-FITC staining principle was adapted for use with the HCA platform with only minor modifications. Even though a higher rate of apoptosis was detected for neurons treated with the positive control staurosporine, the effect was unexpectedly low. This could be due to the short (1.5 hours) exposure to staurosporine as well as due to the staining protocol. Incubation times with staurosporine of up to 24 hours have been reported (Thuret et al., 2003), as well as a wide range of concentrations (Koh et al., 1995; Simenc and Lipnik-Stangelj, 2012). Hence, further dose-effect studies should be performed to determine the optimal concentration of staurosporine as well as the incubation time to induce apoptosis. Moreover, the staining procedure could be optimized by adjusting the Annexin V-FITC applied to the cells as well as through the addition of propidium iodide to discriminate apoptosis and necrosis.

From a technical point, ethanol is described to evaporate by approx. 90% within 24 hours under culture conditions of 37°C and 5% CO_2 (Dolganiuc and Szabo, 2009; Lieberman et al., 2012). Hence, preparation of the initial stock concentration of 5 M and further diluting

the ethanol in media may result in lower final ethanol concentrations applied to the neurons than intended. Thus, in this setting the rate of evaporation is not fully known and may influence the interpretation of the data. Attempts to measure the final ethanol concentrations with a commercially available kit (Amplite™ Ethanol Quantitation Kit, AAT Bioquest) have not resulted in useful data so far. Therefore, measuring the final concentration of ethanol within the media before, during and after the measurement would be advisable.

Another technical point which could be optimized is the supplementation of ethanol in the chronic setting. In this study, ethanol was added for 7 days by removing half of the media and re-applying fresh ethanol supplemented into the media every day for 7 days. It is known that ethanol can influence the expression of adhesion molecules, which may have caused cell detachment (Sacanella and Estruch, 2003). This effect could have been aggravated due to the daily exchange of the media since neurons itself appear to be sensitive to media changes. Hence, adding ethanol on top may reduce shear stress and the risk of cell detachment. Notably, the media used in this study to culture the neurons contains BDNF, a neurotrophic factor that has been suggested to reduce ethanol-induced neurotoxicity (Heaton et al., 2011). BDNF was present in the media during the maintenance and the 7-day chronic ethanol exposure. Hence, this may have influenced the dataset and should be kept in mind.

6.3 MNH assay development

Based on the previously published HCA-based drug screening targeting MMP in iPSC-derived NPCs (Lorenz et al., 2017), I modified and expanded the assay to measure the MMP and neuronal outgrowth in iPSC-derived mature neuronal cells.

To adapt the assay to neurons, one critical step was the splitting process on the assay plate. Mature neurons are more sensitive to enzymatic splitting. Moreover, neuronal cultures may be more heterogeneous than NPCs. Nonetheless, only slight differences between neurons obtained from different iPSC lines was observed, with low batch-to-batch variability. Still, different cell concentrations had to be determined for re-plating on the MNH assay plate. Since NPCs continue to proliferate during the differentiation process to neurons, NPCs were first differentiated into neurons in conventional 6 well cell culture plates before the neurons were counted and seeded on the assay plate in a defined cell number. The defined cell number was essential since the BioApplication used for the evaluation of neuronal branching only allows a certain degree of confluency as described above (section 5.2.1). For the measurement of the MMP, on the other hand, confluency seemed not to play a major role regarding the BioApplication but for the general health. More confluently grown neurons would probably positively influence general health *in vitro* and not only would minimize the issue of cell detachment but also ensure sufficient neuronal connectivity. Even though the best possible compromise between a high number of cells for connectivity and sufficient space between the neurons for the "Neuronal Profiling" BioApplication to work sufficiently was aimed, the "Neuronal Profiling" BioApplication may present as limiting factor in the MNH assay.

Previous studies in the lab determined the concentration of TMRM that was sufficient to measure reliable fluorescence intensity, which needed to be as low as possible to reduce possible influences of the dye on the cells. Using the HCA microscope CellInsight CX7, we determined 0.5 nM TMRM as the most suitable non-quenching concentration. Nevertheless, TMRM concentrations need to be adjusted based on the cell type used and the detection limits of the microscope.

6.4 Genome editing for *KLB* knockout in control iPSC line

In this study, the generation of a human iPSC-based model system to dissect the role of KLB in ethanol consumption was aimed. For the generation of a *KLB* knockout line, the iPSC line XM001 was used. The approach showed promising results where deletions were detected in the target area by Sanger sequencing. Although high levels of gene disruption have been reported via NHEJ in different cell lines, the efficiencies in human stem cells are often substantially lower. In human iPSCs the overall gene disruption rate is typically only between 1–25% when using a single gRNA (Byrne et al., 2014; Xu et al., 2018), which was the case in this experimental design. One option to increase the success rate would be to induce out-of-frame deletions by applying two designed gRNAs inducing two different DSBs, which may increase the chance for insufficient DNA repair.

KLB is highly expressed in adipose tissue, pancreas, and the liver but low in human brain (The Human Protein Atlas). To further validate the selected clones generated in this study and confirm successful knockout, it would be necessary to quantify the RNA expression level for example through qRT-PCR, to assess protein expression via western blot analysis and to perform phenotypic analyses to demonstrate the functional consequences. Overall, genome editing represents a powerful tool for disease modeling in iPSCs and may help to understand the role of KLB in alcohol consumption.

6.5 HT-screening and neurotoxicity assessment

The evaluation of neurotoxicity in human model systems is still in a nascent stage. Recent studies used MEA to investigate the effect of illicit drugs and new psychoactive substances on spontaneous neuronal activity and network activity in rat primary cortical cultures (Zwartsen et al., 2018, 2020). Measurement of spontaneous electrical activity using MEA may be considered as robust assessment of the effects of compounds on neural network function (Vassallo et al., 2017). Nonetheless, there is a need for additional *in vitro* test systems for human cell-based toxicity assessment (Schmidt et al., 2017). To fully capture neurotoxicity *in vitro,* cellular platforms and read-out combinations for different aspects of neurotoxicity need to be established.

Considering the observations made throughout this study, the MNH assay may serve as basis for a more complex HT-amenable assay platform to evaluate neurotoxicity in human iPSC-derived neurons. The MNH assay may serve as toxicity screening to assess the level of toxicity of drugs, substances, or stressors directly on the cells of interest. One could use the assay to compare the susceptibility of neuronal cells from different individuals to stress or drugs, which also enables the identification of possible disease-associated phenotypes (Fig. 30).

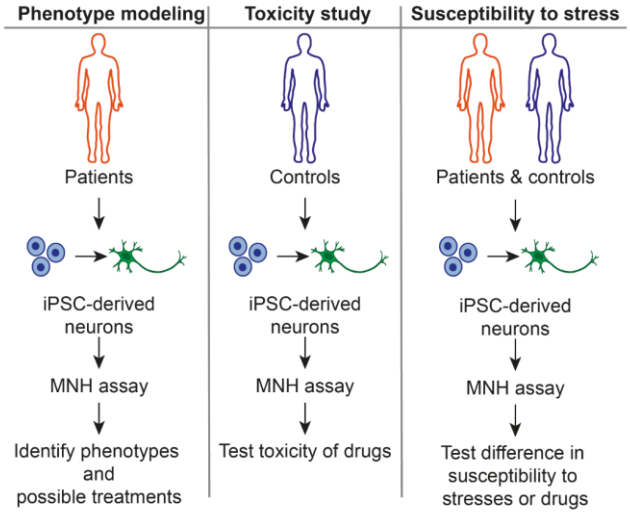

Fig. 30: Schematics of potential applications of the MNH assay.
Figure adapted from the published version: Zink A, Conrad J, Telugu NS, Diecke S, Heinz A, Wanker E, Priller J and Prigione A (2020) Assessment of Ethanol-Induced Toxicity on iPSC-Derived Human Neurons Using a Novel High-Throughput Mitochondrial Neuronal Health (MNH) Assay. *Front. Cell Dev. Biol*. 8:590540. https://doi.org/10.3389/fcell.2020.590540.

Further multiplexing of the assay could, for example, be accomplished through the addition of an apoptotic dye based on Annexin V together with propidium iodide to quantify cell death (Saunders et al., 2014; Gelles and Chipuk, 2016). Several studies underpin the feasibility of assay-multiplexing to assess toxicity using HCA. For the identification and characterization of the effect of cigarette smoke constituents on human bronchial epithelial cells one group multiplexed several staining protocols, which were quantified using high content screening (HCS) (Marescotti et al., 2016). Another study multiplexed readouts for cell viability, mitochondrial integrity, and ROS formation to evaluate their applicability for HCS-based toxicity evaluation (Grimm et al., 2015). For further neurotoxicity evaluation, the MNH assay could be adapted to a fully automated and self-contained system to reduce external influences triggered by changes in the environment (for example changes in temperature and CO_2 during the transport). This could be accomplished through robotics attached to the HCA system enabling transport

of the cell culture plate from the incubator into the HCA system within a controlled environment. A pipetting robot could facilitate and automate media exchanges or the addition of compounds. These factors would probably result in a more robust screening system used for drug development and hazard assessment.

Taken together, the MNH assay enabled to capture the ethanol-induced toxicity in human neurons. The assay may further serve as a potential tool for the evaluation of human neuronal health, for the identification of disease phenotypes and corresponding treatments, and for conducting HT drug discovery and drug toxicity studies in the context of AUD or independent from ethanol toxicity.

6.6 Concluding remarks

Excessive alcohol consumption is a leading risk factor for disease, disability, and death (Griswold et al., 2018). Still, treatment options for alcohol abuse and dependence including AUD are limited and not without risk. Moreover, most drugs of abuse may have inherent neurotoxic effects (Mohammad Ahmadi Soleimani et al., 2016). Understanding the level of ethanol-induced neurotoxicity may enable the development of neuroprotective drugs to reduce the risk for developing neurodegeneration following excessive alcohol consumption.

Hence, the aim of this study was to generate an iPSC-based model system to investigate toxic consequences of ethanol on human neurons. The protocol adapted from Reinhardt et al. (Reinhardt et al., 2013) enabled the generation of many batches of human iPSC-derived neurons containing dopaminergic neurons in a cost effective and reproducible manner. Nevertheless, their potential to release dopamine remains to be studied. My second aim was to address ethanol-induced neurotoxicity in a quantitative HT-amenable

manner. For this, I multiplexed an HCA assay evaluating MMP with another HCA assay measuring neuronal growth complexity. We dubbed the assay Mitochondrial Neuronal Health (MNH) assay. The MMP is known to be an essential parameter for viable cells and is important for ATP generation and the initiation of apoptosis. Using the MNH assay I could show that increasing concentrations of ethanol negatively affected the MMP and neural outgrowth following acute and chronic ethanol exposure in both iPSC-derived neurons from healthy subjects and in iPSC-derived neurons from subjects diagnosed with AUD. Since it was possible to quantitively measure ethanol-induced neurotoxicity I was further interested in the establishment of new drug treatment strategies. Using the MNH assay I performed a proof-of-concept compound screening of 53 FDA approved drugs that are in clinical use for brain diseases and 5 drugs currently used for the treatment of AUD. The screening resulted in the detection of two hit compounds that positively affected the MNH and 21 hit compounds that negatively affected the MNH in the presence of ethanol. Further validation studies are required to confirm the exploratory results. However, the results raise concerns with respect to the potentially enhanced toxicity of compounds when combined with alcohol.

Overall, this work highlights the potential of iPSC-derived model systems to investigate toxic consequences of ethanol on human neurons. Moreover, it addresses the importance of assessing possible toxic effects of compounds on human cell types. The MNH assay, developed in this study, may serve as a tool for the assessment of human mitochondrial and neuronal health. Furthermore, the MNH assay could be optimized for the use in HT drug discovery and drug toxicity screenings.

7. Contributions

In general, Josefin Conrad helped me with the characterization of the AUD-iPSCs and with the generation and characterization of the AUD-NPCs and AUD-neurons. This was part of her bachelor thesis, which I supervised (FU Berlin 2020). More detailed and further author contributions are described as follows:

Figure 8D: Josefin Conrad performed the qPCR of control NPCs with my help during her bachelor thesis (FU Berlin; MDC 2019-2020).

Figure 8F: Josefin Conrad helped with the generation and immunostaining of control neurons during her bachelor thesis (FU Berlin; MDC 2019-2020).

Figure 18A: Blood withdrawal was performed at Charité- Universitätsmedizin Berlin and AUD-iPSCs were generated by the Stem Cell Core facility (MDC and BIH, 2018).

Figure 18B/18C: Josefin Conrad helped with the characterization of the AUD-iPSCs, which was part of her bachelor thesis. She also helped with performing the qPCR and with the immunostainings (FU Berlin; MDC 2019-2020).

Figure 18D: Karyotyping of the AUD-iPSCs was performed by the Stem Cell Core facility (MDC and BIH, 2018).

Figure 19A/19B: Josefin Conrad helped me with the generation and characterization of the AUD-NPCs. She performed the qPCR and helped with the immunostaining. Both were part of her bachelor thesis (FU Berlin; MDC 2019-2020)

Figure 20: Josefin Conrad helped with the generation and characterization of the AUD-neurons. This was part of her bachelor thesis (FU Berlin; MDC 2019-2020).

Contribution

Figure 23: Josefin Conrad assisted with the preparation of the compound plates (FU Berlin; MDC 2019-2020).

Figure 27: Pawel Lisowski performed the PCR to determine KLB expression in different cell lines and helped with the primer design (MDC, 2018-2019).

Figure 28: Pawel Lisowski helped with planning the CRISPR/Cas 9 strategy (MDC, 2018-2019). The master student Tobias Hahn (supervised by Pawel Lisowski) helped to generate the required plasmids and with the transfection into the iPSCs (Hochschule Albstadt-Sigmaringen, 2018).

Figure 29: Tobias Hahn (Hochschule Albstadt-Sigmaringen, 2018) and Josefin Conrad (FU Berlin; MDC 2019-2020) performed the transfection of the cells. Josefin Conrad helped screening the clones via PCR.

8. Bibliography

Abrahao, K. P., Salinas, A. G., and Lovinger, D. M. (2017). Alcohol and the Brain: Neuronal Molecular Targets, Synapses, and Circuits. *Neuron* 96, 1223–1238. doi:10.1016/j.neuron.2017.10.032.

Agabio, R., and Colombo, G. (2014). GABAB receptor ligands for the treatment of alcohol use disorder: preclinical and clinical evidence. *Front. Neurosci.* 8. doi:10.3389/fnins.2014.00140.

Agarwal, D. P. (2001). Genetic polymorphisms of alcohol metabolizing enzymes. *Pathol. Biol.* 49, 703–709. doi:10.1016/S0369-8114(01)00242-5.

Alfonso-Loeches, S., Pascual, M., and Guerri, C. (2013). Gender differences in alcohol-induced neurotoxicity and brain damage. *Toxicology* 311, 27–34. doi:10.1016/j.tox.2013.03.001.

American Psychiatric Association (2013). *Diagnostic and Statistical Manual of Mental Disorders (DSM-5®)*. American Psychiatric Pub.

Arcaniolo, D., Conquy, S., and Tarcan, T. (2015). Flavoxate: present and future. *Eur. Rev. Med. Pharmacol. Sci.* 19, 719–731.

Archer, S. L. (2013). Mitochondrial dynamics--mitochondrial fission and fusion in human diseases. *N. Engl. J. Med.* 369, 2236–2251. doi:10.1056/NEJMra1215233.

Arias-Fuenzalida, J., Jarazo, J., Walter, J., Gomez-Giro, G., Forster, J. I., Krueger, R., et al. (2019). Automated high-throughput high-content autophagy and mitophagy analysis platform. *Sci. Rep.* 9, 1–11. doi:10.1038/s41598-019-45917-2.

Arzua, T., Yan, Y., Jiang, C., Logan, S., Allison, R. L., Wells, C., et al. (2020). Modeling alcohol-induced neurotoxicity using human induced pluripotent stem cell-derived three-dimensional cerebral organoids. *Transl. Psychiatry* 10, 1–21. doi:10.1038/s41398-020-01029-4.

Attilia, F., Perciballi, R., Rotondo, C., Capriglione, I., Iannuzzi, S., Attilia, M. L., et al. (2018). Alcohol withdrawal syndrome: diagnostic and therapeutic methods. *Riv. Psichiatr.* 53, 118–122. Available at: / [Accessed October 6, 2020].

Auta, J., Zhang, H., Pandey, S. C., and Guidotti, A. (2017). Chronic Alcohol Exposure Differentially Alters One-Carbon Metabolism in Rat Liver and Brain. *Alcohol. Clin. Exp. Res.* 41, 1105–1111. doi:10.1111/acer.13382.

Bahmad, H., Hadadeh, O., Chamaa, F., Cheaito, K., Darwish, B., Makkawi, A.-K., et al. (2017). Modeling Human Neurological and Neurodegenerative Diseases: From

Induced Pluripotent Stem Cells to Neuronal Differentiation and Its Applications in Neurotrauma. *Front. Mol. Neurosci.* 10. doi:10.3389/fnmol.2017.00050.

Baliunas, D. O., Taylor, B. J., Irving, H., Roerecke, M., Patra, J., Mohapatra, S., et al. (2009). Alcohol as a risk factor for type 2 diabetes: A systematic review and meta-analysis. *Diabetes Care* 32, 2123–2132. doi:10.2337/dc09-0227.

Banerjee, N. (2014). Neurotransmitters in alcoholism: A review of neurobiological and genetic studies. *Indian J. Hum. Genet.* 20, 20–31. doi:10.4103/0971-6866.132750.

Barres, B. A. (2008). The Mystery and Magic of Glia: A Perspective on Their Roles in Health and Disease. *Neuron* 60, 430–440. doi:10.1016/j.neuron.2008.10.013.

Bates, M. E., Bowden, S. C., and Barry, D. (2002). Neurocognitive impairment associated with alcohol use disorders: implications for treatment. *Exp. Clin. Psychopharmacol.* 10, 193–212. doi:10.1037//1064-1297.10.3.193.

Bliek, A. M. van der, Shen, Q., and Kawajiri, S. (2013). Mechanisms of Mitochondrial Fission and Fusion. *Cold Spring Harb. Perspect. Biol.* 5, a011072. doi:10.1101/cshperspect.a011072.

Boileau, I., Assaad, J.-M., Pihl, R. O., Benkelfat, C., Leyton, M., Diksic, M., et al. (2003). Alcohol promotes dopamine release in the human nucleus accumbens. *Synap. N. Y. N* 49, 226–231. doi:10.1002/syn.10226.

Bonet-Ponce, L., Saez-Atienzar, S., da Casa, C., Flores-Bellver, M., Barcia, J. M., Sancho-Pelluz, J., et al. (2015). On the mechanism underlying ethanol-induced mitochondrial dynamic disruption and autophagy response. *Biochim. Biophys. Acta* 1852, 1400–1409. doi:10.1016/j.bbadis.2015.03.006.

Bookout, A. L., de Groot, M. H. M., Owen, B. M., Lee, S., Gautron, L., Lawrence, H. L., et al. (2013). FGF21 regulates circadian behavior and metabolism by acting on the nervous system. *Nat. Med.* 19, 1147–1152. doi:10.1038/nm.3249.

Brennand, K. J., Simone, A., Jou, J., Gelboin-Burkhart, C., Tran, N., Sangar, S., et al. (2011). Modelling schizophrenia using human induced pluripotent stem cells. *Nature* 473, 221–225. doi:10.1038/nature09915.

Burghes, A. H. M., and Beattie, C. E. (2009). Spinal muscular atrophy: why do low levels of survival motor neuron protein make motor neurons sick? *Nat. Rev. Neurosci.* 10, 597–609. doi:10.1038/nrn2670.

Burté, F., Carelli, V., Chinnery, P. F., and Yu-Wai-Man, P. (2015). Disturbed mitochondrial dynamics and neurodegenerative disorders. *Nat. Rev. Neurol.* 11, 11–24. doi:10.1038/nrneurol.2014.228.

Bustamante, J., Karadayian, A. G., Lores-Arnaiz, S., and Cutrera, R. A. (2012). Alterations of motor performance and brain cortex mitochondrial function

during ethanol hangover. *Alcohol* 46, 473–479. doi:10.1016/j.alcohol.2011.09.027.

Byrne, S. M., Mali, P., and Church, G. M. (2014). GENOME EDITING IN HUMAN STEM CELLS. *Methods Enzymol.* 546, 119–138. doi:10.1016/B978-0-12-801185-0.00006-4.

Campo, M. L., Kinnally, K. W., and Tedeschi, H. (1992). The effect of antimycin A on mouse liver inner mitochondrial membrane channel activity. *J. Biol. Chem.* 267, 8123–8127.

Casañas-Sánchez, V., Pérez, J. A., Quinto-Alemany, D., and Díaz, M. (2016). Sub-toxic Ethanol Exposure Modulates Gene Expression and Enzyme Activity of Antioxidant Systems to Provide Neuroprotection in Hippocampal HT22 Cells. *Front. Physiol.* 7. doi:10.3389/fphys.2016.00312.

Cederbaum, A. I. (2012). Alcohol Metabolism. *Clin. Liver Dis.* 16, 667–685. doi:10.1016/j.cld.2012.08.002.

Cederbaum, A. I., Lu, Y., and Wu, D. (2009). Role of oxidative stress in alcohol-induced liver injury. *Arch. Toxicol.* 83, 519–548. doi:10.1007/s00204-009-0432-0.

Chambers, S. M., Fasano, C. A., Papapetrou, E. P., Tomishima, M., Sadelain, M., and Studer, L. (2009). Highly efficient neural conversion of human ES and iPS cells by dual inhibition of SMAD signaling. *Nat. Biotechnol.* 27, 275–280. doi:10.1038/nbt.1529.

Chan, D. C. (2006). Mitochondrial fusion and fission in mammals. *Annu. Rev. Cell Dev. Biol.* 22, 79–99. doi:10.1146/annurev.cellbio.22.010305.104638.

Charlet, K., Beck, A., and Heinz, A. (2011). "The Dopamine System in Mediating Alcohol Effects in Humans," in *Behavioral Neurobiology of Alcohol Addiction* Current Topics in Behavioral Neurosciences., eds. W. H. Sommer and R. Spanagel (Berlin, Heidelberg: Springer Berlin Heidelberg), 461–488. doi:10.1007/978-3-642-28720-6_130.

Chen, L. B. (1988). Mitochondrial membrane potential in living cells. *Annu. Rev. Cell Biol.* 4, 155–181. doi:10.1146/annurev.cb.04.110188.001103.

Chiang, C.-H., Su, Y., Wen, Z., Yoritomo, N., Ross, C. A., Margolis, R. L., et al. (2011). Integration-free induced pluripotent stem cells derived from schizophrenia patients with a DISC1 mutation. *Mol. Psychiatry* 16, 358–360. doi:10.1038/mp.2011.13.

Chinnery, P. F., and Hudson, G. (2013). Mitochondrial genetics. *Br. Med. Bull.* 106, 135–159. doi:10.1093/bmb/ldt017.

Clark, D. C., and Fawcett, J. (1989). "Does Lithium Carbonate Therapy for Alcoholism Deter Relapse Drinking?," in *Recent Developments in Alcoholism: Treatment*

Research Recent Developments in Alcoholism., ed. M. Galanter (Boston, MA: Springer US), 315–328. doi:10.1007/978-1-4899-1678-5_16.

Clarke, D. D., and Sokoloff, L. (1999). Circulation and Energy Metabolism of the Brain. *Basic Neurochem. Mol. Cell. Med. Asp. 6th Ed.* Available at: https://www.ncbi.nlm.nih.gov/books/NBK20413/ [Accessed July 14, 2020].

Clarke, T.-K., Adams, M. J., Davies, G., Howard, D. M., Hall, L. S., Padmanabhan, S., et al. (2017). Genome-wide association study of alcohol consumption and genetic overlap with other health-related traits in UK Biobank (N=112 117). *Mol. Psychiatry* 22, 1376–1384. doi:10.1038/mp.2017.153.

Costa, L. G. (1998). Neurotoxicity testing: a discussion of in vitro alternatives. *Environ. Health Perspect.* 106, 505–510.

Cui, C., and Koob, G. F. (2017). Titrating Tipsy Targets: The Neurobiology of Low-Dose Alcohol. *Trends Pharmacol. Sci.* 38, 556–568. doi:10.1016/j.tips.2017.03.002.

Daneman, R., and Prat, A. (2015). The Blood–Brain Barrier. *Cold Spring Harb. Perspect. Biol.* 7. doi:10.1101/cshperspect.a020412.

Daniele, J. R., Esping, D. J., Garcia, G., Parsons, L. S., Arriaga, E. A., and Dillin, A. (2017). "High-Throughput Characterization of Region-Specific Mitochondrial Function and Morphology." *Sci. Rep.* 7, 1–16. doi:10.1038/s41598-017-05152-z.

Das, S. K., and Vasudevan, D. M. (2007). Alcohol-induced oxidative stress. *Life Sci.* 81, 177–187. doi:10.1016/j.lfs.2007.05.005.

de Beaurepaire, R. (2018). A Review of the Potential Mechanisms of Action of Baclofen in Alcohol Use Disorder. *Front. Psychiatry* 9. doi:10.3389/fpsyt.2018.00506.

de Beaurepaire, R., Sinclair, J. M. A., Heydtmann, M., Addolorato, G., Aubin, H.-J., Beraha, E. M., et al. (2019). The Use of Baclofen as a Treatment for Alcohol Use Disorder: A Clinical Practice Perspective. *Front. Psychiatry* 9. doi:10.3389/fpsyt.2018.00708.

De Filippis, L., Halikere, A., McGowan, H., Moore, J. C., Tischfield, J. A., Hart, R. P., et al. (2016). Ethanol-mediated activation of the NLRP3 inflammasome in iPS cells and iPS cells-derived neural progenitor cells. *Mol. Brain* 9, 51. doi:10.1186/s13041-016-0221-7.

Dehmelt, L., and Halpain, S. (2004). The MAP2/Tau family of microtubule-associated proteins. *Genome Biol.* 6, 204. doi:10.1186/gb-2004-6-1-204.

Dhaliwal, J. S., Rosani, A., and Saadabadi, A. (2020). "Diazepam," in *StatPearls* (Treasure Island (FL): StatPearls Publishing). Available at: http://www.ncbi.nlm.nih.gov/books/NBK537022/ [Accessed October 22, 2020].

Diana, M. (2011). The Dopamine Hypothesis of Drug Addiction and Its Potential Therapeutic Value. *Front. Psychiatry* 2. doi:10.3389/fpsyt.2011.00064.

Dispersyn, G., Nuydens, R., Connors, R., Borgers, M., and Geerts, H. (1999). Bcl-2 protects against FCCP-induced apoptosis and mitochondrial membrane potential depolarization in PC12 cells. *Biochim. Biophys. Acta BBA - Gen. Subj.* 1428, 357–371. doi:10.1016/S0304-4165(99)00073-2.

Dolganiuc, A., and Szabo, G. (2009). In vitro and in vivo models of acute alcohol exposure. *World J. Gastroenterol. WJG* 15, 1168–1177. doi:10.3748/wjg.15.1168.

Duval, K., Grover, H., Han, L.-H., Mou, Y., Pegoraro, A. F., Fredberg, J., et al. (2017). Modeling Physiological Events in 2D vs. 3D Cell Culture. *Physiology* 32, 266–277. doi:10.1152/physiol.00036.2016.

Dyall, S. D., Brown, M. T., and Johnson, P. J. (2004). Ancient invasions: from endosymbionts to organelles. *Science* 304, 253–257. doi:10.1126/science.1094884.

Ebert, A. D., Yu, J., Rose, F. F., Mattis, V. B., Lorson, C. L., Thomson, J. A., et al. (2009). Induced pluripotent stem cells from a spinal muscular atrophy patient. *Nature* 457, 277–280. doi:10.1038/nature07677.

Erecińska, M., and Silver, I. A. (2001). Tissue oxygen tension and brain sensitivity to hypoxia. *Respir. Physiol.* 128, 263–276. doi:10.1016/s0034-5687(01)00306-1.

Erickson, E. K., Blednov, Y. A., Harris, R. A., and Mayfield, R. D. (2019). Glial gene networks associated with alcohol dependence. *Sci. Rep.* 9, 10949. doi:10.1038/s41598-019-47454-4.

Fairbanks, J., Umbreit, A., Kolla, B. P., Karpyak, V. M., Schneekloth, T. D., Loukianova, L. L., et al. (2020). Evidence-Based Pharmacotherapies for Alcohol Use Disorder: Clinical Pearls. *Mayo Clin. Proc.* 95, 1964–1977. doi:10.1016/j.mayocp.2020.01.030.

Fawcett, J., Clark, D. C., Aagesen, C. A., Pisani, V. D., Tilkin, J. M., Sellers, D., et al. (1987). A Double-blind, Placebo-Controlled Trial of Lithium Carbonate Therapy for Alcoholism. *Arch. Gen. Psychiatry* 44, 248–256. doi:10.1001/archpsyc.1987.01800150060008.

Fernandes, L. M. P., de Andrade, E. F., Monteiro, M. C., Cartágenes, S. C., Lima, R. R., Prediger, R. D., et al. (2017). "Chapter 20 - Ethanol: Neurotoxicity and Brain Disorders," in *Addictive Substances and Neurological Disease*, eds. R. R. Watson and S. Zibadi (Academic Press), 201–215. doi:10.1016/B978-0-12-805373-7.00020-7.

Fernandez, G. M., Lew, B. J., Vedder, L. C., and Savage, L. M. (2017). Chronic intermittent ethanol exposure leads to alterations in brain-derived neurotrophic factor within the frontal cortex and impaired behavioral flexibility in both

adolescent and adult rats. *Neuroscience* 348, 324–334. doi:10.1016/j.neuroscience.2017.02.045.

Fernández-Serrano, M. J., Pérez-García, M., Schmidt Río-Valle, J., and Verdejo-García, A. (2010). Neuropsychological consequences of alcohol and drug abuse on different components of executive functions. *J. Psychopharmacol. Oxf. Engl.* 24, 1317–1332. doi:10.1177/0269881109349841.

Ferreira, M. P., and Willoughby, D. (2008). Alcohol consumption: the good, the bad, and the indifferent. *Appl. Physiol. Nutr. Metab.* 33, 12–20. doi:10.1139/H07-175.

Franklin, T. R., Harper, D., Kampman, K., Kildea, S., Jens, W., Lynch, K., et al. (2009). The GABA B agonist baclofen reduces cigarette consumption in a preliminary double-blind placebo-controlled smoking reduction study. *Drug Alcohol Depend.* 103, 30–36. doi:10.1016/j.drugalcdep.2009.02.014.

Gelles, J. D., and Chipuk, J. E. (2016). Robust high-throughput kinetic analysis of apoptosis with real-time high-content live-cell imaging. *Cell Death Dis.* 7, e2493. doi:10.1038/cddis.2016.332.

Gémes, K., Forsell, Y., Janszky, I., László, K. D., Lundin, A., Leon, A. P. D., et al. (2019). Moderate alcohol consumption and depression – a longitudinal population-based study in Sweden. *Acta Psychiatr. Scand.* 139, 526–535. doi:10.1111/acps.13034.

George, A., and Figueredo, V. M. (2010). Alcohol and arrhythmias: a comprehensive review. *J. Cardiovasc. Med.* 11, 221–228. doi:10.2459/JCM.0b013e328334b42d.

Giorgi, C., Agnoletto, C., Bononi, A., Bonora, M., De Marchi, E., Marchi, S., et al. (2012). Mitochondrial calcium homeostasis as potential target for mitochondrial medicine. *Mitochondrion* 12, 77–85. doi:10.1016/j.mito.2011.07.004.

Giuliano, K. A., DeBiasio, R. L., Dunlay, R. T., Gough, A., Volosky, J. M., Zock, J., et al. (1997). High-Content Screening: A New Approach to Easing Key Bottlenecks in the Drug Discovery Process: *J. Biomol. Screen.* doi:10.1177/108705719700200410.

Goldman, D., Oroszi, G., and Ducci, F. (2005). The genetics of addictions: uncovering the genes. *Nat. Rev. Genet.* 6, 521–532. doi:10.1038/nrg1635.

Goldman, S. A. (2016). Stem and progenitor cell-based therapy of the central nervous system: Hopes, hype and wishful thinking. *Cell Stem Cell* 18, 174–188. doi:10.1016/j.stem.2016.01.012.

Gonzales, R. A., Job, M. O., and Doyon, W. M. (2004). The role of mesolimbic dopamine in the development and maintenance of ethanol reinforcement. *Pharmacol. Ther.* 103, 121–146. doi:10.1016/j.pharmthera.2004.06.002.

Grimm, F. A., Iwata, Y., Sirenko, O., Bittner, M., and Rusyn, I. (2015). High-Content Assay Multiplexing for Toxicity Screening in Induced Pluripotent Stem Cell-Derived Cardiomyocytes and Hepatocytes. *ASSAY Drug Dev. Technol.* 13, 529–546. doi:10.1089/adt.2015.659.

Griswold, M. G., Fullman, N., Hawley, C., Arian, N., Zimsen, S. R. M., Tymeson, H. D., et al. (2018). Alcohol use and burden for 195 countries and territories, 1990–2016: a systematic analysis for the Global Burden of Disease Study 2016. *The Lancet* 392, 1015–1035. doi:10.1016/S0140-6736(18)31310-2.

Grobarczyk, B., Franco, B., Hanon, K., and Malgrange, B. (2015). Generation of Isogenic Human iPS Cell Line Precisely Corrected by Genome Editing Using the CRISPR/Cas9 System. *Stem Cell Rev.* 11, 774–787. doi:10.1007/s12015-015-9600-1.

Grskovic, M., Javaherian, A., Strulovici, B., and Daley, G. Q. (2011). Induced pluripotent stem cells--opportunities for disease modelling and drug discovery. *Nat. Rev. Drug Discov.* 10, 915–929. doi:10.1038/nrd3577.

Guenther, M. G., Frampton, G. M., Soldner, F., Hockemeyer, D., Mitalipova, M., Jaenisch, R., et al. (2010). Chromatin Structure and Gene Expression Programs of Human Embryonic and Induced Pluripotent Stem Cells. *Cell Stem Cell* 7, 249–257. doi:10.1016/j.stem.2010.06.015.

Guo, R., and Ren, J. (2010). Alcohol and Acetaldehyde in Public Health: From Marvel to Menace. *Int. J. Environ. Res. Public. Health* 7, 1285–1301. doi:10.3390/ijerph7041285.

Gupta, R. M., and Musunuru, K. (2014). Expanding the genetic editing tool kit: ZFNs, TALENs, and CRISPR-Cas9. *J. Clin. Invest.* 124, 4154–4161. doi:10.1172/JCI72992.

Handler, J. A., and Thurman, R. G. (1988). Catalase-dependent ethanol oxidation in perfused rat liver. Requirement for fatty-acid-stimulated H2O2 production by peroxisomes. *Eur. J. Biochem.* 176, 477–484. doi:10.1111/j.1432-1033.1988.tb14305.x.

Haorah, J., Ramirez, S. H., Floreani, N., Gorantla, S., Morsey, B., and Persidsky, Y. (2008). Mechanism of alcohol-induced oxidative stress and neuronal injury. *Free Radic. Biol. Med.* 45, 1542–1550. doi:10.1016/j.freeradbiomed.2008.08.030.

Haorah, J., Rump, T. J., and Xiong, H. (2013). Reduction of Brain Mitochondrial β-Oxidation Impairs Complex I and V in Chronic Alcohol Intake: The Underlying Mechanism for Neurodegeneration. *PLoS ONE* 8, e70833. doi:10.1371/journal.pone.0070833.

Harper, C. (2009). The neuropathology of alcohol-related brain damage. *Alcohol Alcohol. Oxf. Oxfs.* 44, 136–140. doi:10.1093/alcalc/agn102.

Bibliography

Harris, A. H. S., Kivlahan, D. R., Bowe, T., and Humphreys, K. N. (2010). Pharmacotherapy of alcohol use disorders in the Veterans Health Administration. *Psychiatr. Serv. Wash. DC* 61, 392–398. doi:10.1176/ps.2010.61.4.392.

Hasin, D. S., Stinson, F. S., Ogburn, E., and Grant, B. F. (2007). Prevalence, correlates, disability, and comorbidity of DSM-IV alcohol abuse and dependence in the United States: results from the National Epidemiologic Survey on Alcohol and Related Conditions. *Arch. Gen. Psychiatry* 64, 830–842. doi:10.1001/archpsyc.64.7.830.

Heaton, M. B., Paiva, M., and Siler-Marsiglio, K. (2011). Ethanol Influences on Bax Translocation, Mitochondrial Membrane Potential, and Reactive Oxygen Species Generation Are Modulated by Vitamin E and Brain-Derived Neurotrophic Factor: VITAMIN E/BDNF REDUCE ETHANOL TOXICITY. *Alcohol. Clin. Exp. Res.* 35, 1122–1133. doi:10.1111/j.1530-0277.2011.01445.x.

Heilig, M., Augier, E., Pfarr, S., and Sommer, W. H. (2019). Developing neuroscience-based treatments for alcohol addiction: A matter of choice? *Transl. Psychiatry* 9, 1–11. doi:10.1038/s41398-019-0591-6.

Heilker, R., Traub, S., Reinhardt, P., Schöler, H. R., and Sterneckert, J. (2014). iPS cell derived neuronal cells for drug discovery. *Trends Pharmacol. Sci.* 35, 510–519. doi:10.1016/j.tips.2014.07.003.

Heinz, A., Beck, A., Wrase, J., Mohr, J., Obermayer, K., Gallinat, J., et al. (2009). Neurotransmitter Systems in Alcohol Dependence. *Pharmacopsychiatry* 42, S95–S101. doi:10.1055/s-0029-1214395.

Heung, J., Poon, J. Y., Tung, C., Yeung, S., and Lam, M. (2018). Confusion in Sobriety: A Case Study on Disulfiram Encephalopathy in a Middle-Aged Male Patient. *Alcohol Alcohol* 53, 497–498. doi:10.1093/alcalc/agy018.

Hines, L. M., and Rimm, E. B. (2001). Moderate alcohol consumption and coronary heart disease: a review. *Postgrad. Med. J.* 77, 747–752. doi:10.1136/pgmj.77.914.747.

Hingorani, R., Deng, J., Elia, J., McIntyre, C., and Mittar, D. (2011). Detection of Apoptosis Using the BD Annexin V FITC Assay on the BD FACSVerse™ System. 12.

Hiroi, N., and Agatsuma, S. (2005). Genetic susceptibility to substance dependence. *Mol. Psychiatry* 10, 336–344. doi:10.1038/sj.mp.4001622.

Hockemeyer, D., and Jaenisch, R. (2016). Induced Pluripotent Stem Cells Meet Genome Editing. *Cell Stem Cell* 18, 573–586. doi:10.1016/j.stem.2016.04.013.

Iannetti, E. F., Willems, P. H. G. M., Pellegrini, M., Beyrath, J., Smeitink, J. A. M., Blanchet, L., et al. (2015). Toward high-content screening of mitochondrial

morphology and membrane potential in living cells. *Int. J. Biochem. Cell Biol.* 63, 66–70. doi:10.1016/j.biocel.2015.01.020.

Ikehara, S., Iso, H., Toyoshima, H., Date, C., Yamamoto, A., Kikuchi, S., et al. (2008). Alcohol consumption and mortality from stroke and coronary heart disease among Japanese men and women: the Japan collaborative cohort study. *Stroke* 39, 2936–2942. doi:10.1161/STROKEAHA.108.520288.

Inak-Girrbach, G. (2019). Modeling Leigh syndrome using patient-specific induced pluripotent stem cells. doi:10.17169/refubium-25988.

Izant, J. G., and McIntosh, J. R. (1980). Microtubule-associated proteins: a monoclonal antibody to MAP2 binds to differentiated neurons. *Proc. Natl. Acad. Sci. U. S. A.* 77, 4741–5. doi:10.1073/pnas.77.8.4741.

Jackson, J., Jambrina, E., Li, J., Marston, H., Menzies, F., Phillips, K., et al. (2019). Targeting the Synapse in Alzheimer's Disease. *Front. Neurosci.* 13. doi:10.3389/fnins.2019.00735.

Jayaram-Lindström, N., Ericson, M., Steensland, P., and Jerlhag, E. (2016). Dopamine and Alcohol Dependence: From Bench to Clinic. *Recent Adv. Drug Addict. Res. Clin. Appl.* doi:10.5772/63144.

Ji, C. (2011). Mechanisms of Alcohol-Induced Endoplasmic Reticulum Stress and Organ Injuries. *Biochem. Res. Int.* 2012, e216450. doi:https://doi.org/10.1155/2012/216450.

Jinek, M., Chylinski, K., Fonfara, I., Hauer, M., Doudna, J. A., and Charpentier, E. (2012). A Programmable Dual-RNA–Guided DNA Endonuclease in Adaptive Bacterial Immunity. *Science* 337, 816–821. doi:10.1126/science.1225829.

Johnson, R. A., Noll, E. C., and Rodney, W. M. (1982). Survival after a serum ethanol concentration of 1 1/2%. *Lancet Lond. Engl.* 2, 1394. doi:10.1016/s0140-6736(82)91285-5.

Jung, M. E. (2015). Alcohol Withdrawal and Cerebellar Mitochondria. *Cerebellum Lond. Engl.* 14, 421–437. doi:10.1007/s12311-014-0598-8.

Kalbáčová, M., Vrbacký, M., Drahota, Z., and Mělková, Z. (2003). Comparison of the effect of mitochondrial inhibitors on mitochondrial membrane potential in two different cell lines using flow cytometry and spectrofluorometry. *Cytometry A* 52A, 110–116. doi:10.1002/cyto.a.10031.

Karadayian, A. G., Bustamante, J., Czerniczyniec, A., Lombardi, P., Cutrera, R. A., and Lores-Arnaiz, S. (2015). Alcohol hangover induces mitochondrial dysfunction and free radical production in mouse cerebellum. *Neuroscience* 304, 47–59. doi:10.1016/j.neuroscience.2015.07.012.

Kelava, I., and Lancaster, M. A. (2016). Stem Cell Models of Human Brain Development. *Cell Stem Cell* 18, 736–748. doi:10.1016/j.stem.2016.05.022.

Bibliography

Kepiro, M., Varkuti, B. H., and Davis, R. L. (2018). "High Content, Phenotypic Assays and Screens for Compounds Modulating Cellular Processes in Primary Neurons," in *Methods in Enzymology* (Elsevier), 219–250. doi:10.1016/bs.mie.2018.09.021.

Kessler, R. C., Berglund, P., Demler, O., Jin, R., Merikangas, K. R., and Walters, E. E. (2005). Lifetime prevalence and age-of-onset distributions of DSM-IV disorders in the National Comorbidity Survey Replication. *Arch. Gen. Psychiatry* 62, 593–602. doi:10.1001/archpsyc.62.6.593.

Kim, D.-S., Lee, J. S., Leem, J. W., Huh, Y. J., Kim, J. Y., Kim, H.-S., et al. (2010). Robust enhancement of neural differentiation from human ES and iPS cells regardless of their innate difference in differentiation propensity. *Stem Cell Rev. Rep.* 6, 270–281. doi:10.1007/s12015-010-9138-1.

Kim, J.-S., He, L., and Lemasters, J. J. (2003). Mitochondrial permeability transition: a common pathway to necrosis and apoptosis. *Biochem. Biophys. Res. Commun.* 304, 463–470. doi:10.1016/s0006-291x(03)00618-1.

Kim, W. H., Hong, F., Jaruga, B., Zhang, Z. S., Fan, S. J., Liang, T. J., et al. (2005). Hepatitis B virus X protein sensitizes primary mouse hepatocytes to ethanol- and TNF-alpha-induced apoptosis by a caspase-3-dependent mechanism. *Cell. Mol. Immunol.* 2, 40–48.

Kim, Y., Hack, L. M., Ahn, E. S., and Kim, J. (2018). Practical outpatient pharmacotherapy for alcohol use disorder. *Drugs Context* 7. doi:10.7573/dic.212308.

Klatsky, A. L. (1999). Moderate Drinking and Reduced Risk of Heart Disease. *Alcohol Res. Health* 23, 15–24.

Koh, J.-Y., Wie, M. B., Gwag, B. J., Sensi, S. L., Canzoniero, L. M. T., Demaro, J., et al. (1995). Staurosporine-Induced Neuronal Apoptosis. *Exp. Neurol.* 135, 153–159. doi:10.1006/exnr.1995.1074.

Koob, G. F. (2013). Theoretical frameworks and mechanistic aspects of alcohol addiction: alcohol addiction as a reward deficit disorder. *Curr. Top. Behav. Neurosci.* 13, 3–30. doi:10.1007/7854_2011_129.

Koppes, L. L. J., Dekker, J. M., Hendriks, H. F. J., Bouter, L. M., and Heine, R. J. (2005). Moderate Alcohol Consumption Lowers the Risk of Type 2 Diabetes: A meta-analysis of prospective observational studies. *Diabetes Care* 28, 719–725. doi:10.2337/diacare.28.3.719.

Kranzler, H. R., and Soyka, M. (2018). Diagnosis and Pharmacotherapy of Alcohol Use Disorder: A Review. *JAMA* 320, 815. doi:10.1001/jama.2018.11406.

Krauss, S. (2001). "Mitochondria: Structure and Role in Respiration," in *Encyclopedia of Life Sciences*, ed.John Wiley & Sons, Ltd (Chichester, UK: John Wiley & Sons, Ltd), a0001380. doi:10.1038/npg.els.0001380.

Kumar, S., Porcu, P., Werner, D. F., Matthews, D. B., Diaz-Granados, J. L., Helfand, R. S., et al. (2009). The role of GABA(A) receptors in the acute and chronic effects of ethanol: a decade of progress. *Psychopharmacology (Berl.)* 205, 529–564. doi:10.1007/s00213-009-1562-z.

Lamarche, F., Carcenac, C., Gonthier, B., Cottet-Rousselle, C., Chauvin, C., Barret, L., et al. (2013). Mitochondrial Permeability Transition Pore Inhibitors Prevent Ethanol-Induced Neuronal Death in Mice. *Chem. Res. Toxicol.* 26, 78–88. doi:10.1021/tx300395w.

Lancaster, M. A., and Huch, M. (2019). Disease modelling in human organoids. *Dis. Model. Mech.* 12. doi:10.1242/dmm.039347.

Lang, E. J., and Davis, S. M. (2002). Lithium neurotoxicity: the development of irreversible neurological impairment despite standard monitoring of serum lithium levels. *J. Clin. Neurosci.* 9, 308–309. doi:10.1054/jocn.2001.0977.

Lee, R. D., An, S. M., Kim, S. S., Rhee, G. S., Kwack, S. J., Seok, J. H., et al. (2005). Neurotoxic effects of alcohol and acetaldehyde during embryonic development. *J. Toxicol. Environ. Health A* 68, 2147–2162. doi:10.1080/15287390500177255.

Li, N., Oquendo, E., Capaldi, R. A., Robinson, J. P., He, Y. D., Hamadeh, H. K., et al. (2014). A Systematic Assessment of Mitochondrial Function Identified Novel Signatures for Drug-Induced Mitochondrial Disruption in Cells. *Toxicol. Sci.* 142, 261–273. doi:10.1093/toxsci/kfu176.

Li, X.-L., Li, G.-H., Fu, J., Fu, Y.-W., Zhang, L., Chen, W., et al. (2018). Highly efficient genome editing via CRISPR–Cas9 in human pluripotent stem cells is achieved by transient BCL-XL overexpression. *Nucleic Acids Res.* 46, 10195–10215. doi:10.1093/nar/gky804.

Lieber, C. S. (1995). Medical Disorders of Alcoholism. *N. Engl. J. Med.* 333, 1058–1065. doi:10.1056/NEJM199510193331607.

Lieber, C. S. (2000). Alcohol: Its Metabolism and Interaction With Nutrients. *Annu. Rev. Nutr.* 20, 395–430. doi:10.1146/annurev.nutr.20.1.395.

Lieberman, R., Kranzler, H. R., Joshi, P., Shin, D.-G., and Covault, J. (2015). *GABRA2* Alcohol Dependence Risk Allele is Associated with Reduced Expression of Chromosome 4p12 GABA $_{A}$ Subunit Genes in Human Neural Cultures. *Alcohol. Clin. Exp. Res.* 39, 1654–1664. doi:10.1111/acer.12807.

Lieberman, R., Kranzler, H. R., Levine, E. S., and Covault, J. (2018). Examining the Effects of Alcohol on GABAA Receptor mRNA Expression and Function in Neural Cultures Generated from Control and Alcohol Dependent Donor Induced Pluripotent Stem Cells. *Alcohol Fayettev. N* 66, 45–53. doi:10.1016/j.alcohol.2017.08.005.

Lieberman, R., Levine, E. S., Kranzler, H. R., Abreu, C., and Covault, J. (2012). Pilot Study of iPS-derived Neural Cells to Examine Biological Effects of Alcohol on

Human Neurons in vitro. *Alcohol. Clin. Exp. Res.* 36, 1678–1687. doi:10.1111/j.1530-0277.2012.01792.x.

Lin, M. T., and Beal, M. F. (2006). Mitochondrial dysfunction and oxidative stress in neurodegenerative diseases. *Nature* 443, 787–795. doi:10.1038/nature05292.

Lipton, R. I. (1994). The effect of moderate alcohol use on the relationship between stress and depression. *Am. J. Public Health* 84, 1913–1917. doi:10.2105/ajph.84.12.1913.

Lorenz, C., Lesimple, P., Bukowiecki, R., Zink, A., Inak, G., Mlody, B., et al. (2017). Human iPSC-Derived Neural Progenitors Are an Effective Drug Discovery Model for Neurological mtDNA Disorders. *Cell Stem Cell* 20, 659-674.e9. doi:10.1016/j.stem.2016.12.013.

Lovinger, D. M., and Roberto, M. (2013). Synaptic Effects Induced by Alcohol. *Curr. Top. Behav. Neurosci.* 13, 31–86. doi:10.1007/7854_2011_143.

Manzo-Avalos, S., and Saavedra-Molina, A. (2010). Cellular and Mitochondrial Effects of Alcohol Consumption. *Int. J. Environ. Res. Public. Health* 7, 4281–4304. doi:10.3390/ijerph7124281.

Marescotti, D., Gonzalez Suarez, I., Acali, S., Johne, S., Laurent, A., Frentzel, S., et al. (2016). High Content Screening Analysis to Evaluate the Toxicological Effects of Harmful and Potentially Harmful Constituents (HPHC). *J. Vis. Exp. JoVE*. doi:10.3791/53987.

Mark, T. L., Kassed, C. A., Vandivort-Warren, R., Levit, K. R., and Kranzler, H. R. (2009). Alcohol and opioid dependence medications: prescription trends, overall and by physician specialty. *Drug Alcohol Depend.* 99, 345–349. doi:10.1016/j.drugalcdep.2008.07.018.

Marzo, I., Brenner, C., Zamzami, N., Susin, S. A., Beutner, G., Brdiczka, D., et al. (1998). The Permeability Transition Pore Complex: A Target for Apoptosis Regulation by Caspases and Bcl-2–related Proteins. *J. Exp. Med.* 187, 1261–1271.

Mason, B. J., Goodman, A. M., Dixon, R. M., Hameed, M. H., Hulot, T., Wesnes, K., et al. (2002). A pharmacokinetic and pharmacodynamic drug interaction study of acamprosate and naltrexone. *Neuropsychopharmacol. Off. Publ. Am. Coll. Neuropsychopharmacol.* 27, 596–606. doi:10.1016/S0893-133X(02)00368-8.

Matias, I., Morgado, J., and Gomes, F. C. A. (2019). Astrocyte Heterogeneity: Impact to Brain Aging and Disease. *Front. Aging Neurosci.* 11. doi:10.3389/fnagi.2019.00059.

Mayfield, R. D., Harris, R. A., and Schuckit, M. A. (2008). Genetic factors influencing alcohol dependence. *Br. J. Pharmacol.* 154, 275–287. doi:10.1038/bjp.2008.88.

McKnight-Eily, L. R., Liu, Y., Brewer, R. D., Kanny, D., Lu, H., Denny, C. H., et al. (2014). Vital signs: communication between health professionals and their patients about alcohol use--44 states and the District of Columbia, 2011. *MMWR Morb. Mortal. Wkly. Rep.* 63, 16–22.

Memberg, S. P., and Hall, A. K. (1995). Dividing neuron precursors express neuron-specific tubulin. *J. Neurobiol.* 27, 26–43. doi:10.1002/neu.480270104.

Mertens, J., Wang, Q.-W., Kim, Y., Yu, D. X., Pham, S., Yang, B., et al. (2015). Differential responses to lithium in hyperexcitable neurons from patients with bipolar disorder. *Nature* 527, 95–99. doi:10.1038/nature15526.

Mignarri, A., Chini, E., Rufa, A., Rocchi, R., Federico, A., and Dotti, M. T. (2013). Lithium neurotoxicity mimicking rapidly progressive dementia. *J. Neurol.* 260, 1152–1154. doi:10.1007/s00415-012-6820-z.

Miguel-Hidalgo, J. J. (2018). Molecular Neuropathology of Astrocytes and Oligodendrocytes in Alcohol Use Disorders. *Front. Mol. Neurosci.* 11. doi:10.3389/fnmol.2018.00078.

Miller, G. (2010). Is Pharma Running Out of Brainy Ideas? *Science* 329, 502–504. doi:10.1126/science.329.5991.502.

Mishra, P. (2016). Interfaces between mitochondrial dynamics and disease. *Cell Calcium* 60, 190–198. doi:10.1016/j.ceca.2016.05.004.

Mohammad Ahmadi Soleimani, S., Ekhtiari, H., and Cadet, J. L. (2016). "Chapter 2 - Drug-induced neurotoxicity in addiction medicine: From prevention to harm reduction," in *Progress in Brain Research* Neuroscience for Addiction Medicine: From Prevention to Rehabilitation - Constructs and Drugs., eds. H. Ekhtiari and M. Paulus (Elsevier), 19–41. doi:10.1016/bs.pbr.2015.07.004.

Morikawa, H., and Morrisett, R. A. (2010). Ethanol action on dopaminergic neurons in the ventral tegmental area: interaction with intrinsic ion channels and neurotransmitter inputs. *Int. Rev. Neurobiol.* 91, 235–288. doi:10.1016/S0074-7742(10)91008-8.

Nath, V., Reneau, J. C., Dertien, J. S., Agrawal, R. G., Guerra, I., Bhakta, Y., et al. (2012). An in vitro model for studying the effects of continuous ethanol exposure on N-methyl-d-aspartate receptor function. *Alcohol Fayettev. N* 46, 3–16. doi:10.1016/j.alcohol.2011.08.003.

Nathan, P. E., Conrad, M., and Skinstad, A. H. (2016). History of the Concept of Addiction. *Annu. Rev. Clin. Psychol.* 12, 29–51. doi:10.1146/annurev-clinpsy-021815-093546.

Neher, E., and Sakaba, T. (2008). Multiple roles of calcium ions in the regulation of neurotransmitter release. *Neuron* 59, 861–872. doi:10.1016/j.neuron.2008.08.019.

Bibliography

Ni, H.-M., Williams, J. A., and Ding, W.-X. (2015). Mitochondrial dynamics and mitochondrial quality control. *Redox Biol.* 4, 6–13. doi:10.1016/j.redox.2014.11.006.

Nieweg, K., Andreyeva, A., van Stegen, B., Tanriöver, G., and Gottmann, K. (2015). Alzheimer's disease-related amyloid-β induces synaptotoxicity in human iPS cell-derived neurons. *Cell Death Dis.* 6, e1709. doi:10.1038/cddis.2015.72.

Olson, H., Betton, G., Robinson, D., Thomas, K., Monro, A., Kolaja, G., et al. (2000). Concordance of the Toxicity of Pharmaceuticals in Humans and in Animals. *Regul. Toxicol. Pharmacol.* 32, 56–67. doi:10.1006/rtph.2000.1399.

Onyekwelu, K. C. (2019). Ethanol. *Psychol. Health - Biopsychosoc. Approach*. doi:10.5772/intechopen.79861.

Oscar-Berman, M. (2003). Alcoholism and the Brain: An Overview. 27, 9.

Oscar-Berman, M., and Marinković, K. (2007). Alcohol: Effects on Neurobehavioral Functions and the Brain. *Neuropsychol. Rev.* 17, 239–257. doi:10.1007/s11065-007-9038-6.

Osna, N. A., Donohue, T. M., and Kharbanda, K. K. (2017). Alcoholic Liver Disease: Pathogenesis and Current Management. *Alcohol Res. Curr. Rev.* 38, 147–161.

Osna, N. A., and Kharbanda, K. K. (2016). Multi-Organ Alcohol-Related Damage: Mechanisms and Treatment. *Biomolecules* 6. doi:10.3390/biom6020020.

Ozkol, H., Bulut, G., Balahoroglu, R., Tuluce, Y., and Ozkol, H. U. (2017). Protective Effects of Selenium, N-Acetylcysteine and Vitamin E Against Acute Ethanol Intoxication in Rats. *Biol. Trace Elem. Res.* 175, 177–185. doi:10.1007/s12011-016-0762-8.

Pérez, M. J., and Quintanilla, R. A. (2017). Development or disease: duality of the mitochondrial permeability transition pore. *Dev. Biol.* 426, 1–7. doi:10.1016/j.ydbio.2017.04.018.

Perry, S. W., Norman, J. P., Barbieri, J., Brown, E. B., and Gelbard, H. A. (2011). Mitochondrial membrane potential probes and the proton gradient: a practical usage guide. *BioTechniques* 50, 98–115. doi:10.2144/000113610.

Piano, M. R. (2017). Alcohol's Effects on the Cardiovascular System. *Alcohol Res. Curr. Rev.* 38, 219–241.

Pratt, O. E., Rooprai, H. K., Shaw, G. K., and Thomson, A. D. (1990). The genesis of alcoholic brain tissue injury. *Alcohol Alcohol. Oxf. Oxfs.* 25, 217–230. doi:10.1093/oxfordjournals.alcalc.a044995.

Prigione, A., Fauler, B., Lurz, R., Lehrach, H., and Adjaye, J. (2010). The Senescence-Related Mitochondrial/Oxidative Stress Pathway is Repressed in Human Induced Pluripotent Stem Cells. *Stem Cells* 28, 721–733. doi:10.1002/stem.404.

Prytkova, I., Goate, A., Hart, R. P., and Slesinger, P. A. (2018). Genetics of Alcohol Use Disorder: A Role for Induced Pluripotent Stem Cells? *Alcohol. Clin. Exp. Res.* 42, 1572–1590. doi:10.1111/acer.13811.

Quertemont, E. (2004). Genetic polymorphism in ethanol metabolism: acetaldehyde contribution to alcohol abuse and alcoholism. *Mol. Psychiatry* 9, 570–581. doi:10.1038/sj.mp.4001497.

Ramachandran, V., Watts, L. T., Maffi, S. K., Chen, J., Schenker, S., and Henderson, G. (2003). Ethanol-induced oxidative stress precedes mitochondrially mediated apoptotic death of cultured fetal cortical neurons. *J. Neurosci. Res.* 74, 577–588. doi:10.1002/jnr.10767.

Ramchandani, V. A., Kwo, P. Y., and Li, T. K. (2001). Effect of food and food composition on alcohol elimination rates in healthy men and women. *J. Clin. Pharmacol.* 41, 1345–1350. doi:10.1177/00912700122012814.

Ramsey, S. E., Engler, P. A., and Stein, M. D. (2005). Alcohol Use Among Depressed Patients: The Need for Assessment and Intervention. *Prof. Psychol. Res. Pract.* 36, 203–207. doi:10.1037/0735-7028.36.2.203.

Reddy, P. H. (2014). Inhibitors of mitochondrial fission as a therapeutic strategy for diseases with oxidative stress and mitochondrial dysfunction. *J. Alzheimers Dis. JAD* 40, 245–256. doi:10.3233/JAD-132060.

Reddy, V. D., Padmavathi, P., Kavitha, G., Saradamma, B., and Varadacharyulu, N. (2013). Alcohol-induced oxidative/nitrosative stress alters brain mitochondrial membrane properties. *Mol. Cell. Biochem.* 375, 39–47. doi:10.1007/s11010-012-1526-1.

Rehm, J. (2011). The Risks Associated With Alcohol Use and Alcoholism. *Alcohol Res. Health* 34, 135–143.

Rehm, J., Mathers, C., Popova, S., Thavorncharoensap, M., Teerawattananon, Y., and Patra, J. (2009). Global burden of disease and injury and economic cost attributable to alcohol use and alcohol-use disorders. *Lancet Lond. Engl.* 373, 2223–2233. doi:10.1016/S0140-6736(09)60746-7.

Reinhardt, P., Glatza, M., Hemmer, K., Tsytsyura, Y., Thiel, C. S., Höing, S., et al. (2013). Derivation and Expansion Using Only Small Molecules of Human Neural Progenitors for Neurodegenerative Disease Modeling. *PloS One* 8, e59252. doi:10.1371/journal.pone.0059252.

Renner, H., Grabos, M., Becker, K. J., Kagermeier, T. E., Wu, J., Otto, M., et al. (2020). A fully automated high-throughput workflow for 3D-based chemical screening in human midbrain organoids. *eLife* 9, e52904. doi:10.7554/eLife.52904.

Roget, N. A. (2009). *Encyclopedia of Substance Abuse Prevention, Treatment, and Recovery*. SAGE.

Bibliography

Ryan, S. D., Dolatabadi, N., Chan, S. F., Zhang, X., Akhtar, M. W., Parker, J., et al. (2013). Isogenic human iPSC Parkinson's model shows nitrosative stress-induced dysfunction in MEF2-PGC1α transcription. *Cell* 155, 1351–1364. doi:10.1016/j.cell.2013.11.009.

Sacanella, E., and Estruch, R. (2003). The effect of alcohol consumption on endothelial adhesion molecule expression. *Addict. Biol.* 8, 371–378. doi:10.1080/13556210310001656376.

Sacks, J. J., Gonzales, K. R., Bouchery, E. E., Tomedi, L. E., and Brewer, R. D. (2015). 2010 National and State Costs of Excessive Alcohol Consumption. *Am. J. Prev. Med.* 49, e73–e79. doi:10.1016/j.amepre.2015.05.031.

SAMHSA (2013). Results from the 2013 National Survey on Drug Use and Health: Summary of National Findings. 184.

Sanchez-Roige, S., Palmer, A. A., Fontanillas, P., Elson, S. L., Adams, M. J., Howard, D. M., et al. (2019). Genome-wide association study meta-analysis of the Alcohol Use Disorder Identification Test (AUDIT) in two population-based cohorts. *Am. J. Psychiatry* 176, 107–118. doi:10.1176/appi.ajp.2018.18040369.

Sanjana, N. E., Shalem, O., and Zhang, F. (2014). Improved vectors and genome-wide libraries for CRISPR screening. *Nat. Methods* 11, 783–784. doi:10.1038/nmeth.3047.

Santos, L. E. C., Silveira, G. A. da, Costa, V. D. C., Batista, A. G., Madureira, A. P., Rodrigues, A. M., et al. (2013). Alcohol Abuse Promotes Changes in Non-Synaptic Epileptiform Activity with Concomitant Expression Changes in Cotransporters and Glial Cells. *PLOS ONE* 8, e78854. doi:10.1371/journal.pone.0078854.

Sari, Y., Johnson, V. R., and Weedman, J. M. (2011). Role of the Serotonergic System in Alcohol Dependence: From Animal Models to Clinics. *Prog. Mol. Biol. Transl. Sci.* 98, 401–443. doi:10.1016/B978-0-12-385506-0.00010-7.

Saunders, D. N., Falkenberg, K. J., and Simpson, K. J. (2014). High-Throughput Approaches to Measuring Cell Death. *Cold Spring Harb. Protoc.* 2014, pdb.top072561-pdb.top072561. doi:10.1101/pdb.top072561.

Scarnati, M. S., Halikere, A., and Pang, Z. P. (2019). Using human stem cells as a model system to understand the neural mechanisms of alcohol use disorders: current status and outlook. *Alcohol Fayettev. N* 74, 83–93. doi:10.1016/j.alcohol.2018.03.008.

Schmidt, B. Z., Lehmann, M., Gutbier, S., Nembo, E., Noel, S., Smirnova, L., et al. (2017). In vitro acute and developmental neurotoxicity screening : an overview of cellular platforms and high-throughput technical possibilities. *Arch. Toxicol.* 91, 1–33. doi:10.1007/s00204-016-1805-9.

Schumann, G., Liu, C., O'Reilly, P., Gao, H., Song, P., Xu, B., et al. (2016). KLB is associated with alcohol drinking, and its gene product β-Klotho is necessary for FGF21 regulation of alcohol preference. *Proc. Natl. Acad. Sci. U. S. A.* 113, 14372–14377. doi:10.1073/pnas.1611243113.

Seneviratne, C., and Johnson, B. A. (2015). Advances in Medications and Tailoring Treatment for Alcohol Use Disorder. *Alcohol Res. Curr. Rev.* 37, 15–28.

Shah, V. C., Kayathi, P., Singh, G., and Lippmann, S. (2015). Enhance Your Understanding of Lithium Neurotoxicity. *Prim. Care Companion CNS Disord.* 17. doi:10.4088/PCC.14l01767.

Sherman, S. P., and Bang, A. G. (2018). High-throughput screen for compounds that modulate neurite growth of human induced pluripotent stem cell-derived neurons. *Dis. Model. Mech.* 11, dmm031906. doi:10.1242/dmm.031906.

Simenc, J., and Lipnik-Stangelj, M. (2012). Staurosporine induces different cell death forms in cultured rat astrocytes. *Radiol. Oncol.* 46, 312–320. doi:10.2478/v10019-012-0036-9.

Slaymaker, I. M., Gao, L., Zetsche, B., Scott, D. A., Yan, W. X., and Zhang, F. (2016). Rationally engineered Cas9 nucleases with improved specificity. *Science* 351, 84–88. doi:10.1126/science.aad5227.

Spanagel, R. (2009). Alcoholism: A Systems Approach From Molecular Physiology to Addictive Behavior. *Physiol. Rev.* 89, 649–705. doi:10.1152/physrev.00013.2008.

Squeglia, L. M., Schweinsburg, A. D., Pulido, C., and Tapert, S. F. (2011). Adolescent Binge Drinking Linked to Abnormal Spatial Working Memory Brain Activation: Differential Gender Effects. *Alcohol. Clin. Exp. Res.* 35, 1831–1841. doi:10.1111/j.1530-0277.2011.01527.x.

Staiger, H., Keuper, M., Berti, L., Hrabě de Angelis, M., and Häring, H.-U. (2017). Fibroblast Growth Factor 21—Metabolic Role in Mice and Men. *Endocr. Rev.* 38, 468–488. doi:10.1210/er.2017-00016.

Stern, Y. (2012). Cognitive reserve in ageing and Alzheimer's disease. *Lancet Neurol.* 11, 1006–1012. doi:10.1016/S1474-4422(12)70191-6.

Sychla, H., Gründer, G., and Lammertz, S. E. (2017). Comparison of Clomethiazole and Diazepam in the Treatment of Alcohol Withdrawal Syndrome in Clinical Practice. *Eur. Addict. Res.* 23, 211–218. doi:10.1159/000480380.

Symersky, J., Osowski, D., Walters, D. E., and Mueller, D. M. (2012). Oligomycin frames a common drug-binding site in the ATP synthase. *Proc. Natl. Acad. Sci. U. S. A.* 109, 13961–13965. doi:10.1073/pnas.1207912109.

Takahashi, K., Tanabe, K., Ohnuki, M., Narita, M., Ichisaka, T., Tomoda, K., et al. (2007). Induction of Pluripotent Stem Cells from Adult Human Fibroblasts by Defined Factors. *Cell* 131, 861–872. doi:10.1016/j.cell.2007.11.019.

Takahashi, K., and Yamanaka, S. (2006). Induction of Pluripotent Stem Cells from Mouse Embryonic and Adult Fibroblast Cultures by Defined Factors. *Cell* 126, 663–676. doi:10.1016/j.cell.2006.07.024.

Talukdar, S., Owen, B. M., Song, P., Hernandez, G., Zhang, Y., Zhou, Y., et al. (2016). FGF21 Regulates Sweet and Alcohol Preference. *Cell Metab.* 23, 344–349. doi:10.1016/j.cmet.2015.12.008.

Tapert, S. F., Brown, G. G., Baratta, M. V., and Brown, S. A. (2004). fMRI BOLD response to alcohol stimuli in alcohol dependent young women. *Addict. Behav.* 29, 33–50. doi:10.1016/j.addbeh.2003.07.003.

Tapia-Rojas, C., Pérez, M. J., Jara, C., and Quintanilla, E. H. V. and R. A. (2017). Ethanol Consumption Affects Neuronal Function: Role of the Mitochondria. *Mitochondrial Dis.* doi:10.5772/intechopen.71611.

Tawa, E. A., Hall, S. D., and Lohoff, F. W. (2016). Overview of the Genetics of Alcohol Use Disorder. *Alcohol Alcohol* 51, 507–514. doi:10.1093/alcalc/agw046.

Thadhani, R., Camargo, C. A., Stampfer, M. J., Curhan, G. C., Willett, W. C., and Rimm, E. B. (2002). Prospective study of moderate alcohol consumption and risk of hypertension in young women. *Arch. Intern. Med.* 162, 569–574. doi:10.1001/archinte.162.5.569.

The Human Protein Atlas Available at: https://www.proteinatlas.org/ENSG00000134962-KLB [Accessed July 1, 2020].

Thomsen, H., Kaatsch, H. J., and Asmus, R. (1994). Magnetic resonance imaging of the brain during alcohol absorption and elimination--a study of the “rising tide phenomenon.” *Blutalkohol* 31, 178–185.

Thomson, J. A., Itskovitz-Eldor, J., Shapiro, S. S., Waknitz, M. A., Swiergiel, J. J., Marshall, V. S., et al. (1998). Embryonic stem cell lines derived from human blastocysts. *Science* 282, 1145–1147. doi:10.1126/science.282.5391.1145.

Thuret, G., Chiquet, C., Herrag, S., Dumollard, J.-M., Boudard, D., Bednarz, J., et al. (2003). Mechanisms of staurosporine induced apoptosis in a human corneal endothelial cell line. *Br. J. Ophthalmol.* 87, 346–352.

Torre, C. D., Campagnolo, M., Cagnin, A., and Briani, C. (2010). Disulfiram-induced peripheral and central neurotoxicity. *Prog. Neuropsychopharmacol. Biol. Psychiatry* 34, 1146–1147. doi:10.1016/j.pnpbp.2010.05.023.

Trantham-Davidson, H., and Chandler, L. J. (2015). Alcohol-induced alterations in dopamine modulation of prefrontal activity. *Alcohol* 49, 773–779. doi:10.1016/j.alcohol.2015.09.001.

Tsujimoto, Y., and Shimizu, S. (2007). Role of the mitochondrial membrane permeability transition in cell death. *Apoptosis Int. J. Program. Cell Death* 12, 835–840. doi:10.1007/s10495-006-0525-7.

Uhl, E. W., and Warner, N. J. (2015). Mouse Models as Predictors of Human Responses: Evolutionary Medicine. *Curr. Pathobiol. Rep.* 3, 219–223. doi:10.1007/s40139-015-0086-y.

Vafai, S. B., and Mootha, V. K. (2012). Mitochondrial disorders as windows into an ancient organelle. *Nature* 491, 374–383. doi:10.1038/nature11707.

van den Brink, W., Addolorato, G., Aubin, H.-J., Benyamina, A., Caputo, F., Dematteis, M., et al. (2018). Efficacy and safety of sodium oxybate in alcohol-dependent patients with a very high drinking risk level: Efficacy and safety of sodium oxybate in alcohol-dependent patients with a very high drinking risk level. *Addict. Biol.* 23, 969–986. doi:10.1111/adb.12645.

Varkuti, B. H., Liu, Z., Kepiro, M., Pacifico, R., Gai, Y., Kameneka, T., et al. (2020). High-Throughput Small Molecule Screen Identifies Modulators of Mitochondrial Function in Neurons. *iScience* 23. doi:10.1016/j.isci.2020.100931.

Vassallo, A., Chiappalone, M., De Camargos Lopes, R., Scelfo, B., Novellino, A., Defranchi, E., et al. (2017). A multi-laboratory evaluation of microelectrode array-based measurements of neural network activity for acute neurotoxicity testing. *NeuroToxicology* 60, 280–292. doi:10.1016/j.neuro.2016.03.019.

Vengeliene, V., Bilbao, A., Molander, A., and Spanagel, R. (2008). Neuropharmacology of alcohol addiction. *Br. J. Pharmacol.* 154, 299–315. doi:10.1038/bjp.2008.30.

Verhulst, B., Neale, M. C., and Kendler, K. S. (2015). The heritability of alcohol use disorders: a meta-analysis of twin and adoption studies. *Psychol. Med.* 45, 1061–1072. doi:10.1017/S0033291714002165.

Volkow, N., and Li, T.-K. (2005). The neuroscience of addiction. *Nat. Neurosci.* 8, 1429–1430. doi:10.1038/nn1105-1429.

Wang, H. (2018). Modeling Neurological Diseases With Human Brain Organoids. *Front. Synaptic Neurosci.* 10. doi:10.3389/fnsyn.2018.00015.

Wang, X., and Schwarz, T. L. (2009). The Mechanism of Kinesin Regulation by Ca++ for Control of Mitochondrial Motility. *Cell* 136, 163–174. doi:10.1016/j.cell.2008.11.046.

Wang, X., Sterr, M., Burtscher, I., Chen, S., Hieronimus, A., Machicao, F., et al. (2018). Genome-wide analysis of PDX1 target genes in human pancreatic progenitors. *Mol. Metab.* 9, 57–68. doi:10.1016/j.molmet.2018.01.011.

Weeden, C. E., and Asselin-Labat, M.-L. (2018). Mechanisms of DNA damage repair in adult stem cells and implications for cancer formation. *Biochim. Biophys. Acta BBA - Mol. Basis Dis.* 1864, 89–101. doi:10.1016/j.bbadis.2017.10.015.

Weintraub, S. J. (2017). Diazepam in the Treatment of Moderate to Severe Alcohol Withdrawal. *CNS Drugs* 31, 87–95. doi:10.1007/s40263-016-0403-y.

WHO (1992). The ICD-10 Classification of Mental and Behavioural Disorders -. Available at: https://www.who.int/classifications/icd/en/bluebook.pdf [Accessed January 31, 2021].

WHO, Management of Substance Abuse Team, and World Health Organization (2018). *Global status report on alcohol and health 2018.* Available at: http://www.who.int/substance_abuse/publications/global_alcohol_report/en/ [Accessed July 14, 2020].

Wilby, M. J., and Hutchinson, P. J. (2004). The Pharmacology of Chlormethiazole: A Potential Neuroprotective Agent? *CNS Drug Rev.* 10, 281–294. doi:10.1111/j.1527-3458.2004.tb00028.x.

Williams, G. S. B., Boyman, L., Chikando, A. C., Khairallah, R. J., and Lederer, W. J. (2013). Mitochondrial calcium uptake. *Proc. Natl. Acad. Sci. U. S. A.* 110, 10479–10486. doi:10.1073/pnas.1300410110.

Wilson, D. F., and Matschinsky, F. M. (2020). Ethanol metabolism: The good, the bad, and the ugly. *Med. Hypotheses* 140, 109638. doi:10.1016/j.mehy.2020.109638.

Winslow, B. T., Onysko, M., and Hebert, M. (2016). Medications for Alcohol Use Disorder. *Am. Fam. Physician* 93, 457–465.

Wise, R. A., and Rompre, P. P. (1989). Brain dopamine and reward. *Annu. Rev. Psychol.* 40, 191–225. doi:10.1146/annurev.ps.40.020189.001203.

Won, E., and Kim, Y.-K. (2017). An Oldie but Goodie: Lithium in the Treatment of Bipolar Disorder through Neuroprotective and Neurotrophic Mechanisms. *Int. J. Mol. Sci.* 18. doi:10.3390/ijms18122679.

Wong, A., and Cortopassi, G. A. (2002). High-throughput measurement of mitochondrial membrane potential in a neural cell line using a fluorescence plate reader. *Biochem. Biophys. Res. Commun.* 298, 750–754. doi:10.1016/S0006-291X(02)02546-9.

Wu, X., Kriz, A. J., and Sharp, P. A. (2014). Target specificity of the CRISPR-Cas9 system. *Quant. Biol.* 2, 59–70. doi:10.1007/s40484-014-0030-x.

Xiao, W., Wang, R.-S., Handy, D. E., and Loscalzo, J. (2018). NAD(H) and NADP(H) Redox Couples and Cellular Energy Metabolism. *Antioxid. Redox Signal.* 28, 251–272. doi:10.1089/ars.2017.7216.

Xu, X., Gao, D., Wang, P., Chen, J., Ruan, J., Xu, J., et al. (2018). Efficient homology-directed gene editing by CRISPR/Cas9 in human stem and primary cells using tube electroporation. *Sci. Rep.* 8, 11649. doi:10.1038/s41598-018-30227-w.

Yan, T., Zhao, Y., and Zhang, X. (2015). Acetaldehyde Induces Cytotoxicity of SH-SY5Y Cells via Inhibition of Akt Activation and Induction of Oxidative Stress. *Oxid. Med. Cell. Longev.* 2016, e4512309. doi:https://doi.org/10.1155/2016/4512309.

Yang, F., and Luo, J. (2015). Endoplasmic Reticulum Stress and Ethanol Neurotoxicity. *Biomolecules* 5, 2538–2553. doi:10.3390/biom5042538.

Young, W. (2009). Review of Lithium Effects on Brain and Blood. *Cell Transplant.* 18, 951–975. doi:10.3727/096368909X471251.

Yu, J., Chau, K. F., Vodyanik, M. A., Jiang, J., and Jiang, Y. (2011). Efficient Feeder-Free Episomal Reprogramming with Small Molecules. *PLoS ONE* 6, e17557. doi:10.1371/journal.pone.0017557.

Zakhari, S. (2006). Overview: how is alcohol metabolized by the body? *Alcohol Res. Health J. Natl. Inst. Alcohol Abuse Alcohol.* 29, 245–254.

Zhang, J. H., Chung, T. D., and Oldenburg, K. R. (1999). A Simple Statistical Parameter for Use in Evaluation and Validation of High Throughput Screening Assays. *J. Biomol. Screen.* 4, 67–73. doi:10.1177/108705719900400206.

Zhang, J., Han, X., and Lin, Y. (2018). Dissecting the regulation and function of ATP at the single-cell level. *PLOS Biol.* 16, e3000095. doi:10.1371/journal.pbio.3000095.

Zhao, M.-T., Chen, H., Liu, Q., Shao, N.-Y., Sayed, N., Wo, H.-T., et al. (2017). Molecular and functional resemblance of differentiated cells derived from isogenic human iPSCs and SCNT-derived ESCs. *Proc. Natl. Acad. Sci. U. S. A.* 114, E11111–E11120. doi:10.1073/pnas.1708991114.

Zhao, Y.-N., Wang, F., Fan, Y.-X., Ping, G.-F., Yang, J.-Y., and Wu, C.-F. (2013). Activated microglia are implicated in cognitive deficits, neuronal death, and successful recovery following intermittent ethanol exposure. *Behav. Brain Res.* 236, 270–282. doi:10.1016/j.bbr.2012.08.052.

Zwartsen, A., Hondebrink, L., de Lange, D. W., and Westerink, R. H. S. (2020). Hyperthermia exacerbates the acute effects of psychoactive substances on neuronal activity measured using microelectrode arrays (MEAs) in rat primary cortical cultures in vitro. *Toxicol. Appl. Pharmacol.* 397, 115015. doi:10.1016/j.taap.2020.115015.

Bibliography

Zwartsen, A., Hondebrink, L., and Westerink, R. H. (2018). Neurotoxicity screening of new psychoactive substances (NPS): Effects on neuronal activity in rat cortical cultures using microelectrode arrays (MEA). *NeuroToxicology* 66, 87–97. doi:10.1016/j.neuro.2018.03.007.

9. Supplementary information

9.1 List of selected compounds from the FDA-approved drug screening library (z65122)

Table 9-A: List of selected compounds from the FDA-approved drug screening library (z65122)

No.	Name	M.w.	Target	Indication	Brief description	CAS Number	MMP rel. to UT (value)	Neurite count rel. to UT (value)
1	Bethanechol chloride	196.68	AChR	Neurological disease	Selective muscarinic receptor agonist without any effect on nicotinic receptors.	590-63-6	Down (0.750)	Down (0.839)
2	Econazole nitrate (Spectazole)	444.7	Anti-infection, Calcium Channel	Neurological disease	$Ca2^{+}$ channel blocker, used as an antifungal medicine that fights infections caused by fungus.	24169-02-6	Down (0.761)	Down (0.701)
3	Acetanilide (Antifebrin)	135.16	n.d	Neurological disease	Aniline derivative and has possess analgesic.	103-84-4	Down (0.630)	Down (0.761)
4	Cefprozil hydrate (Cefzil)	407.44	n.d	Neurological disease	Second-generation cephalosporin type antibiotic.	121123-17-9	Down (0.737)	Down (0.769)

Supplementary

5	Tolterodine tartrate (Detrol LA)	475.57	AChR	Neurological disease	Tartrate salt of tolterodine that is a competitive muscarinic receptor antagonist.	124937-52-6	Down (0.745)	Down (0.780)
6	Azelastine hydrochloride (Astelin)	418.36	Histamine Receptor	Neurological disease	Potent, second-generation, selective, histamine antagonist.	79307-93-0	Down (0.651)	Down (0.806)
7	5-Aminolevulinic acid hydrochloride	167.59	n.d	Neurological disease	Intermediate in heme biosynthesis in the body and the universal precursor of tetrapyrroles.	5451-09-2	Down (0.697)	Down (0.845)
8	Ronidazole	200.15	Anti-infection	Neurological disease	Antiprotozoal agent.	7681-76-7	Down (0.709)	Down (0.799)
9	Miglitol (Glyset)	207.22	Carbohydrate Metabolism	Neurological disease	Oral anti-diabetic drug.	72432-03-2	Down (0.786)	Normal (0.894)
10	Buflomedil HCl	343.85	Adrenergic Receptor	Neurological disease	Vasodilator used to treat claudication or the symptoms of peripheral arterial disease.	35543-24-9	Down (0.529)	Up (1.066)
11	PCI-32765 (Ibrutinib)	440.5	Src	Neurological disease	Potent and highly selective Btk inhibitor with.	936563-96-1	Down (0.652)	Down (0.814)
12	Amoxicillin (Amoxycillin)	365.4	Anti-infection	Neurological disease	Moderate-spectrum, bacteriolytic, β-lactam antibiotic.	26787-78-0	Down (0.619)	Normal (0.909)

13	Cabazitaxel (Jevtana)	835.93	Microtubule Associated	Neurological disease	Semi-synthetic derivative of a natural taxoid.	183133-96-2	Down (0.768)	Down (0.889)
14	Niclosamide (Niclocide)	327.12	STAT	Neurological disease	Inhibits DNA replication and inhibits STAT.	50-65-7	Down (0.728)	Down (0.812)
15	Lurasidone HCl	529.14	Dopamine Receptor	Neurological disease	Antipsychotic, inhibits Dopamine D2, 5-HT2A, 5-HT7, 5-HT1A and noradrenaline α2C.	367514-88-3	Down (0.804)	Down (0.877)
16	D-Phenylalanine	165.19	n.d	Neurological disease	Carboxypeptidase A, endorphinase and enkephalinase inhibitor, enhances endorphin production and diminishes pain.	673-06-3	Down (0.731)	Down (0.871)
17	Palonosetron HCl	332.87	5-HT Receptor	Neurological disease	5-HT3 antagonist used in the prevention and treatment of chemotherapy-induced nausea and vomiting.	135729-62-3	Down (0.803)	Down (0.811)
18	Azelnidipine	582.65	Calcium Channel	Neurological disease	Dihydropyridine calcium channel blocker.	123524-52-7	Down (0.682)	Down (0.872)
19	Dexmedetomidine	200.28	Adrenergic Receptor	Neurological disease	Sedative medication used by intensive care units and anesthetists.	113775-47-6	Down (0.726)	Normal (0.912)

Supplementary

20	Etravirine (TMC125)	435.28	Reverse Transcriptase	Neurological disease	Non-nucleoside reverse transcriptase inhibitor (NNRTI) used for the treatment of HIV.	269055-15-4	Normal (0.904)	Normal (0.921)
21	Oxybutynin chloride	393.95	AChR	Neurological disease	Anticholinergic medication used to relieve urinary and bladder difficulties.	1508-65-2	Down (0.773)	Down (0.833)
22	Tripelennamine HCl	291.82	Histamine Receptor	Neurological disease	H1 antagonist, inhibiting PhIP glucuronidation	154-69-8	Up (0.960)	Up (1.146)
23	Articaine HCl	320.84	n.d	Neurological disease	Dental local anesthetic which contains an additional ester group that is metabolized by estearases in blood and tissue.	23964-57-0	Down (0.768)	Normal (0.960)
24	Doxylamine Succinate	388.46	Histamine Receptor	Neurological disease	Competitively inhibits histamine at H1 receptors with substantial sedative and anticholinergic effects.	562-10-7	Down (0.755)	Normal (0.912)
25	Atomoxetine HCl	291.82	5-HT Receptor	Neurological disease	Selective norepinephrine (NE) transporter inhibitor with Ki of 5 nM, with 15- and 290-fold lower affinity	82248-59-7	Normal (0.910)	Normal (0.955)

					for human 5-HT and DA transporters.			
26	Brinzolamide	383.51	Carbonic Anhydrase	Neurological disease	Potent carbonic anhydrase II inhibitor.	138890-62-7	Normal (0.850)	Normal (0.934)
27	Ropinirole HCl	296.84	Dopamine Receptor	Neurological disease	Selective dopamine D2 receptors inhibitor.	91374-20-8	Down (0.791)	Low (0.886)
28	Azlocillin sodium salt	484.48	Anti-infection	Neurological disease	Acylampicillin with a broad spectrum against bacteria.	37091-65-9	Up (0.935)	Normal (0.956)
29	Azacyclonol	267.37	5-HT receptor	Neurological disease	Drug used to diminish hallucinations in psychotic individuals.	115-46-8	Up (0.955)	Normal (0.940)
30	Reboxetine mesylate	409.5	n.d	Neurological disease	Norepinephrine reuptake inhibitor.	98769-84-7	Normal (0.899)	Down (0.887)
31	Meptazinol HCl	269.81	Opioid Receptor	Neurological disease	Ppioid analgesic, which inhibits [^{3}H]dihydromorphine binding.	59263-76-2	Normal (0.891)	Down (0.880)
32	Nalmefene HCl	375.89	Anti-infection	Neurological disease	Naltrexone analogue with opioid antagonistic property.	58895-64-0	Up (0.964)	Down (0.886)
33	Amidopyrine	231.29	n.d	Neurological disease	Analgesic, anti-inflammatory, and antipyretic properties.	58-15-1	Normal (0.854)	Normal (0.901)
34	Moclobemide	268.74	MAO	Neurological disease	MAO-A (5-HT) inhibitor.	71320-77-9	Up (0.952)	Down (0.862)

Supplementary

35	Lithocholic acid	376.57	FXR	Neurological disease	Acts as a detergent to solubilize fats for absorption.	434-13-9	Normal (0.859)	Down (0.888)
36	Ethambutol HCl	277.23	Anti-infection	Neurological disease	Bacteriostatic antimycobacterial agent, which obstructs the formation of cell wall by inhibiting arabinosyl transferases.	1070-11-7	Down (0.768)	Down (0.875)
37	Acebutolol HCl	372.89	Adrenergic Receptor	Neurological disease	β-adrenergic receptors antagonist used in the treatment of hypertension, angina pectoris and cardiac arrhythmias.	34381-68-5	Up (0.943)	Normal (0.957)
38	Hyoscyamine (Daturine)	289.37	AChR	Neurological disease	AChR inhibitor.	101-31-5	Normal (0.834)	Down (0.888)
39	Procaine (Novocaine) HCl	272.77	Sodium Channel	Neurological disease	Inhibitor of sodium channel, NMDA receptor and nAChR with IC50 of 60 μM, 0.296 mM and 45.5 μM, which is also an inhibitor of 5-HT3 with K_D of 1.7 μM.	51-05-8	Normal (0.886)	Down (0.846)
40	Dicyclomine HCl	345.95	M1 and M3 muscarinic	Neurological disease	Anticholinergic tertiary amine.	67-92-5	Normal (0.924)	Down (0.877)

			receptors antagonist					
41	Flavoxate HCl	427.92	AChR	Neurological disease	Muscarinic AChR antagonist.	3717-88-2	Up (1.018)	Up (1.005)
42	Aclidinium Bromide	564.55	AChR	Neurological disease	Human muscarinic AChR M1, M2, M3, M4 and M5.	320345-99-1	Down (0.789)	Up (1.050)
43	Bismuth Subsalicylate	362.09	COX	Neurological disease	Active ingredient in Pepto-Bismol and inhibits prostaglandin G/H Synthase 1/2.	14882-18-9	Normal (0.899)	Normal (0.910)
44	Diphemanil methylsulfate	389.51	AChR	Neurological disease	Quaternary ammonium anticholinergic, it binds muscarinic acetycholine receptors (mAchR).	62-97-5	Up (0.970)	Down (0.881)
45	Doxapram HCl	432.98	TASK-1, TASK-3, TASK-1/TASK-3	Neurological Disease	TASK-1, TASK-3, TASK-1/TASK-3 heterodimeric channel function	7081-53-0	Up (0.958)	Down (0.886)
46	Methazolamide	236.27	Carbonic Anhydrase	Neurological disease	Carbonic anhydrase inhibitor.	554-57-4	Normal (0.885)	Down (0.884)
47	Bextra (valdecoxib)	314.36	COX	Neurological disease	Potent and selective inhibitor of COX-2.	181695-72-7	Up (0.952)	Normal (0.898)
48	Primidone (Mysoline)	218.25	Sodium channel	Neurological disease	Anticonvulsant of the pyrimidinedione class.	125-33-7	Up (0.961)	Down (0.858)

Supplementary

49	Baclofen	213.661	GABA receptor	AUD drug	Derivative of the neurotransmitter γ-aminobutyric acid (GABA).	1134-47-0	Down (0.631)	Down (0.726)
50	Naltrexone hydrochloride	341.401	Opioid receptor	AUD drug	N-cyclopropylmethyl derivative of oxymorphone. Competitive antagonists at the μ-opioid receptor (MOR).	16590-41-3	Down (0.750)	Down (0.790)
51	Acamprosate calcium	181.211	GABA receptor	AUD drug	NMDA receptor antagonist and positive allosteric modulator of $GABA_A$ receptors.	77337-76-9	Down (0.814)	Down (0.888)
52	Clomethiazole hydrochloride	161.653	GABA receptor	AUD drug	Positive allosteric modulator at the barbiturate/picrotoxin site of the $GABA_A$ receptor.	533-45-9	Up (0.992)	Normal (0.906)
53	Disulfiram	296.52	Dehydrogenase	AUD drug	Inhibitor of the enzyme acetaldehyde dehydrogenase.	97-77-8	Down (0.734)	Normal (0.912)

10. Publications

Zink A, Conrad J, Telugu NS, Diecke S, Heinz A, Wanker E, Priller J, Prigione A. Assessment of Ethanol-Induced Toxicity on iPSC-Derived Human Neurons Using a Novel High-Throughput Mitochondrial Neuronal Health (MNH) Assay. *Front Cell Dev Biol*. 2020 Nov 5;8:590540. doi: 10.3389/fcell.2020.590540. PMID: 33224955; PMCID: PMC7674658.

Laidou S, Alanis-Lobato G, Pribyl J, Raskó T, Tichy B, Mikulasek K, Tsagiopoulou M, Oppelt J, Kastrinaki G, Lefaki M, Singh M, **Zink A**, Chondrogianni N, Psomopoulos F, Prigione A, Ivics Z, Pospisilova S, Skladal P, Izsvák Z, Andrade-Navarro MA, Petrakis S. Nuclear inclusions of pathogenic ataxin-1 induce oxidative stress and perturb the protein synthesis machinery. *Redox Biol*. 2020 May;32:101458. doi: 10.1016/j.redox.2020.101458. PMID: 32145456; PMCID: PMC7058924.

Zink A, Priller J, Prigione A. Pluripotent Stem Cells for Uncovering the Role of Mitochondria in Human Brain Function and Dysfunction. J Mol Biol. 2018 Mar 30;430(7):891-903. doi: 10.1016/j.jmb.2018.02.005. PMID: 29458125.

Inak G, Lorenz C, Lisowski P, **Zink A**, Mlody B, Prigione A. Concise Review: Induced Pluripotent Stem Cell-Based Drug Discovery for Mitochondrial Disease. *Stem Cells*. 2017 Jul;35(7):1655-1662. doi: 10.1002/stem.2637. PMID: 28544378.

Lorenz C, Lesimple P, Bukowiecki R, **Zink A**, Inak G, Mlody B, Singh M, Semtner M, Mah N, Auré K, Leong M, Zabiegalov O, Lyras EM, Pfiffer V, Fauler B, Eichhorst J, Wiesner B, Huebner N, Priller J, Mielke T, Meierhofer D, Izsvák Z, Meier JC, Bouillaud F, Adjaye J, Schuelke M, Wanker EE, Lombès A, Prigione A. Human iPSC-Derived Neural Progenitors Are an Effective Drug Discovery Model for Neurological mtDNA Disorders. *Cell Stem Cell*. 2017 May 4;20(5):659-674.e9. doi: 10.1016/j.stem.2016.12.013. Epub 2017 Jan 26. PMID: 28132834.

11. Selbstständigkeitserklärung

Hiermit erkläre ich, dass ich die vorliegende Arbeit selbständig und unter Verwendung keiner anderen als der von mir angegebenen Quellen und Hilfsmittel verfasst habe. Ferner erkläre ich, dass ich bisher weder an der Freien Universität Berlin noch anderweitig versucht habe, eine Dissertation einzureichen oder mich einer Doktorprüfung zu unterziehen.

Düsseldorf,

Annika Zink